SYNTHESIS OF HRPN-ENCAPSULATED CHITOSAN NANOPARTICLES FOR UPTAKE IN *Carica papaya* L. LEAVES

By

NUR BALQIS BINTI ZAMRI

Thesis Submitted to the School of Graduate Studies, Universiti Putra Malaysia, in Fulfilment of the Requirements for the Degree of Master of Science

December 2024

FBSB 2024 1

Abstract of thesis presented to the Senate of Universiti Putra Malaysia in fulfilment of the requirement for the degree of Master of Science

SYNTHESIS OF HRPN-ENCAPSULATED CHITOSAN NANOPARTICLES FOR UPTAKE IN *Carica papaya* L. LEAVES

By

NUR BALQIS BINTI ZAMRI

December 2024

Chairman : Associate Professor Mas Jaffri bin Masarudin, PhD
Faculty : Biotechnology and Biomolecular Sciences

Carica papaya L. is a favourite tropical fruit worldwide and considered as an economically important crop grown in Malaysia. Unfortunately, outbreak of papaya dieback disease caused by a phytopathogenic bacteria, *Erwinia mallotivora*, had resulted a significant drop in market revenue. Discovery of effector proteins secreted by *E. mallotivora*, have brought a new hope to disease management strategy as they promptly induce defence mechanism like systemic acquired resistance (SAR) against pathogens attack. However, the protein formulations prone to instability which lead to loss of efficiency and efficacy. The application of nanobiotechnology through encapsulation in chitosan biopolymer may be a desirable way to deliver biological compounds into the crops. Chitosan was chosen for its ideal character like biocompatibility, biodegradability, antimicrobial properties, as well as its ability to increase plant immune responses on its own. Thus, this study aimed to synthesis, characterize, and deliver a delivery system of effector protein using chitosan

nanoparticles (CNP) as a vector into papaya leaves. For these purposes, recombinant HrpN protein synthesis, HrpN encapsulation in CNP, physicochemical characterization, *in vitro* HrpN release profiling, fluorescence-based plant uptake assessment, and toxicity evaluation in zebrafish embryos were performed. A selected *E. mallotivora* Type III effector, termed HrpN, was produced as recombinant protein and subjected to encapsulation within the core of chitosan nanoparticles via ionic gelation method. The optimum HrpN-encapsulated chitosan nanoparticles (CNP-HrpN) formulation synthesized spherical CNP-HrpN which had high encapsulation efficiency (>80%) and colloidal stability, influenced by size (particle size distribution = 106.34 ± 2.053 nm) and high homogeneity (polydispersity index = 0.188 ± 0.011). Infrared spectroscopy portrayed the spectra of synthesized nanoparticles which involve bioactive compounds to their vacancies, successfully. *In vitro* HrpN release analysis demonstrated sustained release for over 72 hours. On another note, fluorescence imaging revealed the accumulation of CNP-HrpN in papaya leaves at 24 hour post-delivery. Additionally, CNP-HrpN was found non-toxic towards zebrafish embryos through toxicology evaluation. This study successfully synthesized HrpN-encapsulated chitosan nanoparticles using ionic gelation, characterized their physicochemical properties, and showed sustained HrpN release with successful uptake in papaya leaves, describing its potential as a plant defense delivery system. Further *in vivo* testing in greenhouse condition is recommended to reaffirm this possibility. Hopefully, this study will lay a foundation for developing conceivable biocompatible plant defence tool for better control of plant diseases in future.

Keywords: chitosan nanoparticles, papaya dieback disease, systemic acquired resistance.

SDG: GOAL 2: Zero Hunger

Abstrak tesis yang dikemukakan kepada Senat Universiti Putra Malaysia
sebagai memenuhi keperluan untuk ijazah Master Sains

PENGHASILAN NANOPARTIKEL KITOSAN MENGANDUNGI HRPN UNTUK PENGHANTARAN KE DALAM DAUN BETIK (*Carica papaya* L.)

Oleh

NUR BALQIS BINTI ZAMRI

Disember 2024

Pengerusi : Profesor Madya Mas Jaffri bin Masarudin, PhD
Fakulti : Bioteknologi dan Sains Biomolekul

Carica papaya L. (betik) ialah buah tropika kegemaran di seluruh dunia dan dianggap sebagai tanaman yang penting dari segi ekonomi di Malaysia. Malangnya, wabak penyakit rosot betik yang disebabkan oleh bakteria patogen tumbuhan iaitu *Erwinia mallotivora*, telah mengakibatkan penurunan ketara dalam hasil pasaran. Penemuan protein efektor yang dirembeskan oleh *E. mallotivora* telah membawa harapan baru kepada strategi pengurusan penyakit kerana ia segera merangsang mekanisme pertahanan seperti kerintangan perolehan sistemik (SAR) terhadap serangan patogen. Walau bagaimanapun, formulasi protein tersebut cenderung kepada ketidakstabilan yang membawa kepada kehilangan kecekapan dan keberkesanan. Aplikasi nanobioteknologi melalui penkapsulan dalam biopolimer kitosan mungkin cara yang diinginkan untuk menghantar sebatian biologi ke dalam tanaman. Kitosan dipilih sebagai biopolimer kerana sifatnya yang ideal seperti biokeserasian, biodegradasi, sifat antimikrob, serta kemampuannya untuk

meningkatkan tindak balas tumbuhan secara semula jadi. Oleh itu, kajian ini bertujuan untuk menghasilkan, mencirikan, dan menghantar sistem penghantaran protein efektor menggunakan nanopartikel kitosan (CNP) sebagai vektor ke dalam daun tanaman betik. Untuk tujuan ini, sintesis protein rekombinan HrpN, enkapsulasi HrpN dalam CNP, pencirian fizikokimia, profil pelepasan HrpN secara *in vitro*, penilaian pengambilan tumbuhan berasaskan pendarfluor, dan penilaian ketoksikan pada embrio ikan zebra telah dijalankan. Efektor Type III yang dipilih daripada *E. mallotivora*, yang dikenali sebagai HrpN, dihasilkan sebagai protein rekombinan dan dimasukkan ke dalam teras nanopartikel kitosan melalui kaedah gelasi ionik. Formulasi nanopartikel kitosan mengandungi HrpN (CNP-HrpN) yang optimum menghasilkan CNP-HrpN berbentuk sfera yang mempunyai kecekapan penkapsulan yang tinggi (>80%) dan kestabilan koloid, dipengaruhi oleh saiz (taburan saiz zarah = 106.34 ± 2.053 nm) dan homogeniti yang tinggi (indeks polidispersi = 0.188 ± 0.011). Spektroskopi inframerah berjaya menggambarkan spektrum nanopartikel yang terhasil memasukkan sebatian bioaktif kedalamnya. Analisis pelepasan HrpN secara *in vitro* menunjukkan pelepasan yang berterusan selama lebih dari 72 jam. Dalam nota lain, pengimejan pendarfluor mendedahkan pengumpulan CNP-HrpN dalam daun betik pada 24 jam selepas penghantaran. Selain itu, CNP-HrpN didapati tidak toksik terhadap embrio zebrafish melalui penilaian toksikologi. Kajian ini berjaya menghasilkan nanopartikel kitosan berenkapsulasi HrpN menggunakan gelasi ionik, mencirikan sifat fizikokimianya, dan menunjukkan pelepasan protein yang berterusan dengan pengambilan yang berjaya dalam daun betik, menggambarkan potensinya sebagai sistem penghantaran pertahanan

tumbuhan. Ujian lanjut secara *in vivo* dalam rumah hijau telah disarankan untuk mengesahkan kemungkinan ini. Kajian ini diharap akan meletakkan asas untuk membangunkan alat pertahanan tumbuhan yang biokompatibel untuk kawalan penyakit tumbuhan yang lebih baik di masa depan.

Kata Kunci: kitosan nanopartikel, penyakit mati rosot betik, kerintangan perolehan sistemik.

SDG: MATLAMAT 2: Kebuluran sifar

ACKNOWLEDGEMENTS

All praise to Allah, the Almighty, on whom ultimately, we depend for health, blessings, and guidance. Second, I want to thank my supervisor, Prof. Madya Dr. Mas Jaffri Masarudin, for his good deeds. It was only due to his valuable guidance, cheerful enthusiasm, and ever-friendly nature that I was able to complete this Master successfully.

I want to express my highest gratitude to the members of the Biotechnology and Nanotechnology Research Centre in MARDI. Without their guidance in the lab, an amateur like me would not be able to complete my lab work. They are among the good souls who always give thoughtful feedback and are always aimed at moving me forward. Their timely and efficient contribution in terms of energy, food, and gossip helped to shape me into who I am now.

I am forever indebted to my precious family, especially my mother, Puan Norlaila, and my father, Encik Zamri, as well as my cheerleaders, Aqilah, Nasyriq, Naqib, and Rafiq, who understand me a lot and sacrifice their everything for me. I cannot express how much I love them, and without their support, maybe I would have already quit this study. I would like to thank my housemates and friends for their constant encouragement and for always being available when I need help. Lastly, my gratitude goes to my special one for his unwavering support and love. Special thanks, tribute, and appreciation to all those names who do not appear here. May Allah shower all of you with eternal happiness.

This thesis was submitted to the Senate of Universiti Putra Malaysia and has been accepted as fulfilment of the requirement for the degree of Master of Science. The members of the Supervisory Committee were as follows:

Mas Jaffri bin Masarudin, PhD
Associate Professor
Faculty of Biotechnology and Biomolecular Sciences
Universiti Putra Malaysia
(Chairman)

Nadiya Akmal binti Baharum, PhD
Senior Lecturer
Faculty of Biotechnology and Biomolecular Sciences
Universiti Putra Malaysia
(Member)

Norliza binti Abu Bakar, PhD
Principal Research Officer
Biotechnology & Nanotechnology Research Centre
Malaysian Agricultural Research and Development Institute
(Member)

Noor Azlina binti Masdor, PhD
Principal Research Officer
Industrial Crop Research Centre
Malaysian Agricultural Research and Development Institute
(Member)

_____
ZALILAH MOHD SHARIFF, PhD
Professor and Dean
School of Graduate Studies
Universiti Putra Malaysia

Date: 8 May 2025

TABLE OF CONTENTS

LIST OF TABLES

LIST OF FIGURES

LIST OF ABBREVIATIONS

°C	celcius
Ag	silver
AIC	Akaike information criterion
ANOVA	one-way analysis of variance
ATP	adenosine triphosphate
Au	gold
B	boron
BCIP/NBT	bromo-4-chloro-3-indolyl phosphate/nitro blue tetrazolium
BSA	bovine serum albumin
CEP	comparative export performance
cm^{-1}	reciprocal centimeter
CNP	chitosan nanoparticles
CNP-HrpN	HrpN-encapsulated chitosan nanoparticles
CS	chitosan
Cu	copper
CuO	copper oxide
DC	detergent compatible
ddH_2O	double-distilled water
DLS	dynamic light scattering
DMSO	dimethyl sulfoxide
DNA	deoxyribonucleic acid
DOA	Department of Agriculture
DOS	Department of Statistics
EE	encapsulation efficiency
ETI	effector-triggered immunity
FAO	Food and Agriculture Organisation
FE-SEM	field emission-scanning electron microscopy
FITC	fluorescein-5(6)-isothiocyanate
FTIR	fourier transform infrared
g	gram
H^+	hydrogen ions
HCl	hydrochloric acid
His	histidine
hpa	hectoPascals
hpe	hours post-exposure
hpf	hours post-fertilization
HR	hypersensitive response
hrp	hypersensitive response and pathogenicity
HrpL	hypersensitive response protein L
HrpN	hypersensitive response protein N
HrpS	hypersensitive response protein S
HRPX	hypersensitive response protein X
HR-TEM	high resolution-transmission electron microscopy
IgG	anti-mouse immunoglobulin
IPTG	isopropyl β-D-1-thiogalactopyranoside
kDa	kilo Dalton
kbp	kilobase pair

L	litre
LB	Luria Bertani
LC	lethal concentration
M	molar
MAMPs	microbial-associated molecular patterns
Mn	Manganese
MARDI	Malaysian Agricultural Research and Development Institute
mg	milligram
min	minutes
mL	millilitre
mM	millimolar
MSC	model selection criterion
MTI	MAMP-triggered immunity
MW	molecular weight
NAC	N-acetyl-cysteine
NaOH	sodium hydroxide
Ni-NTA	nickel-nitrilotriacetic
NiO	nickel oxide
nm	nanometer
OD	optical density
OH^-	hydroxide ions
OVA	ovaalbumin
PBS	phosphate buffered saline
PDI	polydispersity index
pI	isoelectric point
ppm	parts-per-million
PCA	protocatechuic acid
PSD	particle size distribution
R^2	correlation factor
RNA	ribonucleic acid
ROS	reactive oxygen species
rpm	revolution per minute
SA	salicylic acid
SAR	systemic acquired resistance
SD	standard deviation
SDS-PAGE	sodium dodecyl sulfate polyacrylamide gel electrophoresis
SSR	self-sufficiency ratio
T3SS	type III secretion system
TPP	sodium tripolyphosphate
v/v	volume per volume
ZFET	zebrafish embryo toxicity
ZnO	zinc oxide
µg	microgram
µL	microlitre

CHAPTER 1

INTRODUCTION

1.1 Research Background

Carica papaya L., or locally referred in Malaysia as “Betik”, is an edible tropical fruit with high economic importance in both domestic consumption and the international market. In 2004, Malaysia became the second-largest papaya exporter in the world by bringing in RM 120 million in export revenues (Roff et al., 2019). However, Malaysia became the fourth-largest papaya exporter from 2019 to 2023. The export volume was lower than other top papaya exporter like Mexico, Guatemala, and Brazil. In 2023, Malaysia's papaya exports fell by 14% to 14,000 tonnes (FAO, 2024). Attacks from *Erwinia mallotivora* led to bacterial dieback disease, which affected the global production chain. The Department of Agriculture (DOA) reported that this crisis resulted in RM 30 million in losses for the whole affected area in Malaysia. Infected trees in 806 hectares of papaya plantations displayed water-soaked symptoms on petioles, leaves, and the apical stem. They experienced a range of damage, from slight impairment to total devastation across various growth stages, potentially resulting in the death of the tree within one to two weeks (Idris et al., 2023). At present, papaya growers have no effective solution to stop the disease from spreading as soon as the symptoms appear on the trees. Researchers are looking into the mode of action of the phytopathogen and performing conventional breeding as well as genetic engineering to synthesize resistant

papaya lines (Tamizi et al., 2022). Despite this progress, it is very difficult for researchers to identify and introduce resistance genes in papaya. In current situation, there is limited knowledge of its natural resistance mechanisms, the absence of naturally resistant cultivars as well as incomplete understanding of *E. mallotivora* pathogenicity and its interaction with host plant (Mohd-Azhar et al., 2021). Flaws in earlier works encourage the idea of using plants own defence mechanisms as deployable, affordable, and green technology.

Pathogens such as bacteria, fungi, and viruses switch on the first line of defence system upon invasion. This stimulates signal transmission via the phloem to the rest of the plant parts, termed systemic acquired resistance (SAR). The SAR phenomenon defends a variety of crop species, where plants will develop tolerance at one site and have resistance to subsequent attacks throughout the entire organism (Malik et al., 2020). Few works in agricultural studies mentioned the ability of SAR elicitors to activate defence signalling pathways, thereby leading to secondary metabolite production and cell wall lignification (Nishad et al., 2020). For example, salicylic acid (SA) is a famous SAR elicitor that recently produce phytoalexins that can act as an antibiotic against a bacterium named *Pseudomonas savastanoi* that causes halo blight in beans (Astha & Sekhon, 2021). Another study on the protection of zucchini plants against viral and fungal pathogens showed that benzothiadiazole derivatives has successfully increase plant resistance at the beginning of the vegetative season (Spychalski et al., 2023). The elicitors provide resistance against disease as well as improving crop quality and quantity through the application of naturally-occurring molecules secreted by pathogens or found in

the environment, or synthetic molecules like peptides or chemical compounds that can replicate the effects of pathogen-derived molecules on plants (Z. Li et al., 2023a). The exogenous proteinaceous hairpin elicitor emerged as one of the substitutes for conventional chemical treatment in managing biotic threats; even though hairpin treatment in the actual field required frequent foliar applications with higher amounts. Hairpin was easy to degrade, especially in a long-term storage period. The intricate anatomical leaf features caused minimal assimilation and interaction of the hairpin with receptors (Kongala et al., 2021; Sabrina Wahid et al., 2021).

Researchers were trying to overcome those limitations by delivering hairpins into plants using the nanoencapsulation approach. In a recent study, hairpins from *Pseudomonas syringae* pv. *syringae* coated with gold nanoparticles were able to penetrate and induce defence responses in tobacco plants. Interestingly, the metal nanoparticulate system required only minimal concentrations of hairpin for successful application (Kongala et al., 2021). Nevertheless, metal nanocarrier matrices trigger environmental harm such as toxicity risks and pollution hazards (Khan et al., 2021). Non-toxic polymer-based chitosan nanoparticles (CNP) appear as an option for biocompatible and biodegradable carriers. CNP protects the encapsulated compounds and boosts their penetration into plant in a sustained release manner. Moreover, chitosan, as a single agent, improves plant resistance and biological processes associated with plant growth through callose deposition and the production of defense-related enzymes, phytoalexins, and proteins (Francesconi et al., 2024; Torres-Rodriguez et al., 2021; Zheng et al., 2021).

Plants have their own specific mechanisms for uptake, transport, and release of nanoparticles with varying physicochemical characteristics, release kinetics, as well as human and environmental concerns. Previous studies with SAR inducer within CNP carriers required direct foliar uptake for fast adsorption and minimal soil interaction, thereby eliciting immunity within plant systems in a safe way (Yavas, 2021).

This study hypothesizes that encapsulating the SAR elicitor within CNP can produce stable nanoparticles with high encapsulation efficiency and sustained delivery in papaya leaves. In this work, we used an ionotropic gelation approach to encapsulate an eco-friendly recombinant hairpin from *E. mallotivora*, termed HrpN. The focus was on optimizing the size, dispersity, morphology, and encapsulation efficiency of synthesized HrpN-encapsulated chitosan nanoparticles (CNP-HrpN). Besides, we observed the CNP-HrpN uptake in papaya leaves via fluorescence tagging and assessed their *in vitro* release kinetics and potential toxicity. The synthesis of CNP-HrpN brings hope to deliver and release HrpN in lab-scale and actual papaya field in a sustainable manner for future papaya dieback disease management.

1.2 Research Objective

The general aim of this study is to develop a chitosan nanoparticles system that encapsulates a selected recombinant hairpin to enhance the uptake of systemic acquired resistance elicitor into papaya leaves. The objectives outlined for this study include:

1. To synthesize chitosan nanoparticles encapsulating the systemic acquired resistance-inducing recombinant protein using ionic gelation methods;
2. To perform physico-chemical characterization of the systemic acquired resistance-inducing recombinant protein encapsulated chitosan nanoparticles; and
3. To assess the release manner and uptake of systemic acquired resistance-inducing recombinant protein encapsulated in chitosan nanoparticles in papaya leaves.

CHAPTER 2

LITERATURE REVIEW

2.1 Papaya (*Carica papaya* L.) and its economic significance

Papaya is an outstanding crop of this nation, supplying its natural vitamins, minerals, bioactive compounds, and secondary metabolites to fruit consumers (Koul et al., 2022a; Xi et al., 2023). Prior findings have shown that, aside from its fruit, different parts of the papaya plant, such as its leaves, flowers, stems, and seeds, have medicinal value due to their antimicrobial and healing properties. Papaya latex contains a variety of industrial enzymes like endopeptidases, papain, caricain, and proteinase, which are practical in the commercial sector (Koul et al., 2022b). For instance, papain serves as a meat tenderising agent within the meat-processing application, while healthcare practitioners utilise papaya leaves for the management of malaria, asthma, and hypertension (Ayodipupo Babalola et al., 2024). The massive papaya cultivation and commercialization contribute to the substantial economic importance. Several factors facilitate the dynamic growth and expansion of the papaya industry in this country, including its export performance, comparative export performance (CEP) index, government support and endorsement, export revenue and productivity, as well as domestic self-sufficiency (Tan et al., 2022).

An annual report by the Food and Agriculture Organisation (FOA) acknowledged the shipment of 58,149 metric tonnes of papaya from Malaysia as the second-largest export value in this world, possessing 21% of market trade in 2004 (N. A. Bakar, 2018). Malaysian Agricultural Research and Development Institute (MARDI) mentioned that Malaysia had a positive CEP index for a continuous nine-year period. This country was doing better than other Asian papaya exporters such as Thailand, Indonesia, the Philippines, Singapore, China, and India from 2000-2008. Consequently, the National Agrofood Policy 2011-2020 approved papaya cultivation by highlighting its potential for continuous export, in addition to other main commodities like rubber and oil palm (Rozana, 2017a).

Malaysia was accountable for 2.38% of the total global papaya exports in 2020. According an international platform for food and agriculture trading statistics called Tridge, Malaysia generated approximately 7.28 million USD in export revenue from papaya, with Singapore being the primary purchaser. Furthermore, the papaya export value increased by 21.85%, and its productivity climbed by 26.28% compared to 2017 (Tan et al., 2023). In 2019, the Malaysian Department of Statistics (DOS) published a report showing that papaya fruits maintained the highest self-sufficiency ratio (SSR) at 153.1%. The self-sufficiency ratio indicates whether the number of fruits can meet the needs of the people. An SSR reaching 100.0% or above indicates that production is sufficient to meet domestic needs. This value shows Malaysia can supply domestic demand for papaya without being strongly dependent on imports. However, Malaysia was unable to rival other regional countries when

its part in worldwide exports declined from 21% in 2002 to 2.6% in 2020 (Rozana, 2017b).

2.2 Emergence of papaya dieback disease

The papaya industry in Malaysia collapsed since the outbreak of papaya dieback disease caused by a phytopathogenic bacteria named *Erwinia mallotivora*. The dieback was first spotted in Southeast Asia a long time earlier, precisely in Java, Indonesia, in 1931. The authorities of Johor State of Agriculture discovered the outbreak in Batu Pahat, Johor, in 2003. There was a possibility that the pathogen entered this country and was transmitted gradually from one plant to another through human intervention or bird and insect as transport agents. Prior observations on trunks, stems, and fruits documented few symptoms like yellowing, greasy appearance, and water-soaked lesions that result in dieback and plant death. The next incident happened in Bidor, Perak, and by the end of 2006, it spread to other regions on the west coast and central Malaysia peninsula, including Pahang, Selangor, Melaka, Negeri Sembilan, and Kedah. Another case in Sabah displayed similar observations, leading the plant pathologist from the Sarawak DOA to execute quarantine procedures and preventive strategies in collaboration with the Sabah DOA (Eng et al., 2020). Malaysia suffered a total loss in its calculated annual yield, valued at USD 58 million or 20000 metric tons, after a million-papaya tress died across 800 hectares of plantations (Wong et al., 2023).

Previous studies referred it as bacterial crown rot and bacterial canker disease (Azhar et al., 2020). According to the International Tropical Fruit Network, this dieback disease had a bad effect on the Malaysia market (Food and Agriculture Organisation, 2022). Widespread worries among farmers and stakeholders were raised after several papaya cultivars in Malaysia, including Eksotika, Sekaki, and Setiawan, were vulnerable to this pathogenic attack (Dayana et al., 2019). *E. mallotivora* is now penetrating Indonesia and the Philippines, with a future threat to papaya cultivation areas in another Southeast Asian region (Suharjo et al., 2021). *E. mallotivora* is a Gram-negative phytobacterium with many flagella distributed all over its rod-structure and belongs to the *Enterobacteriaceae* family. In the biochemical, genetic, and physical traits observed during the advanced stage of papaya dieback infection in Malaysia, the papaya plants did not show any canker symptoms, even though *E. papaya* is well-known for canker formation. In addition, while both *E. mallotivora* and *E. papaya* produced comparable symptoms, the isolates from affected papaya trees showed distinct results in biochemical tests. They discovered *E. mallotivora* with properties like catalase positive, oxidase negative, and the capability to make reducing compounds from sucrose (Sekeli et al., 2019).

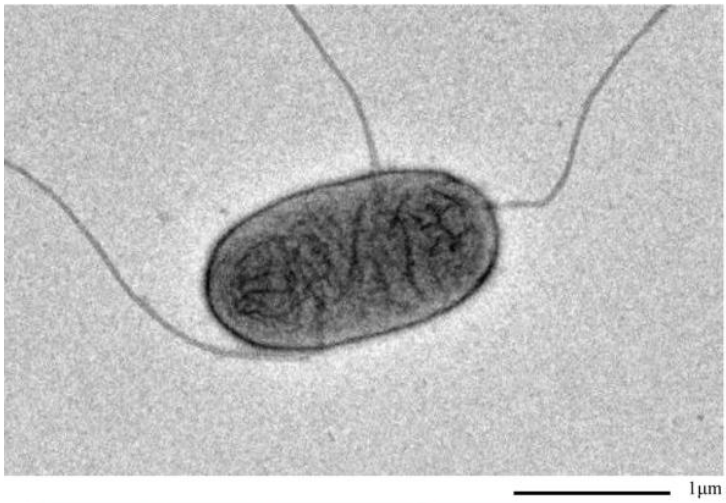

Figure 2.1: *Erwinia mallotivora*
(Source: Amin et al., 2011)

In a few exemplary cases, a diverse range of plant species have been susceptible to bacterial infection from the *Erwinia* genus. The phytopathogenic bacterium belonging to the *Erwinia* genus induces necrosis, wilt, and insidious rot in their hosts. For instance, *Erwinia amylovora* is responsible for triggering necrosis in relation to the fire blight disease on *Sorbus alnifolia* in Korea (Lim et al., 2023). Researchers have also linked *Erwinia pyrifoliae* to the bacterial attack in strawberry plantations in Netherlands and *Erwinia crysanthemi* to the outbreak of bacterial heart rot in pineapple crops in Hawaii (Cano-Reinoso et al., 2021; Jin et al., 2022).

Several publications have listed the symptoms of *E. mallotivora* infection. A scanning electron microscopy analysis visualised the *E. mallotivora* infiltration through various injury points, such as cracks, open wounds, and the degraded exterior tissues of the infected plant. This ultra-structural characterization focuses on the need to minimize plant injuries to prevent bacterial infiltration

(Magdalita et al., 2021). Another past observation provides a disease severity index that facilitates researchers and farmers in building intervention strategies by outlining the five stages of infection. Water-soaked spots appear on petioles and stems during the early stage. The second stage starts after the leaves become yellow-in-colour and black spots are visible on both leaves and fruits. Some plant organs, including petioles, stems, flowers, and leaves, become wilt, while fruits show brown tissue damage in the third stage. As the infection proceeds to the fourth stage, brown lesions begin to develop at the crown. A significant reduction in leaf production happened at the fourth stage. At the end, whole plant parts become rotten, leading to plant death (N. A. Bakar, 2018). Additional transcriptome analysis of *E. mallotivora* during early infection in papaya seedlings showed the increase in 5680 differentially expressed genes activity in response to pathogenic attack. In this study, plants started synthesising secondary metabolites and activating microbial metabolism pathway at 6 hours post-inoculation with *E. mallotivora.* On the fourth day post-inoculation, the signs of papaya dieback disease began to appear because of pathogen colonization. Afterwards, disease severity in plants increased rapidly, reaching 70% in 2 weeks. As the symptoms progressed, all plant parts succumbed to this bacterial infection (Juri et al., 2020). In a study likewise conducted within controlled glasshouse environments, the *Eksotika* cultivar exhibited rapid disease severity during the flowering and fruiting stages. In addition, the bacterial colonization in xylem and phloem directly impairs growth and productivity by disturbing physiological functions, particularly photosynthesis, leading to reduced leaf production (Abu-Bakar et al., 2021a). The DOA Terengganu mentioned that the hanging-leaf or ‘flag-leaf’ symptom

is an easy way to diagnose papaya dieback disease. Awareness of disease symptoms will assist papaya growers to halt the disease from spreading and minimize crop losses in future (Idris et al., 2023b).

Figure 2.2: Manifestation of dieback disease on infected papaya plants. (Source: (R. A. H. Bakar et al., 2023)

2.3 Recent disease management strategies

Current papaya dieback management covered systematic agronomic practices, chemical and fertilizer applications, the use of resistant varieties, and biological controls. The Department of Biosafety in Malaysia provides papaya growers with a set of approaches for their agricultural activities. According to the exclusion program mentioned in the biosecurity manual for the papaya industry, growers must limit vehicle or visitor access to the newly cultivated areas and encourage vehicle tires and shoes sanitization. Therefore, the chance of pathogen infection in the fields will be lower (Department of Biosafety, 2019). A recent spatial modelling analysis conducted in Batu Pahat,

Johor; revealed that papaya plantations nearer to roads are more likely to get affected by dieback disease due to increased human activity and pollution exposure. Hence, choosing the suitable location and landscape for newly planted areas will mitigate papaya dieback in the future (Idris et al., 2023b). If the prevention steps fail, the field will be put in a containment state. Farmers have to check on their papaya trees routinely to remove all the infected parts. When farmers cut down severely infected trees, they typically leave a 1-meter stump behind to allow them to re-shoot. Healthy new shoots growing from the stumps require proper care to support their recovery (Department of Agriculture, 2019). Farmers who fail to destroy papaya plants with dieback symptoms can be charged legally up to RM10,000 under Section 11 of the Plant Quarantine Act 1976 (Nur Adliza Baharom et al., 2018a).

Only a few chemicals are available on the global market for managing papaya dieback. In field applications, insecticides can inhibit vector insects from dispersing bacteria to papaya trees, while copper-based fungicides can lessen the consequences of infection (Abu Bakar et al., 2016). MARDI spent six years before introducing its own Dieback Buster 95 to the public in 2017. This chemical treatment is functional to induce systemic resistance in papaya plants against *E. mallotivora* (Ganisan Krishnen, 2022). Still, chemical product has negative side effects after continuous treatments. Soil quality becomes poor, environment turns polluted, and plant become resistant to pathogens (G. Wang et al., 2022). In a separate study, MARDI found that selected micronutrients like copper (Cu), boron (B), and manganese (Mn) sped up the lignification process in the Eksotika cultivar. This fertiliser serves as a natural

mechanical defence barrier as well as stimulating the development of natural defence enzymes in papaya plants (Nur Adliza Baharom et al., 2018b). Research on genetic engineering and conventional breeding to produce *E. mallotivora*-resistant papaya plants is still ongoing. The horticulture team at MARDI acquired a new hybrid that was resistant to papaya dieback disease after graft seedlings using Viorica papaya variety. Better interaction between scion and rootstock during metabolite transport successfully increases yield production and improves fruit quality (Mohd-Azhar et al., 2021). However, selection for an excellent papaya hybrid requires more data on shelf life from field tests in multilocations (Azhar et al., 2020). Recently, attention has been given to biological control strategies because researchers use microbial antagonists, such as fungi and bacteria, to fight the *Erwinia* pathogen. A report claimed that native endophytic bacteria on papaya can suppress *E. mallotivora* from growing (Paul et al., 2021). In another instance, several *Bacillus* species from rizosphere soil broke down *E. mallotivora* strain BT-MARDI's quorum sensing signal molecules, whereas five *Trichoderma* fungal isolates showed their antimicrobial activity. These microbial antagonists may work in the petri dish or in controlled setup, but the way they interact with other microbes with genetic variation in different environmental settings affect their performance in actual application (Sekeli et al., 2019; Tamizi et al., 2022).

Ongoing research now focuses on the molecular mechanisms and physiological responses related to plant defense mechanism, nutrient uptake, and stress tolerance. Few studies have discovered that dieback symptoms reduce leaf photosynthesis, transpiration, and stomatal conductance. This

confirms that maximizing plant resistance can slow disease growth and reduce photosynthetic losses (Noor Shahida et al., 2016). Molecular research is exploring *E. mallotivora* pathogenicity and host-pathogen interactions. For example, transcriptome analysis identified the main pathways and key cellular processes that took part in the early stages of *E. mallotivora* infection. They explained the importance of secondary metabolite biosynthesis, microbial metabolism, ATP-binding cassette transporters, and activities related to stimulus response, transmembrane transport, lyase, and structural molecule functions. The outcome of another study explained that iron acquisition and metabolism play a vital role in *E. mallotivora* pathogenesis. This mentioned the need to inhibit iron uptake in *E. mallotivora* in future studies (Juri et al., 2020). Besides, structural and phylogenetic analysis detected the presence of nucleotide binding site-leucine rich repeat domains. This domain recognises the effector molecules of *E. mallotivora*. These are the components used by the pathogen to infect and elicit symptoms in the papaya plant (N. S. A. Bakar et al., 2021).

Plant-pathogen interactions have discovered few proteins that are functional during dieback disease management. For example, bioinformatic analysis deciphered the role of a protein, *Em*HrpL, in the pathogen-related mechanism through its phylogenetic relationship with the type III secretion system (T3SS). The T3SS is a complex system in which a set of hypersensitive response and pathogenicity (hrp) genes function at the same time during any pathogenic attack (Tamizi et al., 2020). Moreover, alternative crop protection technology has also come a long way by using the plant resistance inducers to control

pathogen attacks. A recent experiment in an actual field showed that foliar application of a recombinant harpin protein termed Hrp I can induce SAR in papaya plants. This finding proves the possibility of T3SS-related proteins as a potential agent for dieback disease control (R. A. H. Bakar et al., 2023).

Current disease management strategies still have challenges despite these advancements. First, agronomic practises need strict adherence. This can be tough to follow in large-scale farming. Next, chemical treatments come with risks like resistance buildup as well as environmental toxicity. Other than that, resistant crop varieties take years to be developed and need further optimization. Biological control approaches show potential but still need more research and development to make sure they can work efficiently in real-world applications.

2.4 Application of proteinaceous hairpins to induce systemic acquired resistance in plant

By looking at the gaps mentioned in Section 2.3, alternative approaches such as proteinaceous hairpins offer a promising eco-friendly solution. Plant resistance inducers, also recognised as elicitors or effectors, offer an eco-friendly approach to pests and diseases associated with phytosanitary concerns in conventional farming practices (Guarnizo et al., 2020). Based on a review, pathogen inoculation, exogenous application of proteins from microbes or chemical application provides an array of biochemical activators that bind to receptor molecules on plant cells to elicit plant innate immunity (Malik et al., 2020). A conceptual study has illustrated that microbial-

associated molecular patterns (MAMPs) signify MAMP-triggered immunity (MTI). The MTI response defends against any potential pathogenic colonization. Gram-negative phytopathogenic bacteria like *E. mallotivora*. utilise the T3SS, a complex network that secretes effector proteins, toxins, and virulence factors directly into the host cell to suppress MTI and boost pathogenesis. Afterwards, plants use avirulence proteins to detect effectors from pathogens. When they do, they initiate a stronger reaction called effector-triggered immunity (ETI). Hypersensitive response (HR) at the infection site leads to rapid cell death and necrosis. These immune responses activate systemic responses, including SAR (Jiménez-Guerrero et al., 2023).

SAR is one of the best-acquired defence layers in plants. It offers long-term protection to the entire plant systems against different pathogens like bacteria, viruses, oomycetes, and fungi. An experiment reveals SAR efficiently protects the wheat cultivar against wheat foliar diseases throughout its entire growing season (Mapuranga et al., 2023). Normally, SAR not only stimulates defense pathways in the directly affected tissues, but it also initiates systemic responses in unaffected distant tissues and is transmitted across generations (Meena et al., 2022). As evidenced, foliar application of silica nanoparticles elevated SAR in both infected leaves and healthy *Arabidopsis thaliana* roots (Du et al., 2022). Previous discoveries describe the key events that happened during SAR in plants. For instance, the accumulation of reactive oxygen species (ROS) and synthesis of antimicrobial compounds such as phytoalexin, phenol, alkaloids, and tannins, helps the soybean leaves acclimatize to drought stress conditions by inducing stress-response pathways (Ji et al.,

2023). Moreover, cell wall reinforcements, lignification, and callose formation are the hallmarks of the salicylic acid (SA)-dependent signalling pathway for SAR in sorghum (Mutinda et al., 2023).

Some studies also reported the application of exogenous elicitors, which are either naturally occurring or artificially synthesized plant defence-triggering molecules (Bektas, 2022; Xiao et al., 2022; Zehra et al., 2021). Spraying *Panax notoginseng* leaves with a chemical inducer, 2,3-butanediol, successfully synthesized camalexis and enhanced SAR against the leaf pathogen, *Alternaria panx* (Li et al., 2023). 2,6-dichloroisonicotinic acid, one of the most common SAR elicitors in plant research over the past few decades, has made cotton more resistant to cotton leaf curl disease by boosting β-1,3 glucanase and chitinase levels, increasing peroxidase activities, and elevating total protein content (A. Kumari et al., 2020). Hairpins, a cell-free proteinaceous elicitor that hypersensitises gram-negative phytopathogenic bacteria, elevate plant natural defences, giving broad-spectrum and long-lasting resistance in an eco-friendly and sustainable approach (Z. Li et al., 2023b). Hairpins normally have an acidic, hydrophilic, and thermostable nature. Even so, their unique sequences and structural configurations make them prone to chemical denaturation. In a test with tomato plants, hairpin proteins from *Ralstonia solanacearum* produced the antioxidant enzymes catalase, superoxidase dismutase, and peroxidase, which stop the production of excessive ROS (Zhou et al., 2020).

Recent proteomics researches have enabled scientists to explore a few proteinaceous hairpin elicitors, including protease 2, hydrolase, luxR transcriptional regulator, chorismate mutase, hypersensitive response protein N (HrpN), hypersensitive response protein S (HrpS), and hypersensitive response protein L (HrpL) from *E. mallotivora* that are associated with T3SS and may be utilised as treatments for papaya dieback disease (N. A. Bakar et al., 2017). In this context, quantitative real-time analysis described improvement in natriuretic peptide receptor 1 and pathogenesis-related-1-d gene expression in papaya plants inoculated with recombinant HrpN protein because of SAR activation via SA-signalling pathways. Further, foliar application in a greenhouse setting had lower disease severity in HrpN-treated plants compared to untreated ones. Initial brown discoloration symptoms appeared early, but affected leaves dropped between days 6 and 10 post-infection, allowing new shoots to grow (N. A. Bakar, 2018).

A study found that incorporation of hypersensitive response protein X (HRPX) recombinant protein using the heterologous *Escherichia coli* system worked to activate the SAR response in papaya plants. Still, the application of HRPX was not enough to increase plant resistance because of its nature as a regulatory protein (Abu-Bakar et al., 2021). Foliar application with Hrp I and Hrp II in glasshouse and field conditions showed the expression of a few defence genes such as *peroxidase, pathogenesis-related-1-d*, and *osmotin* by Hrp I. Collective field data explained that infected plants treated with Hrp I had lower severity, better growth, and higher fruit production than Hrp II. Different harpin proteins had different efficiency in lowering disease severity in plants. In

addition, they found that stress turned on defence gene expression pathways, which explains the reason why proteinaceous hairpin treatment does not induce defence gene expression in healthy plants (R. A. H. Bakar et al., 2023).

Yet, frequent hairpin application in higher doses was necessary because hairpin structure had minimal interaction with plant leaves receptors. When the hairpin had minimal bioavailability, it had a poor capability to trigger the HR in the system (Nadendla et al., 2018). It is also apparent that limited cell wall osmosis to macromolecules caused the hairpin effect to be transient (Kongala et al., 2021). Nowadays, nanobiotechnology is going to enhance the function of proteinaceous hairpins in agricultural applications. For instance, the encapsulation of 30 nanogram of hairpin in chitosan nanoparticles (CNP) elicited SAR in tobacco plants by upregulating the defensive genes and antioxidants. This finding displayed its future potential as an eco-friendly biopesticide (Kongala et al., 2021). Loading recombinant HrpS, HrpN, and HrpX hairpin proteins onto CNP via ionic gelation method enhanced defence gene expression in papaya. From the significant results, a nanotechnology-based approach might be the most assuring solution for tackling papaya dieback disease (Sabrina Wahid et al., 2021).

2.5 Nanomaterial selection for delivery in agriculture

Nano-based plant disease control agents are safer option than conventional chemical products on the market. In the last few years, several countries have presented their regulatory frameworks to ensure the safety of nanomaterials

in different applications (R. Kumari et al., 2023). As discussed in past works, encapsulating pesticides, fungicides, herbicides, and micronutrients in nano-scale release matrices assist their penetration through plant cuticles and tissues. This allows a gradual release of the encapsulated compounds (Ansari, 2023; Yadav et al., 2023). Previous applications of metallic nanoparticles, including silver (Ag), gold (Au), copper oxide (CuO), zinc oxide (ZnO), and nickel oxide (NiO), worked effectively by being stable in the field. Still, there were concerns raised because these particles stayed in the soil for a long period of time, were hard to break down, and were harmful to the beneficial microbes living in the soil. It makes sense to adopt another alternative for biodegradable nanodelivery systems to solve these issues (Ameen et al., 2021; Dikshit et al., 2021).

Various biopolymers can replace metallic nanoparticles to deliver cargo to plants. The choice of nanomaterials depends on specific applications and cargo properties because different nanoparticles have their own particular characteristics. The process of selecting the suitable nanoparticles is to make sure that the substance reached the location successfully (Mujtaba et al., 2021). From prior studies, nanoparticles could transport nutrients, genetic materials like deoxyribonucleic acid (DNA) or ribonucleic acid (RNA), or biostimulants (Cao et al., 2016; Y. Wang et al., 2023). Another study mentioned that the size and solubility of the payload play roles in nanoparticle selection (Vega-Vásquez et al., 2020). Apart from that, the size and morphology of nanoparticles influence their ability to enter plant cells or tissues because some sizes and shapes work better in one condition than others. Both

factors determine their uptake by selected plant tissues or cells. (Zhang et al., 2022). Genetic material encapsulation in biocompatible biopolymers allowed them to interact with living organisms safely (Santana et al., 2020). Other than that, environmental conditions like temperature, soil pH, and relative humidity significantly influence the nanoparticle uptake in plant systems (Sampathkumar et al., 2020). Different crops have their own specific stimulus and pathways for nanoparticle-based treatments. Optimization steps are necessary to select the right nanomaterials that add value and minimize threats to plants and the environment concurrently (Mittal et al., 2020).

Over the past decades, CNP have been a significant area of interest among the natural biopolymers like pectin, cellulose, and alginates (Ansari, 2023). Chitosan (CS) with varying degrees of deacetylation and molecular weights ranging from 500 to 1400 kDa comes from the chemical deacetylation of second most abundant natural biopolymer, chitin, in an alkaline environment. Chitin is present in the shells of crustaceans, insect cuticles, and the cell walls of fungi (Pellis et al., 2022). In CS structural configurations, amino groups provide flexibility and direct chemical modifications. Previously, CS can adhere to plant surfaces and increase the contact time between agrochemicals and target absorptive surfaces such as leaves and stems as a result from its bioadhesive properties (Valderrama N et al., 2020). CNP is a non-toxic, biodegradable, and biocompatible compound that has characters like being anti-viral, anti-fungal, anti-oxidant, anti-inflammatory, and antimicrobial (Jagdale et al., 2024).

2.6 Application of chitosan nanoparticles as a delivery system in agriculture

Prior studies have described that CNP-encapsulated hexaconazole had the highest loading content of 16.7%, along with sustained release of 99.91% over a prolonged time up to 86 hours. CNP improves this active fungicidal agent efficiency against *Ganoderma boninense* in oil palm because of its high loading capacity, enhanced antifungal activity, thermal stability, and sustained release properties (Maluin et al., 2019). In a preliminary experiment, the copper-loaded CNP sample had the highest antibacterial activity in both an *in vitro* and an artificial soybean bacterial infection. It was better than CS hydrolysate, CS hydrolysate with copper, and CNP. CNP have a high surface area for better bacterial cell interaction, the ability to encapsulate and steadily release antibacterial agents, biocompatibility, and inherent antimicrobial activity. Besides, copper-encapsulated CNP with a size of 89 nm inhibited the growth of bacteria responsible for pomegranate bacterial blight at a concentration of 1000 ppm. CNP has efficient penetration and antimicrobial properties that are comparable to standard antibiotics like streptomycin (Tarakanov et al., 2023).

A recent application of harpin-loaded CNP, with a size of approximately 160 nm and a zeta potential of 30.2 ± 0.7 mV, induced pathogenesis-related proteins, specific marker genes, as well as defense enzymes in tobacco plants. As confirmed in histopathological findings, CNP, with its small dimension and positive zeta potential, was improving hairpin delivery and bioavailability, resulting in increased defense-related protein and enzyme levels in tobacco

plants compared to harpin or CS alone (Kongala et al., 2021). Another study describes that the synthesis of CNP loaded with SA and Ag through the ionic gelation method was capable of decreasing disease severity and the disease index of cassava leaf spot. Nano-sized CNP can assist in cassava leaf spot management due to its biocompatibility with the plants (Hoang et al., 2022). In a physicochemical study, the ZnO-chitosan nanoproducts were between 149 and 257 nm in size and released Zn (II) ions slowly over two weeks. The ZnO-chitosan nanoproducts showed a burst release within 24 hours and had a gradual release over two weeks, which fits the criteria for sustained release. These nanoproducts improve maize seed germination and growth even under salt-stress environment. CNP has a controlled release characteristic to make sure a continuous supply of nutrients and promotes the growth of seeds and seedlings even in challenging conditions (Zungu et al., 2023).

Loading gibberellic acid within a CNP matrix with a molecular weight of 27 kDa and a deacetylation degree of 75-85% boosted the growth of tomato and bean plants because CNP is non-toxic to the plant cellular system (Pereira et al., 2019). A separate work revealed that the application of CNP containing S-nitroso-mercaptosuccinic acid at a concentration of 1 mM. CNP has a high surface area, which helps the compound maintain stability with minimal degradation. High encapsulation efficiency resulted in overexpression of antioxidant activity and a reduction of oxidative stress as well as the nutritional imbalance in the roots stimulated by copper stress (Gomes et al., 2022). Subsequent research also explored the *in-situ* encapsulation of different active compounds (phenylalanine, methionine, salicylic acid, and pyruvate) onto CNP

using the ionic gelation method for avocado callus. Among them, CNP encapsulated with 40 mg/L of methionine had the highest mean record of callus fresh weight and glutathione content, together with a low malondialdehyde concentration of 0.993 nmol/g. CNP was able to hold more active compounds and release them slowly over time because it had porous properties (El-Fadl et al., 2022). Another study mentioned that polyphenols extracted from olive leaf encapsulated in CNP had fungicidal properties in managing Verticillium wilt in tomato plants. The loading efficiency was 58%, while the particle size measured was about 330 nm. Uptake and distribution of the polyphenols became more efficient as nanosized CNP could penetrate easily into tomato plant systems (Mazzotta et al., 2022).

Researchers also employed protocatechuic acid (PCA)-encapsulated CNP to fight the rice blast caused by *Pyricularia oryzae*. Transmission electron microscopy analysis indicated that nanoparticle penetration into fungal cells happened when the optimal size of nanoparticles ranged from 30 to 35 nm. Further anti-fungal assay showed that the nanoparticles were more effective at killing fungi than pure PCA sample, especially at a concentration of 5000 ppm. Based on findings, CNP itself has antimicrobial properties, which can work synchronously with PCA to elevate the overall anti-fungal effect (Pham et al., 2019). Additional study synthesized N-acetyl-cysteine (NAC)-loaded CNP by incorporating 0.5 mg/mL NAC into the CNP solution before ionotropic gelation with tripolyphosphate. Greenhouse experiments confirmed the elevation of the leaf antioxidant pool when the synthesized nanoparticles increased the ascorbic acid content in durum wheat cultivars. From the

observations, CNP can protect NAC from degradation and maintain its stability over a prolonged period in field environments (Picchi et al., 2021). Earlier works showed that CNP has advantages as carriers in increasing disease resistance, stress tolerance, and plant growth (Saritha et al., 2022). Still, there is a constant need to look for the best nanobiotechnology application, dosage, and timing for safe agricultural practices (Moses et al., 2024).

CHAPTER 3

MATERIALS AND METHODS

3.1 Overview of experimental design and workflow

This study follows a step-by-step workflow to achieve three main objectives: (i) synthesizing HrpN-encapsulated chitosan nanoparticles (CNP-HrpN), (ii) characterizing their physico-chemical properties, and (iii) evaluating their uptake in papaya leaves and potential toxicity. First, recombinant HrpN protein is expressed, purified, and encapsulated in chitosan nanoparticles using the ionic gelation method, followed by an encapsulation efficiency study. Next, the nanoparticles undergo physico-chemical characterization. These including particle size and polydispersity index analysis via Dynamic Light Scattering (DLS), chemical interaction analysis using Fourier Transform Infrared Spectroscopy (FTIR), and structural and morphological evaluation using High-Resolution Transmission Electron Microscopy (HRTEM) and Field Emission Scanning Electron Microscopy (FESEM). An *in vitro* HrpN release test is conducted to assess release kinetics. Finally, the uptake of CNP-HrpN in papaya leaves is tracked using fluorescein isothiocyanate (FITC) conjugation, and potential toxicity is evaluated through the Zebrafish Embryo Toxicity Assay (ZFET). This workflow ensures a clear, reproducible methodology to effectively meet the study's objectives, with the following flowchart providing a visual summary of the experimental process.

Objective 1

Synthesis of HrpN-encapsulated chitosan nanoparticles (CNP-HrpN)

- Recombinant HrpN protein expression and purification
- Encapsulation of recombinant HrpN protein in chitosan nanoparticles via ionic gelation
- Encapsulation efficiency study

Objective 2

Physico-chemical characterization of CNP-HrpN properties

- Physico-chemical characterization of CNP-HrpN
  - Dynamic Light Scattering (DLS)
  - Fourier Transform Infrared Spectroscopy (FTIR)
  - High-Resolution Transmission Electron Microscopy (HRTEM)
  - Field Emission Scanning Electron Microscopy (FESEM)
- *In vitro* HrpN release test
- Release kinetics modelling

Objective 3

Assessment of uptake of CNP-HrpN in papaya leaves and its potential toxicity

- *In vitro* CNP-HrpN uptake tracking in papaya leaves
  - Conjugation with fluorescein isothiocyanate (FITC)
- Toxicity evaluation
  - Zebrafish Embryo Toxicity Assay

3.2 Materials

The powder form of low molecular weight chitosan (CS) (MW: 50 kDa–190 kDa, >75% deacetylated), sodium tripolyphosphate (TPP), and fluorescein-5(6)-isothiocyanate (FITC) and the liquid form of dimethyl sulfoxide (DMSO) were procured from Sigma-Aldrich, St. Louis, MO, USA. The Biotechnology and Nanotechnology Research Centre of the Malaysian Agricultural Research and Development Institute (MARDI) in Serdang provided glacial acetic acid, sodium hydroxide (NaOH), hydrochloric acid (HCl), 10X phosphate buffered saline (PBS), and chemical reagents for molecular work. The Horticulture Research Centre in MARDI provided 4-month-old papaya plant leaves for tracking assessment. All chemicals were analytical grade and used without any further purification. Sterilized double-distilled water (ddH_2O) was used for all dilution purposes.

3.3 Expression and purification of recombinant HrpN protein from *Escherichia coli*

The *hrpN* gene (1.392 kbp), which encodes the full-length hairpin from *Erwinia mallotivora*, was obtained from MARDI Serdang. It had already been subcloned into a pET-32b expression vector (N. A. Bakar, 2018). The cloned plasmid was transformed into a competent *Escherichia coli* BL21(DE3*)* strain by chemical transformation and screened for ampicillin resistance at concentrations of 100 µg/mL. Successful bacterial transformation was confirmed through the formation of bacterial colonies on the plate. A single colony of pET-32b/hrpN-transformed BL21 was then cultured overnight in 5.0

mL of Luria Bertani (LB) broth medium at 37˚C. Protein expression was induced by transferring the culture to 400 mL of LB broth medium supplemented with ampicillin and 0.5 mM isopropyl β-D-1-thiogalactopyranoside (IPTG) (Thermo Scientific, USA). The culture was grown for an additional 6 hours at 37 °C after reaching an optical density (OD_{600}) of 0.5. After that, the cells were harvested via centrifugation (2,500 x g, 15 min, 4˚C). The supernatant was thrown away and the pellet was mixed with 10 mL of inclusion bodies. It was rotated with a rotary shaker (15 min, 4˚C) and then centrifuged (20,000 × g, 30 min, 4˚C). The bacterial pellet was resuspended in solubilization buffer (10 mL of Bugbuster reagent (Novogen) supplemented with a tablet of protease inhibitor (Thermo Fisher, USA) and rotated overnight at 4˚C. Following this, the protein suspension was centrifuged (20000 x g, 30 min, 4˚C). The supernatant was collected for large-scale purification. Nickel-nitrilotriacetic (Ni-NTA) columns were used for histidine-(His)-tag protein purification using the AKTAPrime Chromatography System. For verification, about 20 µL of purified HrpN protein was loaded onto two sets of 12% sodium dodecyl sulfate polyacrylamide gel electrophoresis (SDS–PAGE). One set was stained with Coomassie Brilliant Blue R250 and the other one was used for Western Blot. In the Western Blot process, proteins were transferred to a polyvinylidene difluoride membrane and probed with an anti-His antibody. The membrane was incubated with anti-mouse immunoglobulin (IgG) alkaline phosphatase conjugate, washed with buffer, and treated with 5-bromo-4-chloro-3-indolyl phosphate/nitro blue tetrazolium (BCIP/NBT) substrate solution. The bands appeared to show the target protein. Purified HrpN protein was quantified using the detergent compatible

(DC). Protein Assay (BioRad), which is rooted in the Lowry assay principle, with bovine serum albumin (BSA) as a standard. The protein aliquots were subsequently stored at -80 °C.

3.4 Synthesis and optimization of CNP parameters

Nanoparticle were synthesized using ionotropic gelation methods adopted with slight changes. Ionic gelation is a common method used due to its simplicity, low cost, mild processing conditions, and no requirement for toxic solvents (Kuen et al., 2017). CS powder was dissolved in a 1% (v/v) acetic acid solution and stirred overnight at 24^{o}C. The following day, stock solutions of CS and TPP were prepared at concentrations of 1.0 mg/mL in 50 mL centrifuge tubes, accordingly, before being diluted with deionized water to achieve a final working concentration of 0.5 mg/mL for the CS solution and 0.7 mg/mL for the TPP, based on optimal concentrations established in previous studies. The pH of the CS and TPP solutions was adjusted to pH 5 and pH 2, respectively, using 1 M NaOH and 1 M HCl prior to nanoparticle formation. For the synthesis of CNP, TPP solution was gradually added dropwise into the CS solution. The CS and TPP volumes were optimized. A constant volume of CS at 6 mL was used while changing the TPP volumes to 0.0, 0.5, 1.0, 1.5, 2.0, 2.5, 3.0, 3.5, and 4.0 mL. Afterwards, the TPP volume was kept the same at 2.5 mL when CS volumes changed to 0.0, 1.5, 3.0, 4.5, 6.0, and 7.5 mL. HrpN was adjusted to a few concentrations (0.02, 0.04, 0.06, 0.08, and 0.10 mg/mL) using PBS prior to HrpN-encapsulated chitosan nanoparticles (CNP-HrpN) synthesis. Each concentration of HrpN was added drop-by-drop into the 0.5 mg/mL of CS

solution, followed by the addition of 0.7 mg/mL of TPP. The liquid CNP-HrpN was kept at 4 °C for future use.

3.5 Physico-chemical characterizations of nanoparticle samples

The nanoparticles were tested using different characterisation ways to confirm the HrpN encapsulation into CNP. Dynamic light scattering (DLS), field emission-scanning electron microscopy (FE-SEM), high resolution-transmission electron microscopy (HR-TEM) and fourier transform infrared (FTIR) spectroscopy were performed.

3.5.1 Determination of particle size using dynamic light scattering (DLS)

DLS was conducted using a NanoBrook Omni Particle Size and Zeta Potential Analyzer (Brookhaven Instrument, USA) to analyse the particle size distribution (PSD) and polydispersity index (PDI) of the nanoparticle samples. The test parameters were set as follows: 4 runs (15 min per run), 90^{o} backscatter measurement angle, 1.33 material refraction index, 25^{o}C, and water were utilised as the dispersion medium according to quality standards. In a clear disposable cuvette, 100 µL of the sample was mixed in 900 µL of ultra-pure water (1:10 dilution) and sonicated for 5 minutes before measurement. A one-way analysis of variance (ANOVA) was used to assess the variations in PSD and PDI among triplicate samples.

3.5.2 Determination of encapsulation efficiency (EE)

To find the EE, the final amount of HrpN in CNP and the HrpN amount used for encapsulation were compared. CNP-HrpN was transferred to an ultra-centrifugal tube after protein incorporation. Nanoparticle from the CNP-HrpN suspension was separated through centrifugation (15000 rpm, 30 min, 10°C). As CNP-hrpN is larger and potentially denser, it would form a pellet at the tube's bottom. Smaller or less dense particles, such as free proteins, might not sediment as quickly and would remain in the supernatant (the liquid above the pellet). Supernatant of each sample was decanted carefully. The protein content in the supernatant was analysed with a microplate absorbance reader at 690 nm using the DC protein assay method. The supernatant from the unencapsulated CNP suspension was used as a blank. The EE of HrpN was analysed using ANOVA. Triplicate samples were calculated using Equation 3.1:

Encapsulation efficiency (EE) percentage =

$$\frac{\text{(total amount of HrpN used)} - \text{(HrpN amount in supernatant)}}{\text{total amount HrpN used}} \times 100 \qquad (3.1)$$

3.5.3 Determination of surface morphology and particle size using field emission-scanning electron microscopy (FE-SEM)

Surface morphologies and sizes were examined using FE-SEM on a JEOL Scanning Microscope JSM-6400 (beam voltage: 15 kV). The samples were sonicated for 15 minutes before mounting step. This was to avoid nanoparticles from clumping during the drying process. The samples were mounted on aluminium stubs and dried overnight in an incubator. Then, they

were coated with gold using a sputter coater. All prepared stubs were stored in the Electron Microscopy Unit at the Institute of Bioscience, Universiti Putra Malaysia, Malaysia. Imaging was performed at different magnifications. Image J software from the National Institute of Health (version 1.52a) determined nanoparticle diameter, size, and distributions based on the FE-SEM images of 50 individual particles.

3.5.4 Determination of morphological distribution and particle size using high resolution-transmission electron microscopy (HR-TEM)

HR-TEM was employed to elucidate the morphology as well as measure particle size and assess uniformity. The samples were prepared similarly to the FE-SEM analysis by sonicating them for 15 minutes. A small droplet of each sample was then placed on a formvar/carbon film and 400-mesh copper HR-TEM grids. Subsequently, the samples were dried overnight under a lamp. Imaging using JEOL JEM 2100F Field Emission TEM (Tokyo, Japan) were done in the Institute of Bioscience, Universiti Putra Malaysia, Malaysia. Nanoparticle diameters and size distributions were measured by analyzing 50 individual particles using Image J software (version 1.52a) based on the HR-TEM images.

3.5.5 Determination of free functional groups using fourier transform infrared (FTIR) spectroscopy

FTIR spectroscopy confirmed HrpN encapsulation in the CNP-HrpN sample when the CNP-HrpN spectrum showed functional groups from each compound including HrpN. Prior to analysis, liquid samples were freeze-dried to remove

liquid content. Coolsafe 95-15 PRO freeze dryer were used for 72 hours at -90 °C under 0.8-4.0 hPa pressure. The Perkin-Elmer Spectrum 400FT-IR/NIR imaging system recorded the infrared transmittance from powdered samples. Spectra were measured in the range of 650 - 4900 cm^{-1} at a resolution of 8 cm^{-1} in 128 scans at 25 °C.

3.6 *In vitro* release and kinetic study of HrpN from CNP

The release of HrpN from CNP was profiled using the *in vitro* direct dispersion method. Free HrpN in the supernatant was removed by centrifugation at 30,000 x g for 40 min. The pellet was put into another tube with PBS (pH 7.4). HrpN release was monitored up to 72 hours at A_{690}. 1 mL of the released medium was collected at different time points and replaced with the same volume of fresh medium. The total amount of HrpN released over time (0, 1, 2, 3, 6, 9, and 12 hours) was measured using a spectrophotometer at 690 nm. Equation 3.2 was describing the percentage of HrpN released from CNP carrier:

$$\text{Cumulative release percentage} = \frac{HrpN_t}{HrpN_i} \times 100 \qquad (3.2)$$

$HrpN_t$ and $HrpN_i$ represent the amount of HrpN released at time (t) and the initial (i) amount of HrpN encapsulated in the nanoparticle, respectively. The release behavior of CNP-HrpN was then fitted into selected kinetic models including zero-order, first-order, Higuchi, Korsmeyer-Peppas, and Hixson-Crowell. *In vitro* nanoparticle release kinetics were evaluated using the

DDSolver software. The HrpN release data for all nanoparticle formulations followed these equations:

zero-order equation: $F = k_o \times t$

where t is time and k_o is the release rate constant for zero-order kinetics;

first-order equation: $F = 100 \times [1 – Exp (-k_1 \times t)]$

where k_1 represents the release rate constant for the first-order kinetics;

Higuchi's equation: $F = k_H \times t^{0.5}$

where k_H represents the Higuchi release rate constant;

Hixson-Crowell equation: $F = 100 \times [1 - (1 - k_{HC} \times t)^3]$

where k_{HC} is the Hixson-Crowell rate constant;

Korsmeyer-Peppas equation: $F = k_{KP} \times t^n$

where n is the release exponent, showing the HrpN release mechanism. k_{KP} is a constant, describing the structural and geometric characteristics of the carrier.

3.7 Synthesis and visualisation of fluorescently-labelled CNP-HrpN

HrpN was tagged with the fluorescence marker, FITC, before being encapsulated into CNP to monitor the uptake and release of CNP-HrpN in papaya leaves. CS and TPP were prepared as described in Section 3.3. 0.00125 g of FITC powder was dissolved in 5 mL of DMSO at a concentration of 1 mg/mL to prepare a 0.25 mg/mL of FITC solution. FITC stock solution was

stirred in the dark at 25 °C and diluted to 0.05 mg/mL with DMSO. Subsequently, 250 µL of FITC was mixed with 600 µL of CS and 250 µL of HrpN solution (0.5 mg/mL). The mixture was left to incubate for 20 minutes to allow the conjugation of FITC to CS and HrpN structure. 250 µL of TPP (0.7 mg/mL) was then added and resuspended by pipetting to make sure a homogeneous suspension of CNP-HrpN-FITC. The mixture was left to incubate for an additional 20 minutes before further used. All steps were carried out in the dark at 25 °C. Afterwards, 1 mL of freshly prepared samples was added to petri dishes with papaya leaves. The leaves were left to incubate at different time points (0 hour and 24 hours) under laminar airflow. The controls were HrpN and 0.25 mg/mL FITC. Fluorescence microscopy (Olympus, Germany) was used to view the samples at 24-hour time points after incubation. The solution was removed prior to leaf viewing. The leaves were rinsed with distilled water to remove excess FITC. Images were taken using bright field and FITC at 10X magnification.

3.8 Determination of toxicity using zebrafish embryo toxicity (ZFET) assay

A zebrafish embryo model was used to observe how the nanoparticles affected their survivability, hatching process, heart rate, and development. The toxicity study started from 0 to 120 hours post-exposure (hpe). The main stock solutions of freeze-dried CNP and CNP-HrpN were made by diluting them in 1 mL of distilled water. Sub-stocks were prepared in a 96-well microplate. Serial dilutions using embryo media were prepared for concentrations ranging from 10% to 100% (v/v). Untreated embryos in embryo media were used as

controls. The zebrafish embryo toxicity assay followed the fish embryo toxicity test guidelines by the Organisation for Economic Cooperation and Development. One zebrafish per well at 0 hours post-fertilization (0 hpf) was exposed to 200 µL samples in 96-well microplates at seven concentrations (10-100% v/v). Each treatment group and control had 12 embryos. The embryos were kept at 25 °C for 5 days. Survival rate, hatching rate, heart rate, and morphological malformations or teratogenic defect were observed every 24 hours from 0-120 hpe. Images and videos were captured by an inverted microscope with a digital camera. Heartbeats from three selected embryos were counted using a stopwatch for 1 min. Lethal endpoints were identified by coagulation and no heartbeat. Developmental anomalies include pericardial edoema, yolk sac edoema, non-hatched embryos, curved bodies, and bent tails. Toxicity (LC_{50}) values were determined for the sample at 100% (v/v) concentration, described as relatively harmless (>50%), practically non-toxic (80–90%), slightly toxic (50–79%), moderately toxic (10–49%), highly toxic (1–9%), and super toxic (<1%).

3.9 Statistical analysis

Statistical data were analysed using GraphPad Prism version 9.0 software. The data was shown as the mean of replicates. Error bars were calculated from the standard deviation of the mean. Statistical significance was determined using a one-way ANOVA followed by Tukey's post-hoc test. Differences are considered at a level of $p < 0.05$.

CHAPTER 4

RESULTS AND DISCUSSION

4.1 Overview

This chapter discusses the findings of the study, focusing on the synthesis, characterization, and evaluation of CNP encapsulating the recombinant HrpN protein. The analysis begins with the purification and verification of HrpN using SDS-PAGE and Western blot, followed by the optimization and synthesis of CNP-HrpN. Various characterization techniques, including FE-SEM, HR-TEM, and FTIR spectroscopy, were used to assess the morphology, functional groups, and encapsulation efficiency of the nanoparticles. The in vitro release profile of HrpN from CNPs was evaluated, and kinetic modelling was applied to understand the release mechanism. Additionally, the uptake of CNP-HrpN by papaya leaves was visualized using FITC labeling, and the safety of the formulation was assessed through a zebrafish embryo toxicity (ZFET) assay. Together, these findings provide information into the potential of CNPs as a potential nanocarrier for delivering HrpN in a sustained released.

4.2 Analysis of purified recombinant HrpN protein using SDS-PAGE and Western Blot

SDS-PAGE allows protein separation based on their molecular weight, which is important for protein identity confirmation in subsequent Western Blot analysis (Begum et al., 2022). Figure 4.1 shows the SDS-PAGE results from

fractions obtained by the purification process. The purification produced 1 x 10^3 mg L^{-1} (1 µg/µL) of purified recombinant protein per cell culture. From *E. coli* BL21 (DE3) containing pET-32b/HrpN (post-induction with an IPTG) sample, L1-L3 containing a mixture of proteins that producing multiple bands as L1 has total proteins with different sizes, L2 has insoluble proteins that clump together before cell lysis and centrifugation, and L3 has soluble proteins after protein solubilization, including HrpN. L4-L8 has the purified recombinant HrpN protein with differ in protein content from Ni-NTA His-tag purification which resulted in a single band of 30 kDa. A study on recombinant flounder growth hormone protein, where the protein was first expressed as inclusion bodies as HrpN, got similar band patterns. In this study, the protein was solubilized first before going through the same purification methods like HrpN (Choi et al., 2018). There are smearing on the gel. Overloaded samples caused proteins with high concentrations to spread out and smear on the gel. Sample with concentrations that fit the suitable range for the gel type and size can reduce smearing effects (Lee et al., 2021).

In Figure 4.2, the Western Blot from the *E. coli* BL21 (DE3) strain containing pET-32b/HrpN (post-induction with IPTG) verified the appearance of a purified recombinant HrpN protein band with 30 kDa in molecular weight as the protein with the His-tag sequence showed reactivity with the mouse anti-His antibody due to its specificity with the histidine residues available in the His-tag sequence. This result fits the expected size of the purified HrpN in the past literature (N. A. Bakar, 2018). In another study, anti-His monoclonal antibody recognised purified recombinant polygalacturonase inhibiting proteins with

His-tag only (C. Zhang et al., 2016). Notably, both positive and negative controls did not show any bands. The band did not visible in the positive control lane shows that IPTG is necessary for recombinant HrpN protein expression. Past works have explained that the pET-32b vector requires IPTG to induce expression of the cloned gene. The lac repressor is repressed to allow RNA polymerase to bind to the T7 promoter upon IPTG addition. This binding starts the transcription of the gene of interest in the system (Amini et al., 2018). In addition, the negative control, which did not contain the HrpN gene, did not have any bands because His-tag ensured the antibody did not bind or cross-react with other endogenous proteins in the *E. coli* BL21 (DE3) strain.

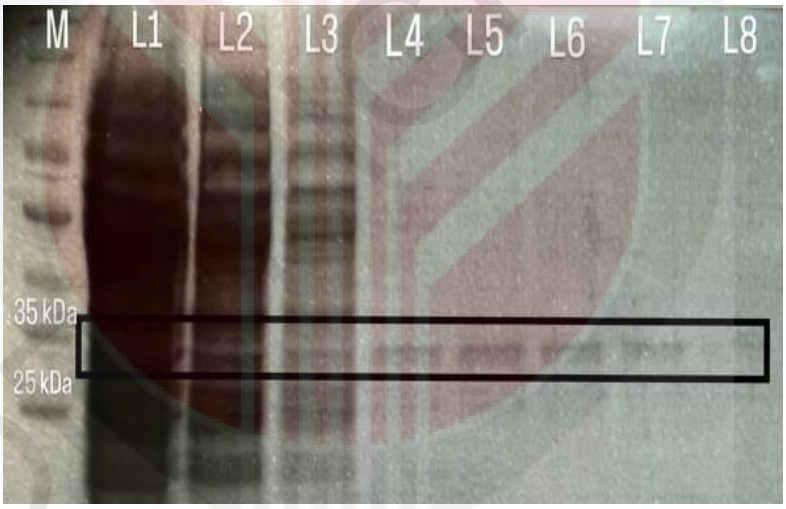

Figure 4.1: Pure recombinant HrpN protein at the expected molecular weight of 30 kDa from SDS-PAGE. M: molecular weight protein marker (range: 10 to 260 kDa); L1: total protein from *E. coli* BL21 (DE3) harbouring pET-32b/HrpN post IPTG-induction; L2: precipitated proteins; 3: supernatant after precipitation; L4-8: eluted protein (fraction 1, 2, 3, 4, 5).

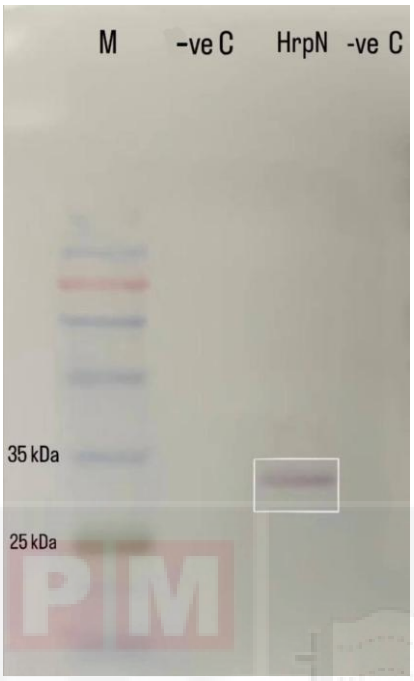

Figure 4.2: Pure recombinant HrpN protein from *E. coli* BL21 (DE3) harbouring pET-32b/HrpN with a molecular weight of 30 kDa reacted with the mouse anti-His antibody in Western Blot. M: molecular weight protein marker (range: 10-260 kDa); +ve C: *E. coli* BL21 (DE3) harbouring pET32b-hrpN without induction with IPTG (negative); HrpN: purified recombinant protein HrpN from *E. coli* BL21 (DE3) harbouring pET32b-hrpN with IPTG induction; -ve C: *E. coli* BL21 (DE3) harbouring pET-32b (negative control).

4.3 Optimization of CNP and HrpN-encapsulated Chitosan Nanoparticles (CNP-HrpN) synthesis

The ionic gelation method was able to form nanoparticles with encapsulated HrpN by maintaining the pH throughout the synthesis process which included CS, HrpN, and TPP. This step was important to make sure an efficient HrpN encapsulation in nanoparticles. CS has a positive charge in an acidic environment because around 90% of deacetylated primary amine groups with a pKa of around 6.5 undergo protonation at pH 5 (Sirviö et al., 2021). HrpN carries a net negative charge at pH 5 as protein becomes negatively charged in an environment with a pH slightly higher than its isoelectric point (pI), which

is 4.56. Acidic residues like aspartic acid and glutamic acids in the protein structure lose their proton because there are more hydroxide ions (OH^-) than hydrogen ions (H^+) in the environment (R. Li et al., 2021; Tokmakov et al., 2021). The positively charged CS can form electrostatic interactions with negatively charged HrpN at an optimal pH. The strong interaction assists the HrpN encapsulation within the CS structure.

A few parameters were optimized to scale up CNP production up to 10 mL for encapsulating HrpN. This crosslinking process was executed at a ten-fold higher volume than typically reported before by Kuen et al. (2020). The volumes of 6 mL for CS and 2.5 mL of TPP were chosen based on from previous work where 600 µL of CS and 250 µL of TPP managed to produce the smallest and lowest PDI nanoparticles for HrpN encapsulation in small-scale (Sabrina Wahid et al., 2021). Varying only one parameter (CS or TPP volumes) at a time enables the study of the effect of the CS or TPP volume on CNP formation in terms of PSD and PDI. In this way, any changes in nanoparticle properties are due to one specific factor and not affected by another parameter. Optimal CS and TPP concentrations and mixing conditions were maintained to make sure the ionic gelation method is reproducible.

As shown in Table 4.1 and Figure 4.3, the smallest nanoparticles, 66.27 ± 1.77 nm, with the lowest PDI of 0.189 ± 0.027, came from a CS: TPP volume ratio of 2.4:1. The homogenously distributed CNP had a PSD below 100 nm. This ratio fits with an earlier study on encapsulating chlorogenic acid and HrpS in similar nanoparticles, where 2.4:1 was the best CS: TPP volume ratio (Rajan

et al., 2019; Sabrina Wahid et al., 2021). Empty nanoparticles are preferred to be below 100 nm before the encapsulation process as encapsulating any active compounds within them will usually increase the particle size above 100 nm (Hoang, Thanh, et al., 2022). Smaller nanoparticles can penetrate various plant cell barriers depending on their size: less than 10 nm for cell walls, up to 40 nm for plasmodesmata, around 1 nm for aquaporins, and up to 1 µm through endocytosis (Gao et al., 2023a).

The effect of various CS volumes on a fixed 2.5 mL of TPP volume were also described. In the absence of CS, TPP was in the form of microaggregates, where the PSD of TPP alone is extremely large at 2239.14 ± 143.81 nm with a PDI of 0.342 ± 0.047. A PDI value greater than 0.300 shows that the particle lacks uniformity, which might contribute to the low performance and stability of the nanoparticles as well as their interaction with biological systems (Rajan et al., 2019). Addition of 1.5 mL of CS gave a significant reduction ($p < 0.001$) in particle size from above 1000 nm to 652.70 ± 39.95 nm. The introduction of CS starts CNP formation through electrostatic interactions with negatively charged TPP (Lima Iida et al., 2020). However, due to the low volume of CS, insufficient bonding between CS and TPP make the particles relatively large and polydisperse. There is a clear decrease in PSD from 200.02 ± 5.89 nm (at 3.0 mL of CS) to 67.65 ± 2.91 nm (at 6.0 mL of CS). PDI values also decreased significantly ($p = 0.0001$) from 0.379 ± 0.035 at 1.5 mL of CS to 0.215 ± 0.024 at 6.0 mL of CS. Increasing CS volume increased the number of available crosslinking sites, which initiate the bonding with TPP, leading to smaller and more uniform nanoparticles, as shown by the PDI value below 0.250. Further

addition of 7.5 mL CS resulted in slight yet insignificant changes in PSD ($p = 0.9999$) and PDI ($p = 0.5680$) to 71.24 ± 0.88 nm and 0.178 ± 0.013, respectively. The amount of CS beyond its optimal volume may lead to potential excess CS that cannot bond with TPP but remains free in suspension.

Next, optimal TPP volume was figured out while keeping CS volume at 6 mL. CS alone had a PSD of 626.21 ± 18.06 nm and a PDI of 0.301 ± 0.030. Putting 0.5 mL of TPP into the mixture lowered the PSD and PDI significantly ($p < 0.0001$) to 162.89 ± 3.83 nm and 0.223 ± 0.013, respectively. The crosslinking process began to occur after the addition of TPP, but at lower TPP volumes, PSD and PDI values stayed high because there were insufficient phosphate groups in TPP structure to bond with the amine groups in the CS backbone (Rajan et al., 2019). Increasing the TPP volume from 1.0 mL to 2.5 mL gradually lessened the PSD and PDI values. From the observation, 2.5 mL of TPP produced nanoparticles with the smallest and uniform particle. This finding was also consistent with a prior study that reported that the higher the amount of anionic phosphate groups available, the more the cross-link can occur with the protonated amine groups within the CS chain in water (Lusiana et al., 2017). Strong electrostatic forces between CS and TPP form a dense network of ionic bonds, which keeps CNP under 100 nm in size. The physical crosslinking also creates steric effects that strengthen internal bonds within each nanoparticle and reduce inter-molecular forces between particles, preventing them from growing larger. The bond lengthening reduces vibrational frequencies, which helps keep the nanoparticles stable and small (Correa et al., 2021). However, a previous study interpreted that excess TPP

beyond its optimal level might lead to over-crosslinking or aggregation of multi-particle rather than expansion of singular particle (Mikušová et al., 2021). This fits with the findings in this study where PSD increased to 113.96 ± 0.62 nm and 129.59 ± 4.32 nm at 3.0 mL of TPP and 4.0 mL of TPP, respectively. The PDI has maintained below 0.300 since the addition of 0.5 mL of TPP. It shows that while the PSD is changing, the nanoparticle sizes are still homogenously distributed. A study on the large-scale production of hydrophobically modified chitosan nanoparticles for encapsulating protocatechuic acid (PCA) had comparable findings (Kuen et al., 2020).

A mixture of 6 mL of CS with 2.5 mL of TPP (2.4:1 volume ratio of CS:TPP) was the best formulation to synthesis small and homogenously-distributed nanoparticles with a PSD of 66.27 ± 1.77 nm and a PDI of 0.189 ± 0.027. This formulation will be used to encapsulate HrpN to make sure high encapsulation efficiency and sustained release for its delivery into plants.

Table 4.1: Particle size distribution (PSD) and polydispersity index (PDI) values for chitosan nanoparticles (CNP) at different chitosan (CS) and sodium tripolyphosphate (TPP) volumes. Statistical analysis using one-way ANOVA and Tukey's post-hoc test at a significance level of $p<0.05$ was done. Columns with distinct letters described a significant difference at $p<0.05$ whereas those with the same letter showed no significant difference.

Volume (mL)		Particle Size Distribution (d.nm ± s.d.)	Polydispersity Index (± s.d.)
TPP	**CS**		
2.5	0.0	2239.14 ± 143.81^{a}	0.342 ± 0.047^{a}
	1.5	652.70 ± 39.95^{b}	0.379 ± 0.035^{a}
	3.0	200.02 ± 5.89^{c}	0.221 ± 0.003^{b}
	4.5	129.69 ± 1.81^{c}	0.223 ± 0.015^{b}
	6.0	67.65 ± 2.91^{c}	0.215 ± 0.024^{b}
	7.5	71.24 ± 0.88^{c}	0.178 ± 0.013^{b}
CS	**TPP**		
6	0.0	626.21 ± 18.06^{a}	0.301± 0.039^{a}
	0.5	162.89 ± 3.83^{b}	0.223± 0.013^{b}
	1.0	80.68 ± 0.75^{c}	0.182± 0.015^{b}
	1.5	76.88 ± 0.79^{c}	0.196± 0.012^{b}
	2.0	73.59 ± 0.94^{c}	0.209± 0.030^{b}
	2.5	66.27 ± 1.77^{c}	0.189± 0.027^{b}
	3.0	113.96 ± 0.62^{d}	0.218± 0.013^{b}
	3.5	117.03 ± 0.95^{d}	0.185±0.002^{b}
	4.0	129.59 ± 4.32^{d}	0.236± 0.015^{b}

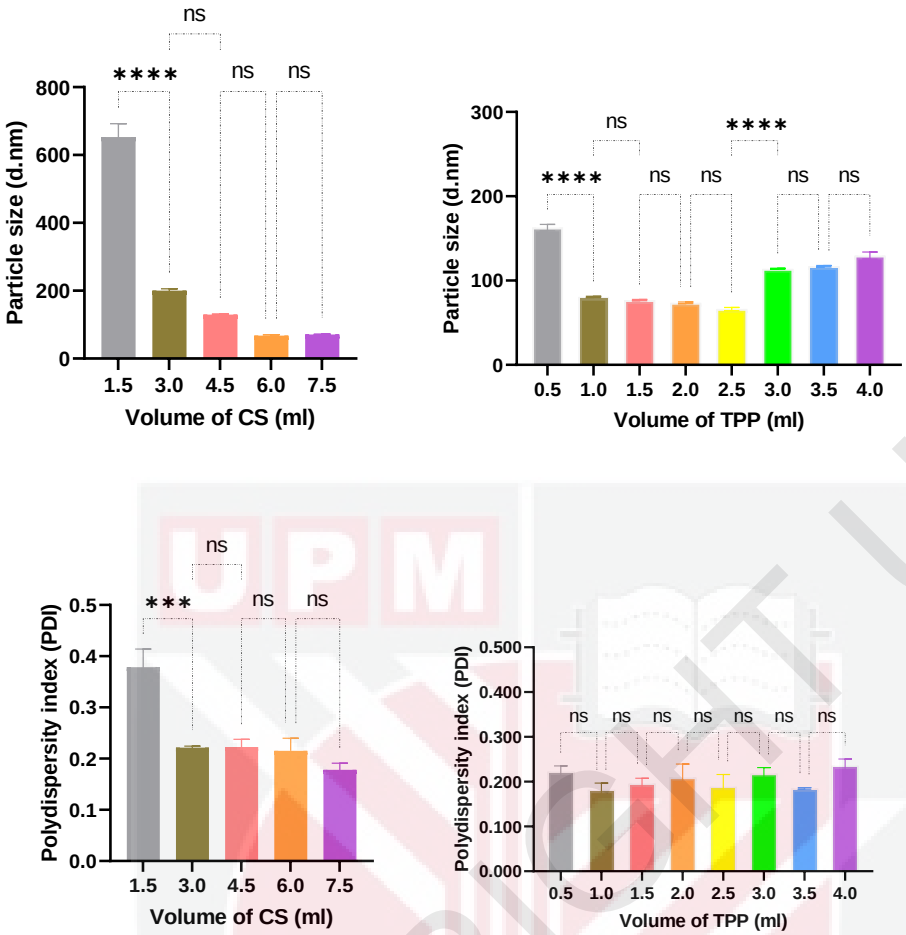

Figure 4.3: Effect of various chitosan (CS) and sodium tripolyphosphate (TPP) volumes on the particle size distribution (top) and polydispersity index (bottom) of chitosan nanoparticles (CNP). Different volumes of CS and TPP were added to 2.5 mL of TPP and 6.0 mL of CS, respectively. The three replicates were simplified as mean ± SD. Statistical analysis using a one-way ANOVA and Tukey's post hoc test was done using GraphPad Prism 9. Significance was described by $p < 0.05$ (*). The * symbol showed a significant difference in PSD and PDI whereas 'ns' had no significant difference when compared to the PSD and PDI of preceding CS and TPP volume.

4.4 Synthesis of HrpN-encapsulated chitosan nanoparticles (CNP-HrpN)

Next, different concentrations of HrpN were encapsulated within the CNP to see its influence on nanoparticle formation. Figure 4.4 shows the schematic possibility of hairpin encapsulation in CNP. Any bioactive materials can be in the core of the CS and TPP nanospheres or attached to their surfaces (Detsi et al., 2020). Encapsulating HrpN within the core of CNP is more suitable than surface binding to provide better protection against physiological environmental factors such as pH changes, temperatures, enzymatic activity, osmotic pressure, humidity, and mechanical forces. In the vast majority, encapsulation keeps the proteins stable and shields it from denaturation during their sustained release in agricultural applications (Bamburowicz-Klimkowska et al., 2019; García-Carrasco et al., 2023).

Figure 4.4: Schematic representation of possible nanoparticle system made of HrpN as hairpin protein, chitosan (CS) and sodium tripolyphosphate (TPP). The HrpN can be encapsulated inside the sphere formed by CS and TPP.

From Table 4.2 and Figure 4.5, the size of CNP-HrpN rose ($p < 0.0001$) by 30% (101.80 ± 1.14 nm) in comparison to empty CNP (78.25 ± 0.08 nm). It

shows that HrpN was trapped successfully inside the core of the nanosphere. Based on prior studies, when gentamicin is encapsulated within the blank CS-TPP matrix, it causes the particle diameter to expand due to swelling when the drug displaces space within the CNP (Buyuk et al., 2020; Simpson et al., 2024). While molecules can be loaded into CNP through either active (incorporation) or passive (incubation) ways, HrpN was entrapped in the CNP using the incorporation method to get high encapsulation efficiency and homogenous distribution. The agent is initially mixed with the CS solution in this method. Then, agent-loaded CNP forms directly once TPP is added to the mixture (Alasas et al., 2024). HrpN encapsulation likely happened when the carbonyl and hydroxyl groups of HrpN formed hydrogen bonds with the amino groups of CS. The negatively charged phosphate groups in TPP interact with the positively charged amine groups of CS. These interactions help trap and stabilise HrpN in the nanoparticles via strong ionic bonds.

Adding HrpN concentrations from 0.02 mg/mL to 0.04 mg/mL led to synthesis of bigger nanoparticles (106.34 ± 2.05 nm). As the concentration of HrpN increases, more molecules were present to bind with CS, leaving fewer CS to form ionic interactions with TPP. This fits with previous findings where increasing deferoxamine mesylate concentrations produced larger CNP due to the weakening of ionic interactions between TPP and CS (Lazaridou et al., 2020). The PSD had insignificant changes after the concentration of HrpN was increased above 0.04 mg/mL ($p = 0.1364$). The nanoparticle system was nearing its saturation point as it had already encapsulated as much HrpN as possible. Additional ingredient loading beyond the optimal concentration point

has only a minor impact on particle size (Omer et al., 2021). Figure 4.5 also shows that the CNP-HrpN size falls within the range of 100-200 nm regardless of any HrpN concentrations used. Many studies implement particles in this size range because they work best as nanocarriers in agricultural applications. Particles below 200 nm in size can penetrate plant stomata via apoplast pathway to the xylem and phloem vessels. Cellular uptake to tissues and organs of these nanoparticles occurred efficiently in sustained release manner without using much cellular energy (Esquivel et al., 2015; Hoang, Le Thanh, et al., 2022; Picchi et al., 2021). The PDI varies insignificantly, but the nanoparticle systems remain homogenously distributed across all HrpN concentrations used. The PDI of the population of both empty CNP and CNP with encapsulated was sometimes influenced by various factors such as surface area and free energy in the system, as well as forces of attraction or repulsion between particles (Hassan et al., 2018; Simpson et al., 2024).

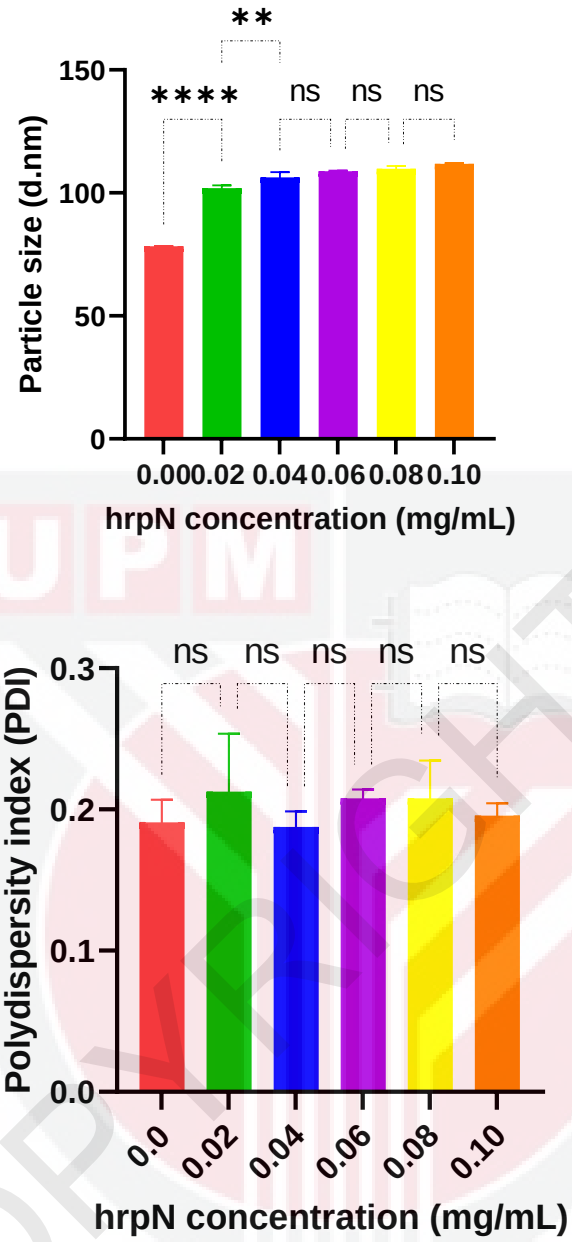

Figure 4.5: Effect of different HrpN concentration on the particle size distribution (PSD) and polydispersity index (PDI) of HrpN-encapsulated chitosan nanoparticles (CNP-HrpN) from dynamic light scattering analysis. Mean ± SD was data from three replicates. One-way ANOVA test and Tukey's post-hoc test with a significance level of $p < 0.05$ was done using GraphPad Prism 9. Significance was described by $p<0.05$ when compared to the PSD and PDI of preceding HrpN concentration. The * showed PSD and PDI had significant difference and more * meant higher significance whereas 'ns' indicated no significant difference.**

Table 4.2: Analysis of particle size distribution (PSD), polydispersity index (PDI), encapsulation efficiency (EE) and theoretical HrpN loading of HrpN-encapsulated chitosan nanoparticles (CNP-HrpN) at different HrpN concentrations. One-way ANOVA and Tukey's post hoc test was done at significance level of $p<0.05$. Columns with distinct letters had a significant difference whereas columns with same letter had no significant difference.

HrpN concentration (mg/mL)	Particle size distribution (nm ± sd)	Polydispersity index (± sd)	Encapsulation efficiency (%)	HrpN loading (mg/mL)
0	78.25± 0.08^{a}	0.191± 0.016^{a}	-	-
0.02	101.8± 1.14^{b}	0.213± 0.041^{a}	85.83 ± 3.31^{a}	0.017
0.04	106.34± 2.05^{c}	0.188± 0.011^{a}	81.84 ± 3.43^{a}	0.032
0.06	108.76± 0.31^{d}	0.208±0.006^{a}	62.11 ± 8.31^{b}	0.037
0.08	109.84± 1.15^{d}	0.208± 0.027^{a}	54.55 ± 4.55^{b}	0.044
0.10	111.86± 0.30^{d}	0.195± 0.009^{a}	53.59 ± 5.57^{b}	0.054

4.5 Encapsulation efficiency (EE) of Hrpn in CNP

EE test was used to figure out the best CNP-HrpN system with strong encapsulation potential by quantifying the total amount of HrpN within the CNP carrier relative to the total HrpN utilised for encapsulation by using a UV-VIS spectrophotometer. HrpN at concentrations of 0.02 mg/mL and 0.04 mg/mL was encapsulated more than 80% in nanoparticles carrier, as described in Figure 4.6 and Table 4.2. As stated before, a carrier system can be considered a good way to deliver a material in maximum amount and efficiency when it has over 80% of its EE value (Muhaimin et al., 2020). There is a pattern showing that lower HrpN concentrations have higher EE. The EE dropped significantly ($p = 0.0078$) to 62.11% when the concentration of HrpN was

increased to 0.06 mg/mL. As the concentration of protein increases, the number of binding sites present in the CS backbone reduces. When the carrier cannot fit all the protein molecules, this leads to saturation and a decrease in EE. Findings from previous works on enzymes were similar to what was observed in HrpN. Steric interaction between protein structure and viscosity of the solution might be another reason that makes it difficult for the protein to accommodate into the CNP structure. A further increase in protein concentration does not affect the particle size (Pirozzi et al., 2023).

The EE is between 50% and 60% when the HrpN concentration used were more than 0.04 mg/mL. It means that even though the EE decreases, at least half of the proteinaceous elicitor at these concentrations has been encapsulated successfully in CNP. Negatively charged HrpN molecules were strongly attracted to positively charged CS molecules because proteins with a low pI encapsulate better in a carrier under pH conditions higher than their pI value. This electrostatic attraction causes loading ingredient to gather around the glucosamine units of CS, which are deacetylated and have amine groups prior to TPP addition (Marques Gonçalves et al., 2023). As an instance, ovalbumin (OVA) and bovine serum albumin (BSA) were similar in size. Yet, OVA gave off stronger negative surface charge as it had a lower pI than BSA. OVA had a higher EE than BSA because it had a better attraction to positively charged CS (Koppolu et al., 2014).

From the calculation of theoretical protein loading, 0.04 mg/mL is the best HrpN concentration that can be used for CNP-HrpN formation, compared to 0.02 mg/mL. EE is greater for nanoparticle samples with 0.02 mg/mL HrpN than for those with 0.04 mg/mL HrpN. Yet, the amount of protein loaded is two-fold lower than CNP with 0.04 mg/mL of HrpN. The higher protein loading means that more protein amount is available in the system to make the treatment more effective. To get a better understanding on HrpN encapsulation, an *in vitro* HrpN release study is necessary. From these findings, the mix of CS to TPP and the HrpN concentration affect the physical properties of CNP-HrpN. Tailoring nanoparticles can make them work much better in biological systems.

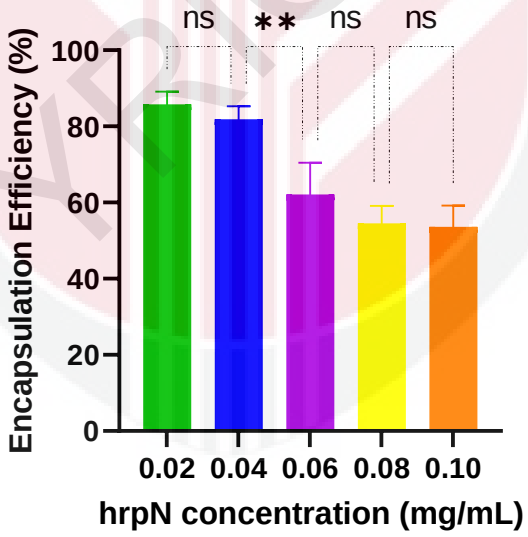

Figure 4.6: Effect of HrpN concentration on the encapsulation efficiency (EE) of HrpN within chitosan nanoparticles (CNP). The EE decreased with an increase in HrpN concentration. The three replicates were simplified as mean ± SD. Statistical analysis using a one-way ANOVA and Tukey's post hoc test was done using GraphPad Prism 9. Significance was described by p < 0.05 (*). The * symbol showed a significant difference in PSD and PDI whereas 'ns' had no significant difference when compared to the PSD and PDI of preceding TPP volume.

4.6 Morphological analysis of CNP and CNP-HrpN by field emission-scanning electron microscopy (FE-SEM) and high resolution-transmission electron microscopy (HR-TEM)

FE-SEM and HR-TEM studied the morphology of both CNP and CNP-HrpN. FESEM examined external surface topology as well as particle size. HR-TEM looked out for the internal structure and the particle dispersion at the atomic scale (Venkateshaiah et al., 2020). FE-SEM images have CNP with a mean size of 32.49 ± 3.84 nm in Figure 4.7(a). These sphere and smooth nanoparticles with a diameter between 20 and 40 nm were spreading evenly. This is in accordance with the theory that CNP usually have a spherical shape as a carrier in most agricultural studies (Hoang, Thanh, et al., 2022). Spherical-shaped nanoparticles are easily taken up by plant cells because they move easily in plant systems and are less toxic than nanoparticles with other shapes. Their smooth surface reduces physical injury to the tissues during delivery (Balusamy et al., 2023). Non-spherical nanoparticles tend to accumulate in irregular way, causing localized toxicity. Besides, spherical shape usually exists in stable dispersion and lower surface energy in aqueous environment. This reduces the chance for aggregation that can lead to physical blockages and reactive oxygen species in host vascular systems. (Gao et al., 2023b; Muzammil et al., 2023). In Figure 4.7, FE-SEM images show CNP-HrpN nanoparticles ranging from 20 to 60 nm in size, with spherical shapes at 0.04 (b) mg/mL and 0.10 mg/mL (c) of HrpN concentrations. The nanoparticle clusters are evenly spaced and look uniform at lower protein concentration. In contrast, the nanoparticles tend to aggregate due to viscosity at higher concentrations (Zarzar et al., 2023). Dark and dense inner morphology of CNP-HrpN was seen in Figure 4(d) of HR-TEM images. This means that only

a few electrons were able to pass through due to HrpN encapsulation. The particle size of CNP-HrpN in DLS, FE-SEM, and HR-TEM have different readings for some reasons. In a liquid, DLS measures both hydrodynamic size of particles and their surrounding solvent layer. Conversely, HR-TEM and FE-SEM take pictures of particles when they were dry. Smaller particles resulted from the solvent evaporation during sample preparation. In addition, a conductive coating applied during FE-SEM sample preparation improves conductivity and image quality but can also increase the measured size of the sample. Not to mention, particle clustering can also affect size readings because DLS detects larger hydrodynamic sizes in the presence of clusters. In contrast, HR-TEM and FE-SEM measure single particles rather than in their aggregate form after sample preparation (Jia et al., 2023). The width of the curve in a normal distribution shows how much the particle sizes vary. A narrow curve describes the sample is more homogenous with less size variation, vice versa, a wider curve shows a bigger range of sizes. CNP seen under FE-SEM (a) had a narrow curve which indicates that the particles are homogenous in size (mean of 32.493 ± 3.838 nm). In contrast, the curve for CNP-HrpN (0.04 mg/mL) (b) is broader than CNP which indicates greater differences in particle size (mean of 39.40 ± 4.88 nm) after HrpN encapsulation. Encapsulation of HrpN at higher concentrations (0.10 mg/mL) (c), causing a broadest range of particle sizes (38.98 ± 6.53 nm), as shown by the widest distributions. The sample might contain two populations of particles which come from aggregation. These images from two different microscopy approaches help us to view the clearer morphology and size distribution of synthesised nanoparticles.

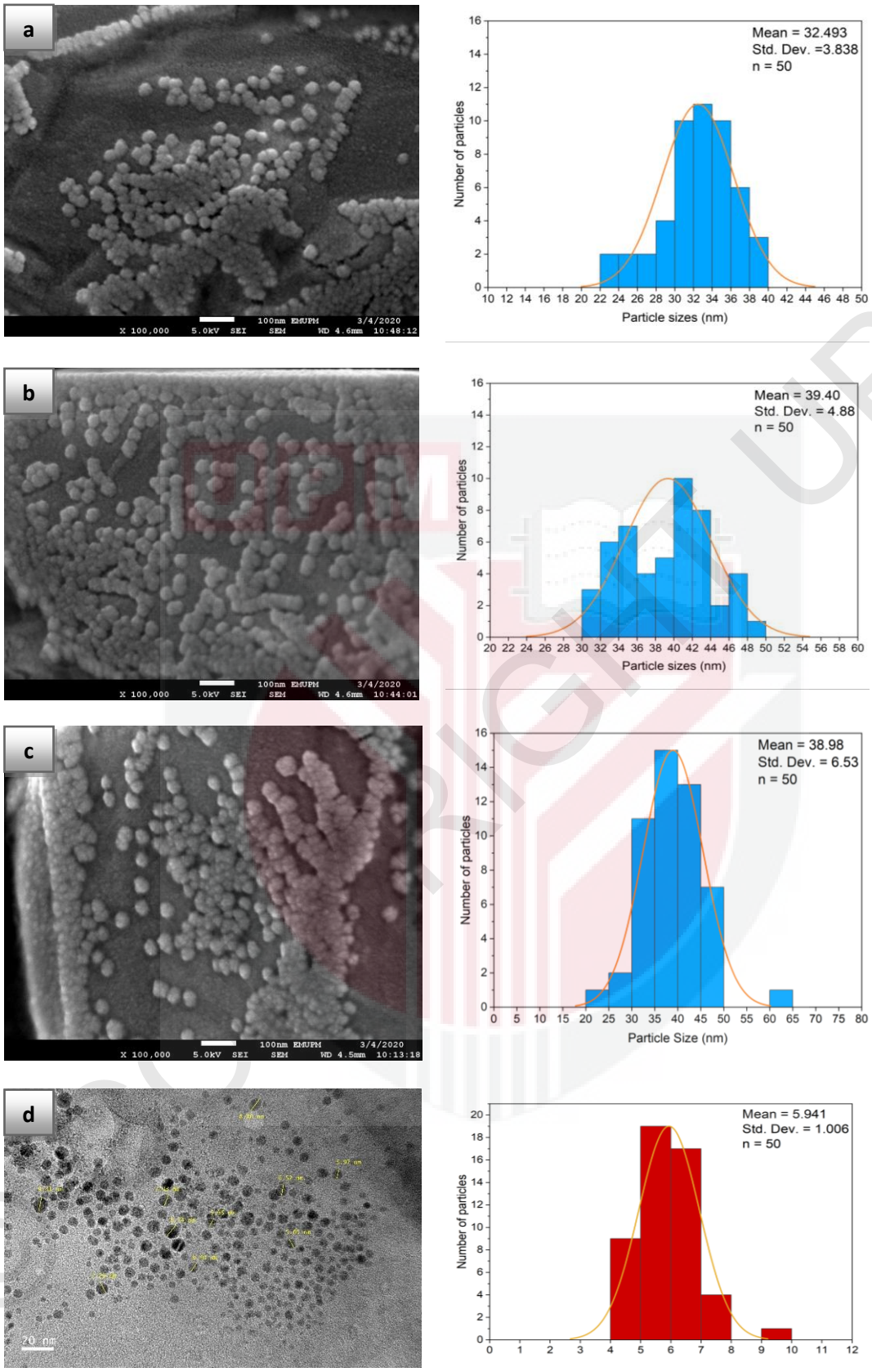

Figure 4.7: Morphology (left) and normal distribution (right) from field-emission scanning electron microscopy - (a) CNP, CNP-HrpN prepared at HrpN concentrations; (b) 0.04 mg/ml, (c) 0.10 mg/ml, and (d) high-

resolution transmission electron microscopy of CNP-HrpN prepared at HrpN concentration 0.04 mg/ml.

4.7 Functional group analysis of CNP and CNP-HrpN via fourier transform infrared (FTIR) spectroscopy

Fourier transform infrared (FTIR) spectroscopy was used to figure out different chemical composition in CNP and CNP-HrpN structures. These groups acting like fingerprints for these compounds. Transmittance from CS, TPP, CNP, HrpN, and CNP-HrpN samples are shown in Figure 4.8 and Table 4.3. The shifts or missing peaks tell the interactions between the carrier and HrpN. The explanation for each transmittance came from Virtual Textbook of Organic Chemistry by William Reusch (Reusch, 1999). The CS spectrum displays a broad peak ranging from 3200 cm^{-1} to 3500 cm^{-1}, with the most noticeable peak occurring at 3357 cm^{-1}.The peak was produced by stretching vibrations from hydrogen bonding between O−H (hydroxyl group) and primary amine groups. Stretching vibrations of C=O, bending vibrations of N-H, and stretching vibrations of C-N at peaks 1650 cm^{-1}, 1585 cm^{-1}, and 1375 cm^{-1}, respectively, corresponding to the functional groups of amides I, amide II, and amide III. In the TPP spectrum, two absorption peaks of phosphate functional groups were identified at 1133 cm^{-1} and 887 cm^{-1} within the range of 1220 cm^{-1} – 1080 cm^{-1} for stretching vibrations of P=O and the range of 850 cm^{-1} – 900 cm^{-1} for stretching vibrations of P-O-P.

When the peaks between 3200 cm^{-1} - 3500 cm^{-1} became wider and the peak at 3357 cm^{-1} of CS shifted to 3304 cm^{-1} at CNP spectrum, it suggests that stronger hydrogen bond interactions have occurred between CS and TPP

molecules during CNP formation. The peak at 1133 cm^{-1} in the TPP spectrum showing vibrations of P=O stretching appears at 1056 cm^{-1} in the CNP spectrum because of ionic interactions between amino groups of CS and phosphate groups of TPP. Electrostatic interaction between the amino group of CS and the phosphate group of TPP accompanied by hydrogen bonding via C=O stretching, N−H carbonyl bending, and C-N stretching from amide I, amide II, and amide III, respectively.

The peaks of amide functional groups in HrpN were compared with those in the CNP-HrpN spectrum to confirm the encapsulation of HrpN. In past studies, the amide region was the backbone to the core structure of proteins. Among these regions, amide I is particularly sensitive to changes in protein structure originating from vibrations in the C=O bond of the amide group. Amide II and III were bending in the N-H bond and stretching in the C-N bond, respectively. These vibrations give information on the protein structure (Ji et al., 2020). After HrpN was encapsulated in CNP, the CNP-HrpN spectrum no longer showed sharp peaks related to the movement of amide I, II, and III groups seen in both HrpN and CS spectra. HrpN has now become part of CNP structure following intra- and inter-molecular bonds formation between HrpN and CNP. The specific 955 cm-1 peak in the HrpN spectrum that is related to C-H bond vibrations help us to recognise HrpN from other compounds. It shifted noticeably to a peak of 944 cm-1 in the CNP-HrpN spectrum. The interaction of HrpN and the encapsulating material leads to shifts in vibrational frequencies of C-H bonds in HrpN. CNP-HrpN are facing changes that can be seen in other protein-nanoparticle systems like BSA. For example, the broader

peak in the hydroxyl and amine regions of the CS spectrum after interacting with TPP is consistent with similar observations in other CS-based nanoparticle systems which indicates stronger interactions of a more complex network. Protein encapsulation in nanoparticles also leads to shifts, broadening, or even the disappearance of amide peaks (Alhazmi, 2019). FTIR showed changes in the HrpN structure or its molecular interactions with the encapsulating material as well as confirming HrpN encapsulation within carrier matrix.

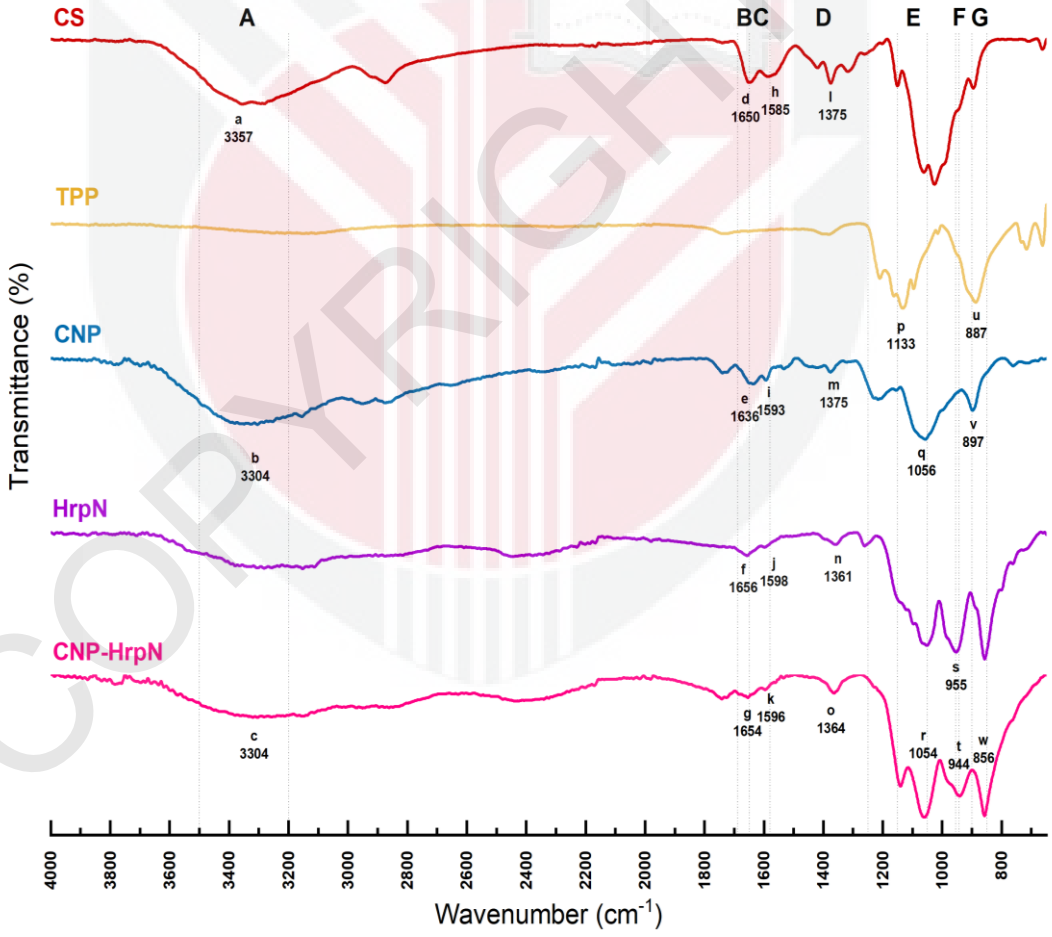

Figure 4.8: Spectra of fourier transform infrared (FTIR) spectroscopy. The FTIR samples are chitosan (CS), sodium tripolyphosphate (TPP), chitosan nanoparticles (CNP), HrpN, and HrpN-encapsulated chitosan nanoparticles (CNP-HrpN). Essential functional groups were labelled with letters.

Table 4.3: Functional groups and their percentages of transmittance in CS, TPP, CNP, HrpN, and CNP-HrpN through fourier transform infrared (FTIR) spectroscopy.

Functional group (range)	Peak	Sample	Wavenumber (cm^{-1})	Transmittance (%)	Label
(A)	Broad	CS	3357	77.97	a
3200 cm^{-1} – 3500 cm^{-1}	Broad	CNP	3304	89.01	b
-OH (hydroxyl) and -NH_2 (amine) stretching vibration	Broad	CNP-HrpN	3304	93.33	c
(B)	Strong	CS	1650	84.68	d
1650 cm^{-1} – 1690 cm^{-1}	Strong	CNP	1636	95.35	e
	Strong	HrpN	1656	93.59	f
C=O stretching, amide I	Strong	CNP-HrpN	1654	96.43	g
(C)	Medium	CS	1585	86.56	h
1580 cm^{-1} – 1650 cm^{-1}	Medium	CNP	1593	95.93	i
	Medium	HrpN	1598	94.91	j
N-H bending, amide II	Medium	CNP-HrpN	1596	97.69	k
(D)	Medium	CS	1375	84.43	l
1250 cm^{-1} – 1020 cm^{-1}	Medium	CNP	1376	97.19	m
	Medium	HrpN	1361	95.34	n
C-N stretching, amide III	Medium	CNP-HrpN	1364	97.12	o

Table 4.3: Continued

(E)	Medium	TPP	1133	67.17	p
1050 cm^{-1} – 1150 cm^{-1}	Medium	CNP	1056	86.69	q
P=O stretching, phosphate	Medium	CNP-HrpN	1054	77.78	r
(F)	Strong	HrpN	955	93.00	s
880 cm-1 – 995 cm-1 C-H bending, alkene	Medium	CNP-HrpN	944	95.00	t
(G)	Strong	TPP	897	70.71	u
850 cm^{-1} – 900 cm^{-1}	Strong	CNP	897	91.23	v
P-O-P asymmetrical stretching vibration, phosphate	Strong	CNP-HrpN	856	85.09	w

4.8 *In vitro* release profiles of HrpN from CNP

An *in vitro* release experiment studied how HrpN was released from CNP to mimic the *in vivo* biological systems conditions during real applications. The release of HrpN was tested in PBS with a pH of 7.4 for 72 hours to stimulate physiological pH. The choice of PBS was made because enzymes and transporters in plant cells work best at this pH to perform proper biochemical reactions (Pecherina et al., 2021). Figure 4.9 shows that almost 99% of HrpN was released from CNP in 3 days in biphasic release pattern. Firstly, CNP-

HrpN released 50% of HrpN within 6 hours in an initial rapid burst. Next, plateau release by 72 hours was achieved in a slower and sustained release in the second phase. Several works have shown a common biphasic release pattern for protein release. By that means, CNP provides a condition for sustained release of protein biomolecules which is beneficial to obtain both immediate and sustained effects in delivery application (Sedyakina et al., 2020). Mechanisms like polymer swelling, degradation, erosion, and cargo diffusion can drive the protein out through the polymer network. These processes give effect to both ways and rates of protein release. Polymer swelling can increase the porosity of the CNP which assists in quicker diffusion. Degradation and erosion of the polymer network help the gradual release of the encapsulated ingredient (Zaman et al., 2022).

HrpN has a similar two-phase release pattern to the common release behavior of other proteins encapsulated in CNP like surface desorption and matrix diffusion. Loosely bound HrpN proteins to the nanoparticle surface are quickly released when exposed to the release medium. This mechanism is helpful for applications that need a fast effect as it allows for the release of a small portion of the encapsulated protein. After the initial burst, HrpN is gradually and steadily released as it diffuses through the dense cross-linked structure of the CNP. Protein that is more securely entrapped in the internal structure has slow movement to ensure a prolonged release over an extended period. A review explained that the structural properties of CNP such as particle size, cross-linking density, and porosity, affect the release kinetics of encapsulated cargo. As an example, a highly cross-linked structure may slow down the

release due to the complicated diffusion pathway. Meanwhile, nanoparticle with high porosity can speed up the release of the protein. Smaller CNP sizes with their higher surface area-to-volume ratio tend to cause an initial rapid release because a larger portion of the encapsulated protein is adsorbed on the surface and readily available for immediate release when exposed to the release medium (Herdiana et al., 2022). CNP can work to deliver and release HrpN in a sustained manner as long as factors like nanoparticle size, surface characteristics, polymer composition, as well as environmental conditions are in an optimal condition.

Table 4.3: *In vitro* release of HrpN from CNP. The release percentages and concentrations of HrpN after 72 hours.

Concentration of HrpN used for encapsulation (mg/mL)	Concentration of HrpN loaded in CNP (mg/mL)	Percentage of HrpN release after 72 hours (%)	Concentration of HrpN release after 72 hours (mg/mL)
0.02	0.017	98.79 ± 1.15	0.017
0.04	0.032	99.56 ± 3.96	0.032
0.06	0.037	99.04 ± 1.85	0.037
0.08	0.044	99.18 ± 1.40	0.044
0.10	0.054	99.59 ± 1.14	0.054

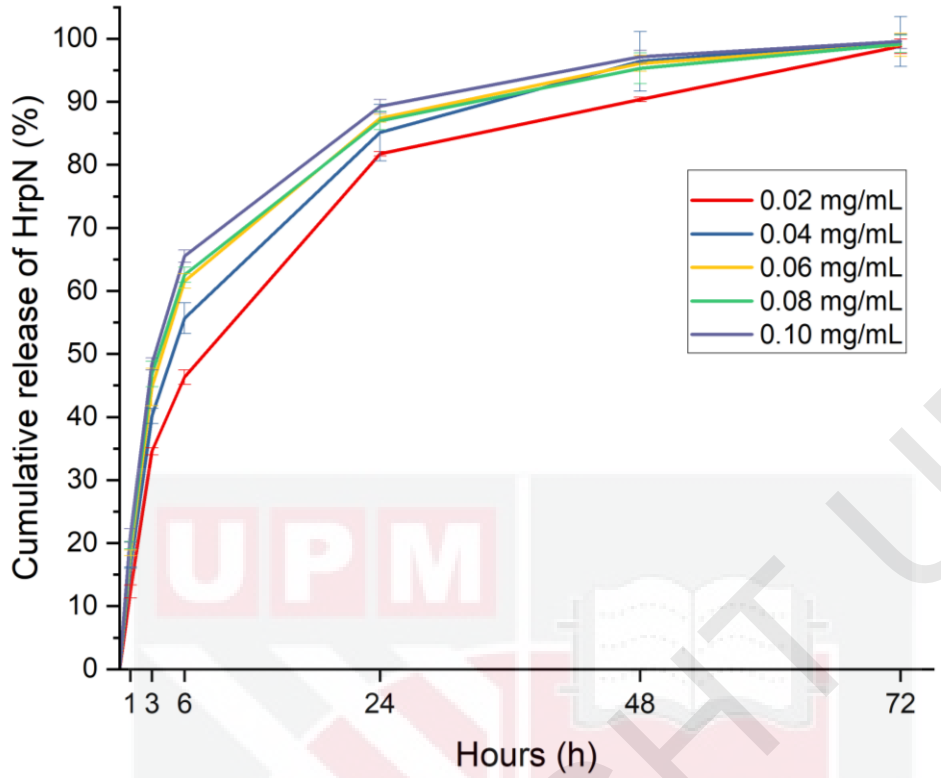

Figure 4.9: Cumulative *in vitro* release profile of encapsulated HrpN from CNP in PBS solution (pH 7.4) over 72-hour period. Replicates were presented as mean ± SD (n=3).

4.9 Release Kinetic Modelling of HrpN from CNP

Five different models like first-order, zero-order, Hixson-Crowell, Korsmeyer-Peppas, and Higuchi, were used in release kinetics study (Sikhondze et al., 2023a). DD Solver software integrated the cumulative percentage of HrpN release data to assess how well each model fit based on correlation factor (R^2), Akaike information criterion (AIC), and model selection criterion (MSC) values. The R^2 describes how well the model tells the data variance. An R^2 higher than 0.95 show a strong fit in linear regression as it means that the model explains the data very well with little left unexplained. AIC finds the right balance between how well a model fits the data and how simple the model is. The data

that has a lower AIC value fits the model well in a simple way. Comparison of different models select the best fit with a MSC value greater than 3 (Concha et al., 2022).

Each CNP-HrpN formulation tested with five different HrpN concentrations shown in Table 4.4 fit well with first-order kinetic model. It indicates a concentration-dependent release mechanism where the rate at which HrpN is released is directly proportional to how much of the protein is still left inside the nanoparticle. This was supported by R^2 higher than 0.950, MSC greater than 3 and the lowest AIC for all CNP-HrpN formulations. Similarly, other studies that follow first-order kinetics show that the release rate of metronidazole was also directly proportional to the amount of metronidazole remaining inside the core of the nanoparticle. Higher initial concentrations create a steeper concentration gradient which speeds up the release rate especially at the beginning. This is a typical behaviour of small molecules and proteins from polymeric carriers (Sikhondze et al., 2023b).

The release of HrpN also fits well with the Korsmeyer-Peppas model. The Korsmeyer-Peppas model uses the *n* value to show how the HrpN is released from its carrier. It tells whether the release happens mainly through diffusion, the relaxation of the polymer, or the breakdown of the polymer through erosion. Values below 0.5 typically indicate Fickian diffusion; values from 0.5 to 0.85 suggest a non-Fickian diffusion, suggesting a mix of diffusion and polymer relaxation (anomalous transport), whereas values over 0.85 show a Case II transport mechanism where polymer chain relaxation has a big impact on the release rate (Hammad Ayaz et al., 2022). HrpN has *n* value below 0.50 and

fits both first-order and Korsmeyer-Peppas kinetic models. This means HrpN is mainly released from CNP by moving through the diffusion of the polymer because of the concentration difference. The rate of release depends on how much HrpN is still inside the carrier. Changes in the polymer have little impact and diffusion is the main factor for sustained kinetics.

In zero-order kinetics, the release rate of a compound stays constant over time, no matter the concentration. This does not work for HrpN because its release rate slows down as the amount of HrpN decreases. So, zero-order kinetics does not accurately describe how HrpN is released from CNP. The Higuchi model then explains compound release from a carrier through diffusion, assuming the carrier stays the same along the process. By that means, the Higuchi model does not fit with the HrpN release mechanisms because CNP-HrpN swells and degrades over time. The Hixson-Crowell model stated that the geometry of the carrier maintains during the compound release. The dissolution only happens in layers parallel to its surface and not in a random manner. As the release of HrpN altered the geometry of the polymeric material, the Hixson-Crowell kinetic model may not work well to describe CNP-HrpN. In contrast, the first-order is good model to show how release depends on the amount of HrpN left inside. At the same time, the Korsmeyer-Peppas model helps explain how the HrpN diffuses out and how factors like CNP relaxation and degradation affect the release over time.

Table 4.4: Mathematical model fit for CNP-HrpN with different HrpN concentrations. The correlation factor (R^2), corrected correlation factor (R^2-adj), Akaike information criterion (AIC), and model selection criterion (MSC) for each model was showed. The mean ± SD (n=3) represents the replicates.

HrpN in CNP (mg/mL)	Model	Equation	Evaluation criteria					
			k	R^2	R^2 adjusted	AIC	MSC	*n*
0.02	Zero- order	$F=k^0 \times t$	1.702	0.234	0.234	52.597	-0.066	-
0.04			1.764	-0.087	-0.087	54.379	-0.416	-
0.06			1.771	-0.428	-0.428	55.430	-0.687	-
0.08			1.768	-0.559	-0.559	55.636	-0.776	-
0.10			1.793	-0.723	-0.723	56.188	-0.877	-
0.02	First-order	$F=100 \times [1- Exp (-k^1 \times t)]$	0.101	0.959	0.959	35.064	2.856	-
0.04			0.142	0.965	0.965	33.722	3.027	-
0.06			0.172	0.966	0.966	32.936	3.062	-
0.08			0.181	0.957	0.957	34.028	2.826	-
0.10			0.197	0.970	0.970	31.891	3.173	-
0.02	Higuchi	$F=k^H \times t^{0.5}$	13.314	0.866	0.866	42.105	1.683	-
0.04			13.973	0.759	0.759	45.328	1.093	-
0.06			14.162	0.626	0.626	47.361	0.657	-
0.08			14.168	0.578	0.578	47.791	0.532	-
0.10			14.424	0.509	0.509	48.651	0.379	-
0.02	Hixson-Crowell	$F=100 \times [1 - (1-k^{HC} \times t)^3]$	0.020	0.873	0.873	41.807	1.733	-
0.04			0.020	0.769	0.769	45.065	1.136	-
0.06			0.021	0.631	0.0631	47.290	0.669	-
0.08			0.021	0.568	0.568	47.919	0.510	-
0.10			0.021	0.503	0.503	48.726	0.367	-

Table 4.4: Continued

0.02	Korsmeyer-Peppas $F = k^{KP} \times t^n$	23.418	0.954	0.943	37.710	2.416	0.350
0.04		28.665	0.940	0.925	39.017	2.145	0.308
0.06		32.537	0.922	0.903	39.955	1.892	0.277
0.08		33.724	0.922	0.903	38.647	1.889	0.267
0.10		35.689	0.913	0.891	40.260	1.778	0.257

4.10 Visualisation of *in vitro* uptake of HrpN from CNP by papaya leaves using fluorescein isothiocyanate (FITC)

The leaf is an ideal entry point for CNP-HrpN application as it makes sure quick absorption while also triggering SAR concurrently. Foliar spraying allows nanoparticles like CNP-HrpN to enter through stomata and the cuticle before activating plant defense pathways and strengthening resistance against future attacks. Foliar delivery offers a direct, efficient, and controlled way to enhance both growth and immunity unlike soil application which faces nutrient loss and environmental interference (Jeon et al., 2022). Fluorescein isothiocyanate (FITC)-tagged chitosan nanoparticles (CNP-HrpN-FITC) were synthesised to visualise *in vitro* uptake of CNP and CNP-HrpN within papaya plant leaves. FITC is a stable and biocompatible fluorescence-emitting molecule that is suitable for *in vivo* localisation in plant study. The potential toxic effects that can disrupt the natural physiological processes of the plant cells is very low (Chandra et al., 2015). The amine groups (-NH2) bond with the isothiocyanate group (R-N=C=S) to attach FITC to the CNP (De Matteis et al., 2022). In this study, protein labelling through chemical conjugation was done before HrpN encapsulation in the CNP. FITC reacts with the primary amine groups on the HrpN backbone to form a covalent amide bond. The pre-encapsulation

fluorescent labelling step make sure that the fluorescent tag is securely attached to the protein. This step allows for consistent fluorescence signals while tracking protein accumulation inside the cells (Chaganti et al., 2018; Sornay et al., 2022).

Qualitative fluorescence microscopy observations started at hour 0 after treatment to set a baseline for FITC fluorescence in papaya plant leaves, which can confirm that any emitted fluorescence later is due to nanoparticle uptake and not residual free FITC. Subsequent assessments were done 24 hours after incubation to track the nanoparticle uptake. The green fluorescence in Figure 4.10 shows that HrpN is delivered into papaya plant cells. FITC labelled on HrpN make it visible inside the cellular environment. There were no fluorescent signals in the leaves from any of the treatments at hour-0. From the images shown, FITC-tagged nanoparticles and proteins molecules had not yet entered the plant cells. The lack of fluorescence also proves that there was no background fluorescence from the labelling and incubation.

After 24 hours, a set of fluorescent green signals were detected in the leaves of papaya plants treated with HrpN-FITC, CNP-FITC, and CNP-HrpN-FITC. Those treated with CNP-HrpN showed higher green fluorescence than leaves treated with HrpN or CNP as single agents. The stronger fluorescence visualised that encapsulation of HrpN inside CNP assists in protein uptake into the plant cells better. The nanoparticles protect HrpN from degrade prematurely, which enables efficient delivery into papaya leaves. No green signals were seen in the leaves treated with control treatments either distilled

water, HrpN, FITC, CNP, or CNP-HrpN. From this observation, the lack of fluorescence in the control leaves confirms that the fluorescence emitted is not due to non-specific binding or natural auto-fluorescence from the plant tissues itself. FITC signals accumulated within cells only when they were encapsulated within carriers containing amino functional groups, like CNP. The amino functional groups on the CS interact with the plant cell membranes to enhance the internalisation of nanoparticles (Hassan et al., 2018). The signals appearance is proof that recombinant HrpN proteins have been successfully delivered into the papaya plant cells by CNP as a carrier.

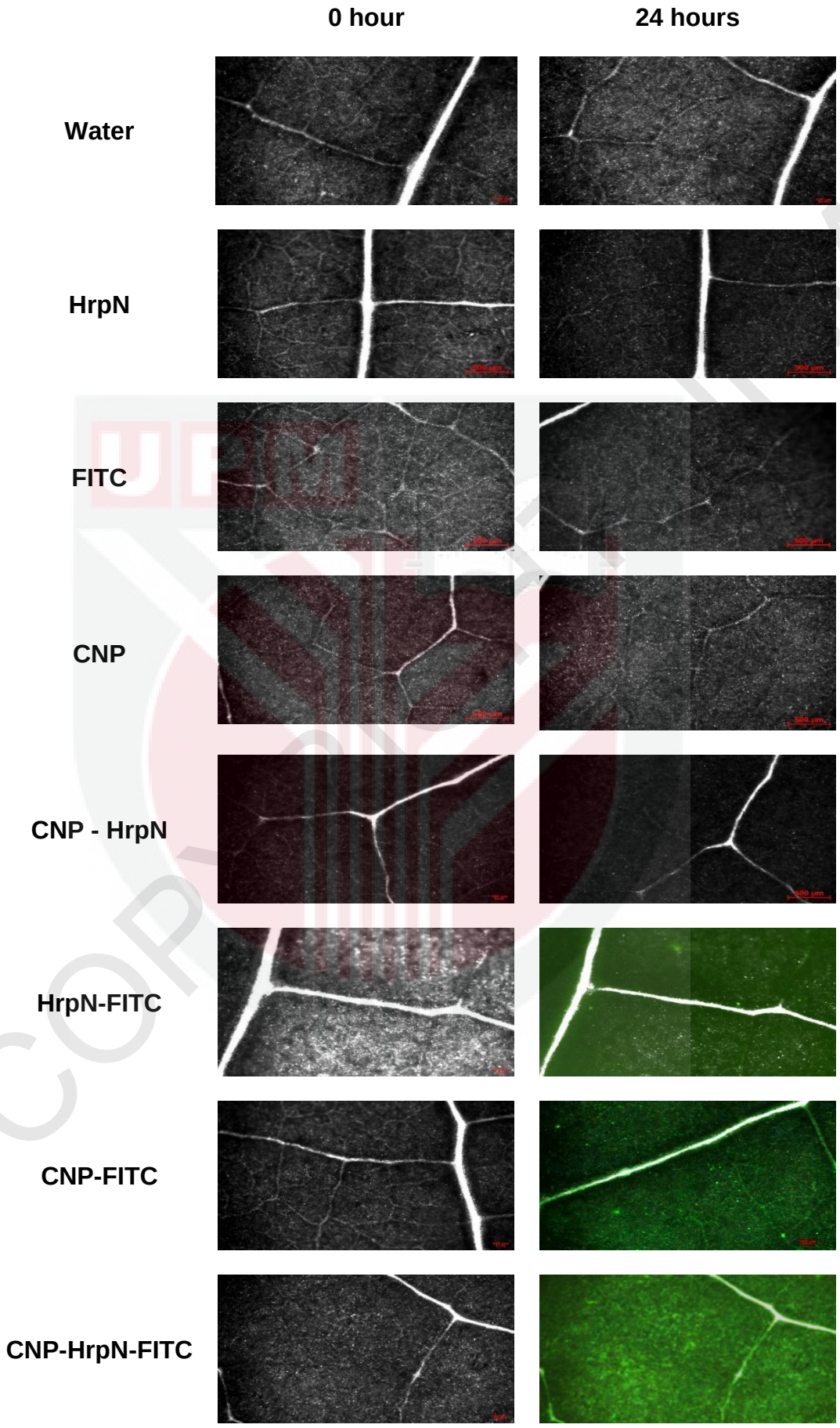

Figure 4.10: Overlay microscopy images of papaya leaves treated with water, HrpN, FITC, CNP, CNP-HrpN, HrpN-FITC, CNP-FITC, and CNP-HrpN-FITC at both 0 and 24-hour incubation periods.

4.11 *In vitro* toxicity test of CNP and CNP-HrpN using zebrafish embryo toxicity (ZFET) assay

Zebrafish embryos were used in preliminary test to check on the toxicity of both empty CNP and CNP-HrpN. Zebrafish shares many conserved genes with higher vertebrates. This making it easier to predict how the results might apply to more complex organisms like human. It was preferred over rodents as this animal has a rapid embryonic growth, cheap, and easy to maintain in laboratory settings (Bauer et al., 2021). Several parameters were monitored at different time points; 0, 24, 48, 72, 96, and 120 hours following CNP and CNP-HrpN exposure. The survival rate of zebrafish embryos (before hatching) and larvae (after hatching) exposed to CNP and CNP-HrpN was being checked over a 5-day period. The reason is to see acute effects of the treatments on embryos and larvae or any delayed or cumulative impacts on the overall viability of the zebrafish. As shown in Figure 4.11, embryos subjected to CNP at 10% (v/v) concentrations survived more than 72 hours post-fertilization (hpf). For CNP-HrpN cases, the survival rate only started to decrease after 96 hours after fertilization (hpf). Less than 50% of the embryos survived at concentrations above 80% (v/v). By this fact, treatment with CNP-HrpN was seen to have a greater survival rate than CNP.

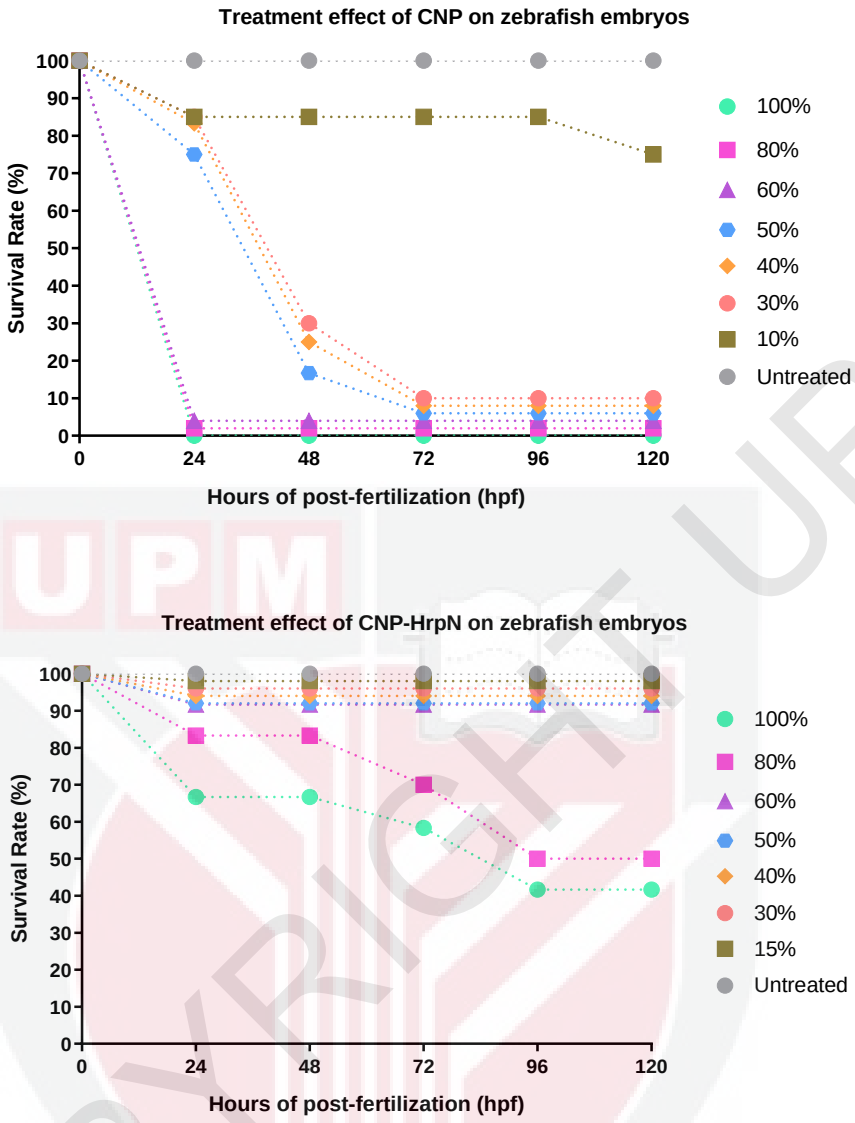

Figure 4.11: Survival rate of zebrafish embryos in 0 to 120 hours after treatment with CNP concentrations ranging from 10 to 100% (v/v) (top) and CNP-HrpN concentrations ranging from 15 to 100% (v/v) (below). Embryos exposed to 10% (v/v) CNP was alive after 72 hours post-fertilization (hpf). Less than 50% survived at concentrations over 80% (v/v) after 96 hours post-fertilization (hpf). The assay was done on 12 embryos.

Median lethal concentration at 50% (LC_{50}) was determined to measure the amount of a substance that causes the death of 50% of a test subject. This is to figure out the short-term acute toxicity caused by the samples. Samples with an LC_{50} of 100% (v/v) are completely harmless, those between 80% and 90% (v/v) are almost non-toxic, LC_{50} ranging from 50% to 79% (v/v) are mildly toxic, and LC_{50} between 10% and 49% (v/v) are moderately toxic. Samples with LC50 between 1% and 9% (v/v) are highly toxic. Those below 1% (v/v) are extremely toxic (Zahir et al., 2021). CNP is moderate toxic to the zebrafish embryos with LC_{50} of 15.97% in Figure 4.12. Meanwhile, CNP-HrpN is non-toxic with LC_{50} of 80.2%. The difference in toxicity may happen because organisms react differently based on the physical properties of nanomaterials. CNP is smaller than CNP-HrpN so its larger surface area relative to volume makes the nanoparticles more reactive in the environment surrounding zebrafish embryos to trigger potential adverse interactions with the zebrafish embryos (Martinez et al., 2017).

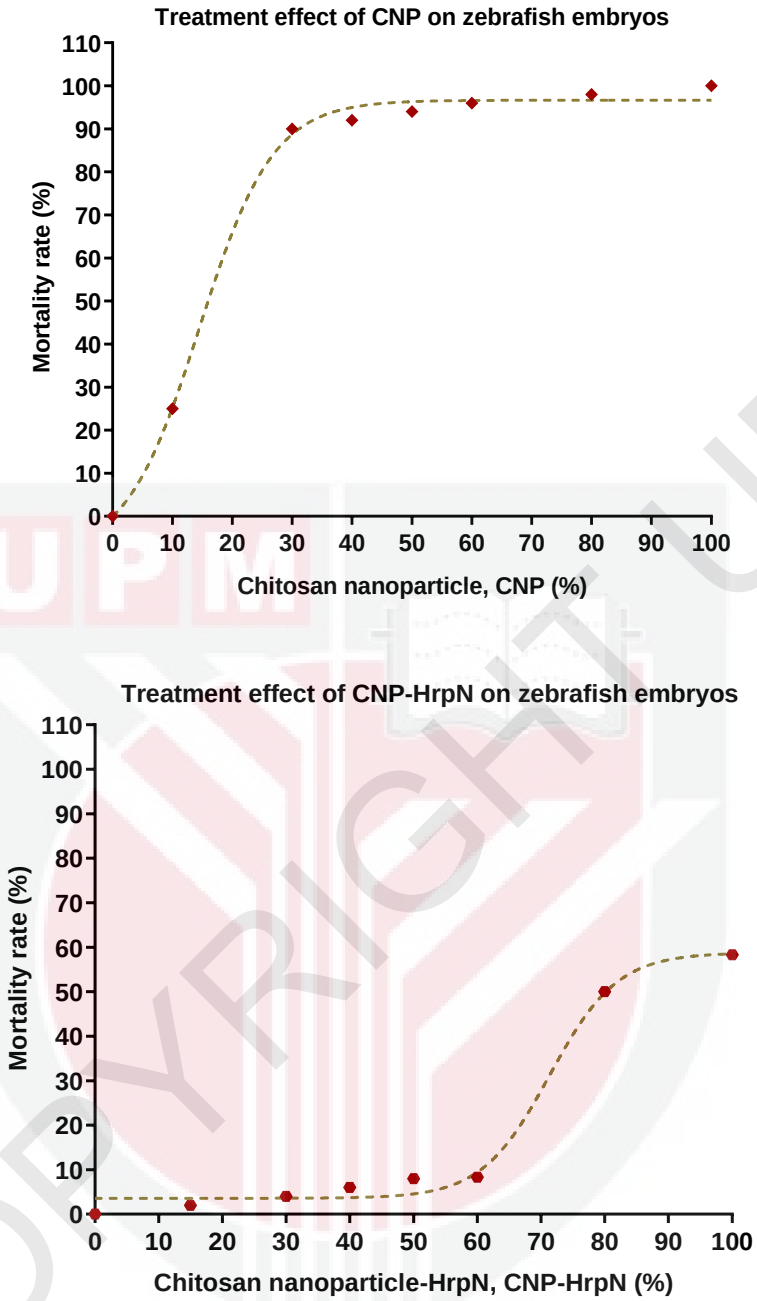

Figure 4.12: Effect of CNP concentrations ranging from 10 to 100% (v/v) (left) and CNP-HrpN concentrations ranging from 15 to 100% (v/v) (right) on zebrafish embryos mortality after 120 hours post-fertilization (hpf). The LC_{50} values of CNP and CNP-HrpN in zebrafish embryos were 15.97% (v/v) and 80.2% (v/v), respectively. Assay was done on 12 animals.

The hatching rate of zebrafish was then supervised from 0 to 120 hours to observe any vital effects on the embryos development. Figure 4.13 shows that CNP moderately affects hatching by reducing the hatching rate. Recent studies have shown that CNP might affect eggshell permeability and disrupting normal embryonic development which led to oxidative stress and low hatching rate (Bhoopathy et al., 2021). At the same time, all concentrations of CNP-HrpN showed a high hatching rate. It suggests that CNP-HrpN is nearly non-toxic and does not adversely affect the hatching process.

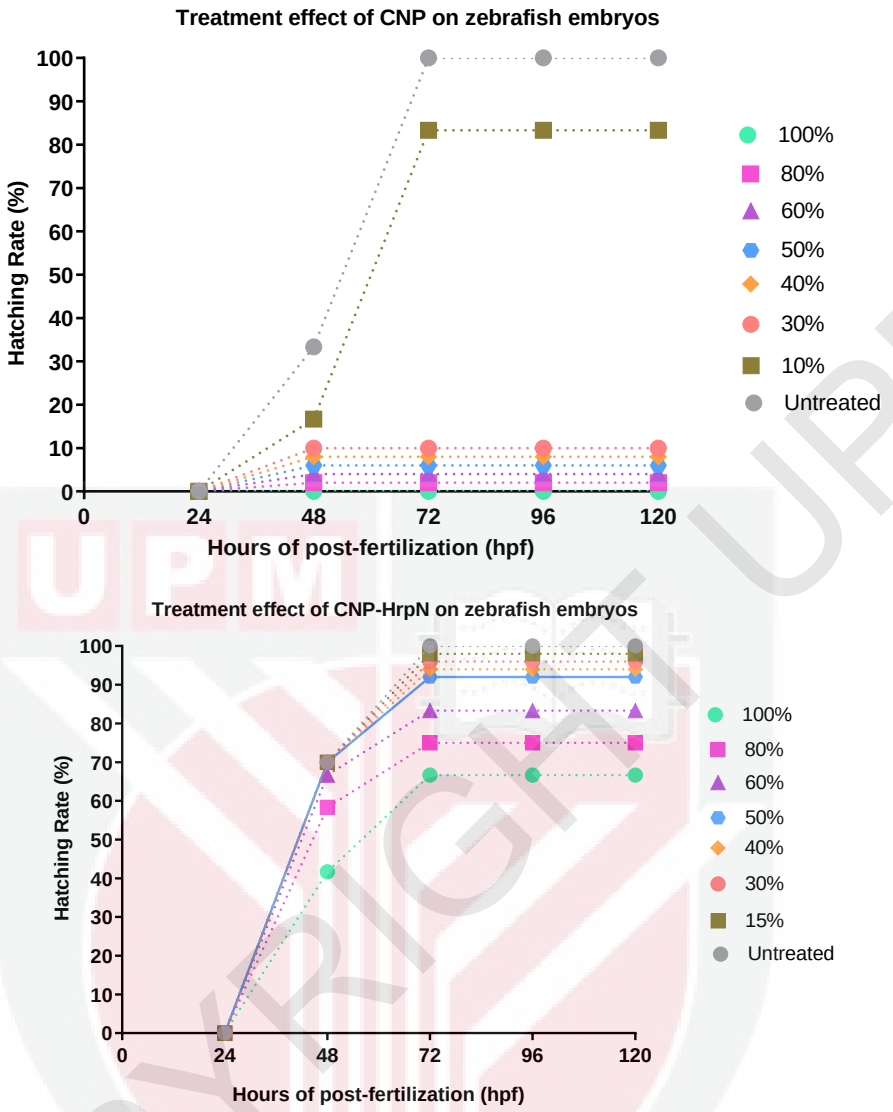

Figure 4.13: Hatching rate of zebrafish embryos from 0 to 120 hours after exposure to CNP at concentrations ranging from 10 to 100% (v/v) (left) and CNP-HrpN at concentrations from 15 to 100% (v/v) (right). Empty CNP had a low hatching rate (>10%) at concentrations more than 30% (v/v). CNP-HrpN had a high hatching rate (>60%) at all concentrations. Data were collected from 12 animals.

From the observation in Figure 4.13, zebrafish embryos have a heart rate of 140 beats per minute after being exposed to CNP and 162 heartbeats per minute post-exposure to CNP-HrpN. This finding fits with a previous studies showing that the normal heart rate of zebrafish embryos is similar to humans which is ranging from 120 to 180 beats per minute. (De Luca et al., 2014). After 96 hours of exposure, both CNP and CNP-HrpN did not affect the cardiac function of zebrafish larvae. The treatment of low concentrations of both nanomaterials do not affect heart development and function of cardiovascular.

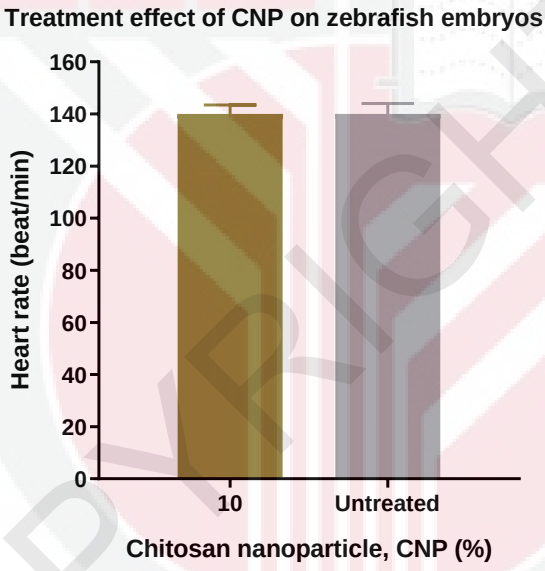

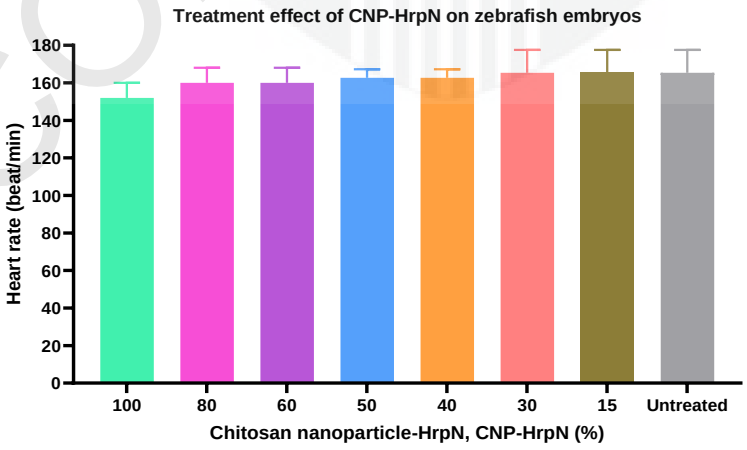

Figure 4.14: Effect of CNP at concentrations of 10% (v/v) (left) and CNP-HrpN at concentrations ranging from 15 to 100% (v/v) (right) on the heart rate of zebrafish embryos at 96 hpf. No result was available for CNP at concentrations of 30-100% (v/v) concentrations as the zebrafish went mortal. Data were collected from 3 animals.

Then, embryos were observed for any abnormal signs such as pericardial swelling, not able to hatch, edema in yolk sac, curvy bodies, and bending tails starting from 0 to 120 hours after treatments. From the observation in a study, defects or indicator of toxicity also can be scoliosis, yolk sac issues, and pericardial edema (Rizeq et al., 2019). CNP was said to be toxic, still it did not induce any physical alterations in zebrafish embryos before or after hatching. Besides, no symptom was observed in the embryos and larvae exposed to CNP at 10% (v/v) and CNP-HrpN at 15-100% (v/v). Briefly, CNP and CNP-HrpN tested at different concentrations, did not cause any teratogenic defects in zebrafish embryos or larvae. Studying CNP and CNP-HrpN with a zebrafish model is useful to figure out if they are safe for agricultural use, especially for delivering bioagents like recombinant HrpN protein. More studies on oxidative stress, liver function, and brain activity are required as CNP is toxic to zebrafish embryos in this study, even though it is well-known as a safe biopolymer in multiple applications.

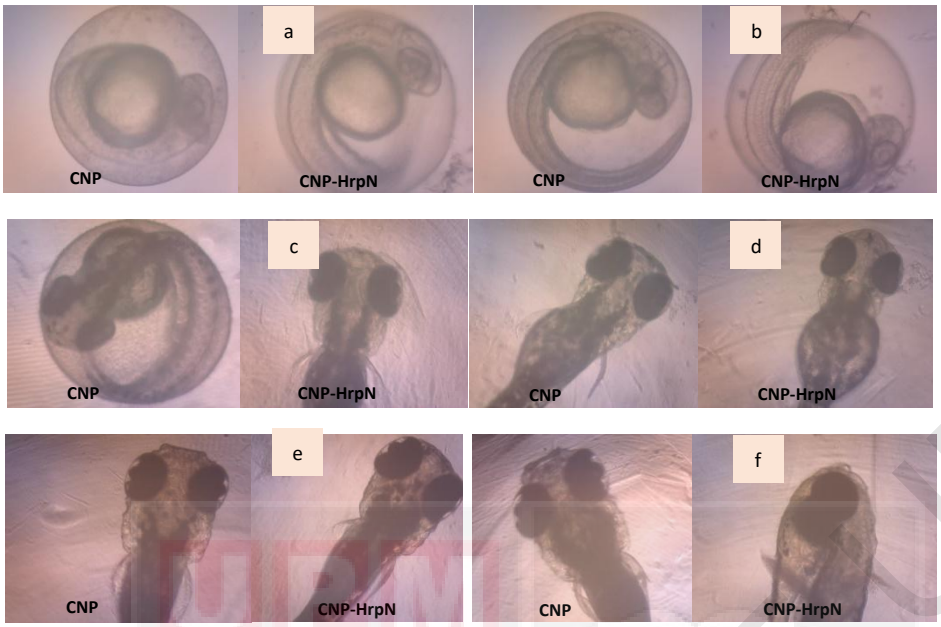

Figure 4.15: Development of zebrafish embryos and larvae at a) 0 hpf, b) 24 hpf, c) 48 hpf, d) 72 hpf, e) 96 hpf and f) 120 hpf after treatment with CNP at a concentration of 10% (v/v) (top) and CNP-HrpN at concentration of 50% (v/v) (below). Images were taken by an inverted microscope at 100X (a and b) and 40X magnification (c-f)

CHAPTER 5

CONCLUSION AND RECOMMENDATION

5.1 Conclusion

This study described the synthesis of a nanocarrier to encapsulate a selected hairpin from *Erwinia mallotivora* via ionic gelation. Prior to encapsulation, a hairpin of interest from *E. mallotivora* HrpN was expressed and purified at a molecular size of 30 kDa as a recombinant protein in the *Escherichia coli* system. The CNP-HrpN formulation was spherical in shape with a homogenous particle size of 106.34 ± 2.053 nm. This showed that the sample preparation gave a good control in terms of particle size and morphology. Encapsulation efficiency of 80% explained that the chitosan-TPP complex was able to entrap HrpN within the nanoparticles. A low polydispersity index of 0.188 ± 0.011 showed that the CNP-HrpN was stable in terms of colloidal particles for efficient delivery.

Fourier transform infrared spectroscopy observed the HrpN within the CNP-HrpN spectra, showing that the nanoparticle retained the compounds successfully. *In vitro* release test described these nanoparticles released the HrpN slowly over 72 hours for lasting benefits in next applications. The HrpN followed a predictable pattern in first-order mechanisms when the HrpN release rate slowed down as its amount decreased. Fluorescence imaging via FITC labelling visualised the uptake of CNP-HrpN in papaya leaves within a relatively short timeframe of 24 hours. The nano-delivery system was able to enter the papaya leaf tissue and deliver HrpN to target sites within the plant.

CNP-HrpN was non-toxic and well-tolerated by zebrafish embryos. In brief, chitosan nanoparticles as a nanocarrier can deliver HrpN into papaya leaves and releasing it in sustained release manner without any side effects.

5.2 Future recommendation

In the future, additional *in vivo* testing should be conducted on papaya plants in a greenhouse setting to see how well CNP-HrpN boosts immune responses in living organisms. This will provide more information on how to use this nano-delivery system in agricultural applications. Also, more studies should explore the encapsulation of various recombinant hairpin proteins in CNP. Experimenting with various recombinant hairpin proteins may foster a better approach to combat papaya dieback disease. We also need to prolong the *in vitro* release test beyond 72 hours to observe how long the CNP can keep releasing its contents and measure the degree of resistance acquired by the CNP-HrpN delivery system through quantitative expression profiling on systemic acquired resistance-responsive genes. To improve its delivery, a study on the routes of CNP-HrpN internalization is a must to understand how nanoparticles penetrate into plant cells. Next, future work should extend the time points for cellular tracking to learn how long CNP-HrpN reside within cells. CNP-HrpN can be applied in papaya seed priming as this method is cheap and does not harm the environment. Future works also can test CNP-HrpN against different crops and diseases to widen its application in agriculture.

REFERENCES

Abu Bakar, N., Badrun, R., Sohaime, Z., Waznul, M., & Zaidan, A. (2016). Technology to improve papaya defence against papaya dieback pathogen via application of chemicals and recombinant proteins. In *Buletin Teknologi MARDI, Bil* (Vol. 10).

Abu-Bakar, N., Juri, N. M., Abu-Bakar, R. A. H., Sohaime, M. Z., Badrun, R., Sarip, J., Hassan, M. A., & Ahmad, K. (2021a). Recombinant protein foliar application activates systemic acquired resistance and increases tolerance against papaya dieback disease. *Asian Journal of Agriculture and Rural Development*, *11*(1), 1–9. https://doi.org/10.18488/journal.ajard.2021.111.1.9

Abu-Bakar, N., Juri, N. M., Abu-Bakar, R. A. H., Sohaime, M. Z., Badrun, R., Sarip, J., Hassan, M. A., & Ahmad, K. (2021b). Recombinant protein foliar application activates systemic acquired resistance and increases tolerance against papaya dieback disease. *Asian Journal of Agriculture and Rural Development*, *11*(1), 1–9. https://doi.org/10.18488/journal.ajard.2021.111.1.9

Alasas, A. B., Mohtar, N., Amirah, *, & Gazzali, M. (2024). Preparation, Characterization and in Vitro Drug Release Evaluation of Chitosan Nanoparticles for Atovaquone. In *Malaysian Journal of Medicine and Health Sciences* (Vol. 20, Issue SUPP1).

Alhazmi, H. A. (2019). FT-IR spectroscopy for the identification of binding sites and measurements of the binding interactions of important metal ions with bovine serum albumin. *Scientia Pharmaceutica*, *87*(1). https://doi.org/10.3390/scipharm87010005

Ameen, F., Alsamhary, K., Alabdullatif, J. A., & ALNadhari, S. (2021). A review on metal-based nanoparticles and their toxicity to beneficial soil bacteria and fungi. In *Ecotoxicology and Environmental Safety* (Vol. 213). Academic Press. https://doi.org/10.1016/j.ecoenv.2021.112027

Amin, N. M., Bunawan, H., Redzuan, R. A., & Jaganath, I. B. S. (2011). Erwinia mallotivora sp., a new pathogen of papaya (Carica papaya) in peninsular Malaysia. *International Journal of Molecular Sciences*, *12*(1), 39–45. https://doi.org/10.3390/ijms12010039

Amini, Y., Tafaghodi, M., Jamehdar, S. A., Meshkat, Z., Moradi, B., & Sankian, M. (2018). Heterologous Expression, Purification, and Characterization of the HspX, Ppe44, and EsxV Proteins of

Mycobacterium tuberculosis. In *Reports of Biochemistry & Molecular Biology* (Vol. 6, Issue 2). www.RBMB.net

Ansari, M. A. (2023). Nanotechnology in Food and Plant Science: Challenges and Future Prospects. In *Plants* (Vol. 12, Issue 13). Multidisciplinary Digital Publishing Institute (MDPI). https://doi.org/10.3390/plants12132565

Astha, & Sekhon, P. S. (2021). Biochemical basis of systemic acquired resistance induced by different Systemic Acquired Resistance (SAR) elicitors in Brassica cultivars challenge inoculated with downy mildew pathogen. *Journal of Applied and Natural Science*, *13*(1), 301–307. https://doi.org/10.31018/jans.v13i1.2548

Ayodipupo Babalola, B., Ifeolu Akinwande, A., Otunba, A. A., Ebenezer Adebami, G., Babalola, O., & Nwuofo, C. (2024). Therapeutic benefits of Carica papaya: A review on its pharmacological activities and characterization of papain. In *Arabian Journal of Chemistry* (Vol. 17, Issue 1). Elsevier B.V. https://doi.org/10.1016/j.arabjc.2023.105369

Azhar, H. M., Johari, S., Sulastri, J. N., Razali, M., Zulfa, M. R. M., Faimah, G. N., Mariatulqabtiah, A. R., Hassan, M. A., Sarip, J., Sulastri Jaafar, N., Mustaffa, R., Zulda, M., Razikin, M., Ghazali, N. F., Razak, M. A., & Mohd Azhar, H. (2020). Field performance of selected papaya hybrids for tolerance to dieback disease (Prestasi ladang bagi hibrid betik terpilih untuk kerintangan terhadap penyakit mati rosot). In *J. Trop. Agric. and Fd. Sc* (Vol. 48, Issue 1).

Bakar, N. A. (2018). Induction of Systemic Acquired Resistance in Papaya by Foliar Application of HrpN Recombinant Protein for Increased Resistance against Papaya Dieback Pathogen. *Current Investigations in Agriculture and Current Research*, *2*(3). https://doi.org/10.32474/ciacr.2018.02.000136

Bakar, N. A., Barun, R., Rozano, L., Ahmad, L., Redzuan, R. A., Firdaus, M., Raih, M., & Tarmizi, A. A. (2017). Identification and Validation of Putative Erwinia mallotivora Effectors proteins via Quantitative Proteomics and Real Time Analysis. In *J. Agric. Food. Tech* (Vol. 7, Issue 9). http://pfam.xfam.org/

Bakar, N. S. A., Saidi, N. B., Rozano, L., Abdullah, M. P., & Supian, S. (2021). In-silico characterization and expression analysis of NB-ARC genes in response to Erwinia mallotivora in Carica papaya. *Sains Malaysiana*, *50*(9), 2591–2602. https://doi.org/10.17576/jsm-2021-5009-08

Bakar, R. A. H., Abu Bakar, N., Ahmad, K., Shaharuddin, N. A., Abdul Wahab, M. A., & Juri, N. M. (2023). RECOMBINANT PROTEIN APPLICATION INDUCED DEFENSE MECHANISM IN HOST PLANT AGAINST PAPAYA DIEBACK DISEASE. *Jurnal Teknologi*, *85*(6), 187–199. https://doi.org/10.11113/jurnalteknologi.v85.20092

Balusamy, S. R., Joshi, A. S., Perumalsamy, H., Mijakovic, I., & Singh, P. (2023). Advancing sustainable agriculture: a critical review of smart and eco-friendly nanomaterial applications. In *Journal of Nanobiotechnology* (Vol. 21, Issue 1). BioMed Central Ltd. https://doi.org/10.1186/s12951-023-02135-3

Bamburowicz-Klimkowska, M., Poplawska, M., & Grudzinski, I. P. (2019). Nanocomposites as biomolecules delivery agents in nanomedicine. In *Journal of Nanobiotechnology* (Vol. 17, Issue 1). BioMed Central Ltd. https://doi.org/10.1186/s12951-019-0479-x

Bauer, B., Mally, A., & Liedtke, D. (2021). Zebrafish embryos and larvae as alternative animal models for toxicity testing. In *International Journal of Molecular Sciences* (Vol. 22, Issue 24). MDPI. https://doi.org/10.3390/ijms222413417

Begum, H., Murugesan, P., & Tangutur, A. D. (2022). Western blotting: A powerful staple in scientific and biomedical research. In *BioTechniques* (Vol. 73, Issue 1, pp. 59–69). Future Science Ltd. https://doi.org/10.2144/btn-2022-0003

Bektas, Y. (2022). FytoSol, a Promising Plant Defense Elicitor, Controls Early Blight (Alternaria solani) Disease in the Tomato by Inducing Host Resistance-Associated Gene Expression. *Horticulturae*, *8*(6). https://doi.org/10.3390/horticulturae8060484

Bhoopathy, S., Inbakandan, D., Thirugnanasambandam, R., Kumar, C., Sampath, P., Bethunaickan, R., Raguraman, V., & Vijayakumar, G. K. (2021). A comparative study on chitosan nanoparticle synthesis methodologies for application in aquaculture through toxicity studies. *IET Nanobiotechnology*, *15*(4), 418–426. https://doi.org/10.1049/nbt2.12047

Buyuk, N. I., Arayici, P. P., Derman, S., Mustafaeva, Z., & Yucel, S. (2020). Synthesis of chitosan nanoparticles for controlled release of amiodarone. *Indian Journal of Pharmaceutical Sciences*, *82*(1), 131–138. https://doi.org/10.36468/pharmaceutical-sciences.630

Cano-Reinoso, D. M., Soesanto, L., Kharisun, & Wibowo, C. (2021). Fruit collapse and heart rot disease in pineapple: Pathogen

characterization, ultrastructure infections of plant and cell mechanism resistance. *Biodiversitas*, *22*(5), 2477–2488. https://doi.org/10.13057/biodiv/d220504

Cao, L., Zhang, H., Cao, C., Zhang, J., Li, F., & Huang, Q. (2016). Quaternized chitosan-capped mesoporous silica nanoparticles as nanocarriers for controlled pesticide release. *Nanomaterials*, *6*(7). https://doi.org/10.3390/nano6070126

Chaganti, L. K., Venkatakrishnan, N., & Bose, K. (2018). An efficient method for FITC labelling of proteins using tandem affinity purification. *Bioscience Reports*, *38*(6). https://doi.org/10.1042/BSR20181764

Chandra, S., Chakraborty, N., Dasgupta, A., Sarkar, J., Panda, K., & Acharya, K. (2015). Chitosan nanoparticles: A positive modulator of innate immune responses in plants. *Scientific Reports*, *5*. https://doi.org/10.1038/srep15195

Choi, T. J., Geletu, T. T., & Choi, T. (2018). High level expression and purification of recombinant flounder growth hormone in E. coli. *Journal of Genetic Engineering and Biotechnology*, *16*(2), 347–355. https://doi.org/10.1016/j.jgeb.2018.03.006

Concha, L., Pires, A. L. R., Moraes, A. M., Mas-Hernández, E., Berres, S., & Hernandez-Montelongo, J. (2022). Cost Function Analysis Applied to Different Kinetic Release Models of Arrabidaea chica Verlot Extract from Chitosan/Alginate Membranes. *Polymers*, *14*(6). https://doi.org/10.3390/polym14061109

Correa, R. F., Colucci, G., Halla, N., Pinto, J. A., Santamaria-Echart, A., Blanco, S. P., Fernandes, I. P., & Barreiro, M. F. (2021). Development of chitosan microspheres through a green dual crosslinking strategy based on tripolyphosphate and vanillin. *Molecules*, *26*(8). https://doi.org/10.3390/molecules26082325

Dayana, M., Taha, M., Saidi, N. B., Rahim, R. A., Kalsom, U., Shah, M., & Hashim, A. M. (2019). *IN VITRO STUDIES OF LACTIC ACID BACTERIA AGAINST THE CAUSATIVE AGENT OF PAPAYA DIEBACK DISEASE*.

De Luca, E., Zaccaria, G. M., Hadhoud, M., Rizzo, G., Ponzini, R., Morbiducci, U., & Santoro, M. M. (2014). ZebraBeat : A flexible platform for the analysis of the cardiac rate in zebrafish embryos. *Scientific Reports*, *4*. https://doi.org/10.1038/srep04898

De Matteis, V., Rizzello, L., Cascione, M., Pellegrino, P., Singh, J., Manno, D., & Rinaldi, R. (2022). Sustainable Synthesis of FITC Chitosan-Capped Gold Nanoparticles for Biomedical Applications. *Clean Technologies*, *4*(4), 942–953. https://doi.org/10.3390/cleantechnol4040058

Department of Agriculture. (2019). *INVASIVE ALIEN SPECIES IN MALAYSIA 2018*.

Department of Biosafety. (2019). *BIOLOGY OF PAPAYA*. www.biosafety.gov.my

Detsi, A., Kavetsou, E., Kostopoulou, I., Pitterou, I., Pontillo, A. R. N., Tzani, A., Christodoulou, P., Siliachli, A., & Zoumpoulakis, P. (2020). Nanosystems for the encapsulation of natural products: The case of chitosan biopolymer as a matrix. In *Pharmaceutics* (Vol. 12, Issue 7, pp. 1–68). MDPI AG. https://doi.org/10.3390/pharmaceutics12070669

Dikshit, P. K., Kumar, J., Das, A. K., Sadhu, S., Sharma, S., Singh, S., Gupta, P. K., & Kim, B. S. (2021). Green synthesis of metallic nanoparticles: Applications and limitations. In *Catalysts* (Vol. 11, Issue 8). MDPI. https://doi.org/10.3390/catal11080902

Du, J., Liu, B., Zhao, T., Xu, X., Lin, H., Ji, Y., Li, Y., Li, Z., Lu, C., Li, P., Zhao, H., Li, Y., Yin, Z., & Ding, X. (2022). Silica nanoparticles protect rice against biotic and abiotic stresses. *Journal of Nanobiotechnology*, *20*(1). https://doi.org/10.1186/s12951-022-01420-x

El-Fadl, R. E. A., Mahdi, A. A., Abdelhamid, A. E., Magid, M. R. A., & Hassan, A. H. (2022). Enhancing the biochemical constituents in avocado callus using encapsulated chitosan nanoparticles. *Egyptian Journal of Chemistry*, *65*(12), 769–782. https://doi.org/10.21608/EJCHEM.2022.113494.5176

Eng, L., Siaw San, H., & Poili, E. (2020). *ETIOLOGY OF PAPAYA DIEBACK IN TAWAU, SABAH*. http://www.ncbi.

Esquivel, R., Juárez, J., Almada, M., Ibarra, J., & Valdez, M. A. (2015). Synthesis and characterization of new thiolated chitosan nanoparticles obtained by ionic gelation method. *International Journal of Polymer Science*, *2015*. https://doi.org/10.1155/2015/502058

FAO. (2024). *MAJOR TROPICAL FRUITS Market Review Preliminary Results 2023*.

Food and Agriculture Organisation. (2022). *MAJOR TROPICAL FRUITS*.

Francesconi, S., Tagliavento, V., Ciarroni, S., Sestili, F., & Balestra, G. M. (2024). Chitosan- and gallic acid-based (NPF) displayed antibacterial activity against three Pseudomonas spp. plant pathogens and boosted systemic acquired resistance in kiwifruit and olive plants. *Pest Management Science*, *80*(3), 1300–1313. https://doi.org/10.1002/ps.7861

Ganisan Krishnen. (2022). Management of papaya bacterial disease with induced systemic resistance approach. *Buletin Teknologi MARDI*, 137–148.

Gao, M., Chang, J., Wang, Z., Zhang, H., & Wang, T. (2023a). Advances in transport and toxicity of nanoparticles in plants. In *Journal of Nanobiotechnology* (Vol. 21, Issue 1). BioMed Central Ltd. https://doi.org/10.1186/s12951-023-01830-5

Gao, M., Chang, J., Wang, Z., Zhang, H., & Wang, T. (2023b). Advances in transport and toxicity of nanoparticles in plants. In *Journal of Nanobiotechnology* (Vol. 21, Issue 1). BioMed Central Ltd. https://doi.org/10.1186/s12951-023-01830-5

García-Carrasco, M., Valdez-Baro, O., Cabanillas-Bojórquez, L. A., Bernal-Millán, M. J., Rivera-Salas, M. M., Gutiérrez-Grijalva, E. P., & Heredia, J. B. (2023). Potential Agricultural Uses of Micro/Nano Encapsulated Chitosan: A Review. In *Macromol* (Vol. 3, Issue 3, pp. 614–635). Multidisciplinary Digital Publishing Institute (MDPI). https://doi.org/10.3390/macromol3030034

Gomes, D. G., Debiasi, T. V., Pelegrino, M. T., Pereira, R. M., Ondrasek, G., Batista, B. L., Seabra, A. B., & Oliveira, H. C. (2022). Soil Treatment with Nitric Oxide-Releasing Chitosan Nanoparticles Protects the Root System and Promotes the Growth of Soybean Plants under Copper Stress. *Plants*, *11*(23). https://doi.org/10.3390/plants11233245

Guarnizo, N., Oliveros, D., Murillo-Arango, W., & Bermúdez-Cardona, M. B. (2020). Oligosaccharides: Defense inducers, their recognition in plants, commercial uses and perspectives. In *Molecules* (Vol. 25, Issue 24). MDPI AG. https://doi.org/10.3390/molecules25245972

Hammad Ayaz, Muhammad Ahmad, Mustafa Kazmi, Husnain Ahmed, Talib Hussain, Ishtiaq Jeelani, Ume Habiba, & Muhammad Akram Choohan. (2022). Formulation and evaluation of 5-fluorouracil controlled release chronotherapeutic drug delivery system (CTDDS)

for colorectal cancer. *Journal of Contemporary Pharmacy*, *6*(2), 65–72. https://doi.org/10.56770/jcp2022624

Hassan, U. A., Hussein, M. Z., Alitheen, N. B., Ariff, S. A. Y., & Masarudin, M. J. (2018). In vitro cellular localization and efficient accumulation of fluorescently tagged biomaterials from monodispersed chitosan nanoparticles for elucidation of controlled release pathways for drug delivery systems. *International Journal of Nanomedicine*, *13*, 5075–5095. https://doi.org/10.2147/IJN.S164843

Herdiana, Y., Wathoni, N., Shamsuddin, S., & Muchtaridi, M. (2022). Drug release study of the chitosan-based nanoparticles. In *Heliyon* (Vol. 8, Issue 1). Elsevier Ltd. https://doi.org/10.1016/j.heliyon.2021.e08674

Hoang, N. H., Le Thanh, T., Thepbandit, W., Treekoon, J., Saengchan, C., Sangpueak, R., Papathoti, N. K., Kamkaew, A., & Buensanteai, N. (2022). Efficacy of Chitosan Nanoparticle Loaded-Salicylic Acid and-Silver on Management of Cassava Leaf Spot Disease. *Polymers*, *14*(4). https://doi.org/10.3390/polym14040660

Hoang, N. H., Thanh, T. Le, Sangpueak, R., Treekoon, J., Saengchan, C., Thepbandit, W., Papathoti, N. K., Kamkaew, A., & Buensanteai, N. (2022). Chitosan Nanoparticles-Based Ionic Gelation Method: A Promising Candidate for Plant Disease Management. In *Polymers* (Vol. 14, Issue 4). MDPI. https://doi.org/10.3390/polym14040662

Idris, N. H., Azman, M., Teri, S. S., Mohd Hata, E., & Ishak, M. H. I. (2023a). Spatial modelling of papaya dieback disease occurrence. *Malaysian Journal of Society and Space*, *19*(3). https://doi.org/10.17576/geo-2023-1903-03

Idris, N. H., Azman, M., Teri, S. S., Mohd Hata, E., & Ishak, M. H. I. (2023b). Spatial modelling of papaya dieback disease occurrence. *Malaysian Journal of Society and Space*, *19*(3). https://doi.org/10.17576/geo-2023-1903-03

Jagdale, S., Agarwal, B., Dixit, A., & Gaware, S. (2024). Chitosan as excellent bio-macromolecule with myriad of anti-activities in biomedical applications – A review. In *International Journal of Biological Macromolecules* (Vol. 257). Elsevier B.V. https://doi.org/10.1016/j.ijbiomac.2023.128697

Jeon, H. W., Park, A. R., Sung, M., Kim, N., Mannaa, M., Han, G., Kim, J., Koo, Y., Seo, Y. S., & Kim, J. C. (2022). Systemic Acquired Resistance-Mediated Control of Pine Wilt Disease by Foliar

Application With Methyl Salicylate. *Frontiers in Plant Science*, *12*. https://doi.org/10.3389/fpls.2021.812414

Ji, Y., Yang, X., Ji, Z., Zhu, L., Ma, N., Chen, D., Jia, X., Tang, J., & Cao, Y. (2020). DFT-Calculated IR Spectrum Amide I, II, and III Band Contributions of N-Methylacetamide Fine Components. *ACS Omega*, *5*(15), 8572–8578. https://doi.org/10.1021/acsomega.9b04421

Ji, Y., Yue, L., Cao, X., Chen, F., Li, J., Zhang, J., Wang, C., Wang, Z., & Xing, B. (2023). Carbon dots promoted soybean photosynthesis and amino acid biosynthesis under drought stress: Reactive oxygen species scavenging and nitrogen metabolism. *Science of the Total Environment*, *856*. https://doi.org/10.1016/j.scitotenv.2022.159125

Jia, Z., Li, J., Gao, L., Yang, D., & Kanaev, A. (2023). Dynamic Light Scattering: A Powerful Tool for In Situ Nanoparticle Sizing. In *Colloids and Interfaces* (Vol. 7, Issue 1). MDPI. https://doi.org/10.3390/colloids7010015

Jiménez-Guerrero, I., López-Baena, F. J., Borrero-de Acuña, J. M., & Pérez-Montaño, F. (2023). Membrane vesicle engineering with “à la carte” bacterial-immunogenic molecules for organism-free plant vaccination. In *Microbial Biotechnology* (Vol. 16, Issue 12, pp. 2223–2235). John Wiley and Sons Ltd. https://doi.org/10.1111/1751-7915.14323

Jin, Y. J., Kong, H. G., Yang, S. I., Ham, H., Lee, M.-H., & Park, D. S. (2022). Species-Specific Detection and Quantification of Erwinia pyrifoliae in Plants by a Direct SYBR Green Quantitative Real-Time PCR Assay. *PhytoFrontiers™*, *2*(4), 371–379. https://doi.org/10.1094/phytofr-09-21-0069-r

Juri, N. M., Samsuddin, A. F., Abdul Murad, A. M., Tamizi, A. A., Shaharuddin, N. A., & Bakar, N. A. (2020). Discovery of pathogenesis related and effector genes of erwinia mallotivora in Carica papaya (Eksotika I) seedlings via transcriptomic analysis. *International Journal of Agriculture and Biology*, *23*(5), 1021–1032. https://doi.org/10.17957/IJAB/15.1382

Juri, N. M., Samsuddin, A. F., Murad, A. M. A., Tamizi, A. A., Hassan, M. A., & Bakar, N. A. (2020). In silico analysis and functional characterization of fhub, a component of erwinia mallotivora ferric hydroxamate uptake system. *Jurnal Teknologi*, *82*(3), 83–90. https://doi.org/10.11113/jt.v82.13635

Khan, M., Khan, M. S. A., Borah, K. K., Goswami, Y., Hakeem, K. R., & Chakrabartty, I. (2021). The potential exposure and hazards of metal-based nanoparticles on plants and environment, with special emphasis on ZnO NPs, TiO2 NPs, and AgNPs: A review. In *Environmental Advances* (Vol. 6). Elsevier Ltd. https://doi.org/10.1016/j.envadv.2021.100128

Kongala, S. I., Nadendla, S. R., & Mamidala, P. (2021). Internalization and induction of defense responses in tobacco by harpinPss conjugated gold nanoparticles as a foliar spray. *Colloids and Interface Science Communications*, *43*. https://doi.org/10.1016/j.colcom.2021.100438

Koppolu, B. prasanth, Smith, S. G., Ravindranathan, S., Jayanthi, S., Suresh Kumar, T. K., & Zaharoff, D. A. (2014). Controlling chitosan-based encapsulation for protein and vaccine delivery. *Biomaterials*, *35*(14), 4382–4389. https://doi.org/10.1016/j.biomaterials.2014.01.078

Koul, B., Pudhuvai, B., Sharma, C., Kumar, A., Sharma, V., Yadav, D., & Jin, J. O. (2022a). Carica papaya L.: A Tropical Fruit with Benefits beyond the Tropics. In *Diversity* (Vol. 14, Issue 8). MDPI. https://doi.org/10.3390/d14080683

Koul, B., Pudhuvai, B., Sharma, C., Kumar, A., Sharma, V., Yadav, D., & Jin, J. O. (2022b). Carica papaya L.: A Tropical Fruit with Benefits beyond the Tropics. In *Diversity* (Vol. 14, Issue 8). MDPI. https://doi.org/10.3390/d14080683

Kuen, C. Y., Fakuraz, S., Othman, S. S., & Masarudin, M. J. (2017). Increased loading, efficacy and sustained release of silibinin, a poorly soluble drug using hydrophobically-modified chitosan nanoparticles for enhanced delivery of anticancer drug delivery systems. *Nanomaterials*, *7*(11). https://doi.org/10.3390/nano7110379

Kuen, C. Y., Galen, T., Fakurazi, S., Othman, S. S., & Masarudin, M. J. (2020). Increased cytotoxic efficacy of protocatechuic acid in A549 human lung cancer delivered via hydrophobically modified-chitosan nanoparticles as an anticancer modality. *Polymers*, *12*(9). https://doi.org/10.3390/POLYM12091951

Kumari, A., Sangha, M., Vasmatkar, P., Akhatar, J., Archana, K., Manjeet Kaur, S., Pashupat, V., Javed, A., & Dharmender, P. (2020). Role of 2,6 Dichloroisonicotinic acid inducing resistance in cotton against cotton leaf curl disease. In *Article in Research Journal of Biotechnology* (Vol. 15, Issue 5). https://www.researchgate.net/publication/341042840

Kumari, R., Suman, K., Karmakar, S., Mishra, V., Lakra, S. G., Saurav, G. K., & Mahto, B. K. (2023). Regulation and safety measures for nanotechnology-based agri-products. In *Frontiers in Genome Editing* (Vol. 5). Frontiers Media SA. https://doi.org/10.3389/fgeed.2023.1200987

Lazaridou, M., Christodoulou, E., Nerantzaki, M., Kostoglou, M., Lambropoulou, D. A., Katsarou, A., Pantopoulos, K., & Bikiaris, D. N. (2020). Formulation and in-vitro characterization of chitosan-nanoparticles loaded with the iron chelator deferoxamine mesylate (DFO). *Pharmaceutics*, *12*(3). https://doi.org/10.3390/pharmaceutics12030238

Lee, Y. J., Inzana, T. J., & Lee, Y. (2021). Extraction and Electrophoretic Analysis of Bacterial Lipopolysaccharides and Outer Membrane Proteins. *Bio-Protocol*, *11*(24). https://doi.org/10.21769/BioProtoc.4263

Li, R., Xiong, Y. L., & Li, R. (2021). Sensitivity of oat protein solubility to changing ionic strength and pH. *Journal of Food Science*, *86*(1), 78–85. https://doi.org/10.1111/1750-3841.15544

Li, T. Y., Ye, C., Zhang, Y. J., Zhang, J. X., Yang, M., He, X. H., Mei, X. Y., Liu, Y. X., Zhu, Y. Y., Huang, H. C., & Zhu, S. S. (2023). 2,3-Butanediol from the leachates of pine needles induces the resistance of Panax notoginseng to the leaf pathogen Alternaria panax. *Plant Diversity*, *45*(1), 104–116. https://doi.org/10.1016/j.pld.2022.02.003

Li, Z., Liu, J., Ma, W., & Li, X. (2023a). Characteristics, Roles and Applications of Proteinaceous Elicitors from Pathogens in Plant Immunity. In *Life* (Vol. 13, Issue 2). MDPI. https://doi.org/10.3390/life13020268

Li, Z., Liu, J., Ma, W., & Li, X. (2023b). Characteristics, Roles and Applications of Proteinaceous Elicitors from Pathogens in Plant Immunity. In *Life* (Vol. 13, Issue 2). MDPI. https://doi.org/10.3390/life13020268

Lim, Y.-J., Oh, H., Lee, M.-H., Roh, E., Ham, H., Park, D. S., Park, D. H., & Lee, Y. H. (2023). First Report of Fire Blight Caused by Erwinia amylovora on Korean Mountain Ash (Sorbus alnifolia) in Korea. *Research in Plant Disease*, *29*(1), 79–81. https://doi.org/10.5423/rpd.2022.28.4.79

Lima Iida, A. S., Luz, K. N., Barros-Alexandrino, T. T., Fávaro-Trindade, C. S., de Pinho, S. C., Garrido Assis, O. B., & Martelli-Tosi, M. (2020).

Investigation of TPP-Chitosomes particles structure and stability as encapsulating agent of cholecalciferol. *Polimeros*, *29*(4). https://doi.org/10.1590/0104-1428.04119

Lusiana, R. A., Protoningtyas, W. P., Wijaya, A. R., Siswanta, D., Mudasir, & Santosa, S. J. (2017). Chitosan-tripoly phosphate (CS-TPP) synthesis through cross-linking process: The effect of concentration towards membrane mechanical characteristic and urea permeation. *Oriental Journal of Chemistry*, *33*(6), 2913–2919. https://doi.org/10.13005/ojc/330626

Magdalita, P. M., Selda Rivarez, M. P., Dela Cueva, F. M., Pascual, A. O. S., & Trinidad, L. C. (2021). Ultrastructural Characterization and Field Performance of Papaya Regrowth Selections Recovered From Bacterial Crown Rot Infection For Disease Tolerance Breeding. In *Philippine Journal of Crop Science* (Vol. 46, Issue 3). PJCS. https://cabidigitallibrary.org

Malik, N. A. A., Kumar, I. S., & Nadarajah, K. (2020). Elicitor and receptor molecules: Orchestrators of plant defense and immunity. In *International Journal of Molecular Sciences* (Vol. 21, Issue 3). MDPI AG. https://doi.org/10.3390/ijms21030963

Maluin, F. N., Hussein, M. Z., Yusof, N. A., Fakurazi, S., Idris, A. S., Hilmi, N. H. Z., & Daim, L. D. J. (2019). Preparation of chitosan-hexaconazole nanoparticles as fungicide nanodelivery system for combating Ganoderma disease in oil palm. *Molecules*, *24*(13). https://doi.org/10.3390/molecules24132498

Mapuranga, J., Chang, J., Zhao, J., Liang, M., Li, R., Wu, Y., Zhang, N., Zhang, L., & Yang, W. (2023). The Underexplored Mechanisms of Wheat Resistance to Leaf Rust. In *Plants* (Vol. 12, Issue 23). Multidisciplinary Digital Publishing Institute (MDPI). https://doi.org/10.3390/plants12233996

Marques Gonçalves, M., Florencio Maluf, D., Pontarolo, R., Ketzer, C., Almouazen, E., Chevalier, Y., & Claude Bernard Lyon, U. (2023). *Negatively charged chitosan nanoparticles prepared by ionotropic gelation for 1 encapsulation of positively charged proteins 2 3*.

Martinez, C. S., Igartúa, D. E., Calienni, M. N., Feas, D. A., Siri, M., Montanari, J., Chiaramoni, N. S., Alonso, S. del V., & Prieto, M. J. (2017). Relation between biophysical properties of nanostructures and their toxicity on zebrafish. In *Biophysical Reviews* (Vol. 9, Issue 5, pp. 775–791). Springer Verlag. https://doi.org/10.1007/s12551-017-0294-2

Mazzotta, E., Muzzalupo, R., Chiappetta, A., & Muzzalupo, I. (2022). Control of the Verticillium Wilt on Tomato Plants by Means of Olive Leaf Extracts Loaded on Chitosan Nanoparticles. *Microorganisms*, *10*(1). https://doi.org/10.3390/microorganisms10010136

Meena, M., Yadav, G., Sonigra, P., Nagda, A., Mehta, T., Swapnil, P., Harish, & Marwal, A. (2022). Role of elicitors to initiate the induction of systemic resistance in plants to biotic stress. *Plant Stress*, *5*. https://doi.org/10.1016/j.stress.2022.100103

Mikušová, V., Mikuš, P., & Piozzi, A. (2021). *Advances in Chitosan-Based Nanoparticles for Drug Delivery*. https://doi.org/10.3390/ijms2217

Mittal, D., Kaur, G., Singh, P., Yadav, K., & Ali, S. A. (2020). Nanoparticle-Based Sustainable Agriculture and Food Science: Recent Advances and Future Outlook. In *Frontiers in Nanotechnology* (Vol. 2). Frontiers Media S.A. https://doi.org/10.3389/fnano.2020.579954

Mohd-Azhar, H., Sarip, J., Ghazali, N. F., Zulfa, M., Razikin, M., & Mariatulqabtiah, A. R. (2021). TOLERANCE LEVEL OF GRAFTED PAPAYA PLANTS AGAINST PAPAYA DIEBACK DISEASE. In *Malays. Appl. Biol* (Vol. 50, Issue 1).

Moses, S., Taiye, C., Oladele, B., Simon-Ilogho, K., Edewor, B., & Adebukola, F. (2024). Effect of technological innovation on sustainability practices in the agricultural sector. In *Journal of Entrepreneurship Education* (Vol. 27, Issue 1).

Muhaimin, M., Yusnaidar, Y., Syahri, W., Latief, M., & Chaerunisaa, A. Y. (2020). Microencapsulation of macaranga gigantea leaf extracts: Production and characterization. *Pharmacognosy Journal*, *12*(4), 716–724. https://doi.org/10.5530/pj.2020.12.104

Mujtaba, M., Wang, D., Carvalho, L. B., Oliveira, J. L., Espirito Santo Pereira, A. Do, Sharif, R., Jogaiah, S., Paidi, M. K., Wang, L., Ali, Q., & Fraceto, L. F. (2021). Nanocarrier-Mediated Delivery of miRNA, RNAi, and CRISPR-Cas for Plant Protection: Current Trends and Future Directions. In *ACS Agricultural Science and Technology* (Vol. 1, Issue 5, pp. 417–435). American Chemical Society. https://doi.org/10.1021/acsagscitech.1c00146

Mutinda, S., Mobegi, F. M., Hale, B., Dayou, O., Ateka, E., Wijeratne, A., Wicke, S., Bellis, E. S., & Runo, S. (2023). Resolving intergenotypic Striga resistance in sorghum. *Journal of Experimental Botany*, *74*(17), 5294–5306. https://doi.org/10.1093/jxb/erad210

Muzammil, S., Ashraf, A., Siddique, M. H., Aslam, B., Rasul, I., Abbas, R., Afzal, M., Faisal, M., & Hayat, S. (2023). A review on toxicity of nanomaterials in agriculture: Current scenario and future prospects. In *Science Progress* (Vol. 106, Issue 4). SAGE Publications Ltd. https://doi.org/10.1177/00368504231221672

Nadendla, S. R., Rani, T. S., Vaikuntapu, P. R., Maddu, R. R., & Podile, A. R. (2018). HarpinPss encapsulation in chitosan nanoparticles for improved bioavailability and disease resistance in tomato. *Carbohydrate Polymers*, *199*, 11–19. https://doi.org/10.1016/j.carbpol.2018.06.094

Nishad, R., Ahmed, T., Rahman, V. J., & Kareem, A. (2020). Modulation of Plant Defense System in Response to Microbial Interactions. In *Frontiers in Microbiology* (Vol. 11). Frontiers Media S.A. https://doi.org/10.3389/fmicb.2020.01298

Noor Shahida, Y., Awang, Y., Sijam, K., Noriha, M. A., & Satar, M. G. M. (2016). Biochemical changes and leaf photosynthesis of erwinia mallotivora infected papaya (Carica papaya) seedlings. *American Journal of Plant Physiology*, *11*(1), 12–22. https://doi.org/10.3923/ajpp.2016.12.22

Nur Adliza Baharom, Farah Huda Sjafni Suherman, & Mohd Nazaruddin Anuar. (2018). Supplementation of selected micronutrients as alternative approach in managing papaya dieback disease. *Buletin Teknologi MARDI*, 105–113.

Omer, A. M., Ziora, Z. M., Tamer, T. M., Khalifa, R. E., Hassan, M. A., Mohy-Eldin, M. S., & Blaskovich, M. A. T. (2021). Formulation of quaternized aminated chitosan nanoparticles for efficient encapsulation and slow release of curcumin. *Molecules*, *26*(2). https://doi.org/10.3390/molecules26020449

Pathania, N., Magdalita, Pablito., Cueva, F. de la., Herradura, Lorna., Waje, Aira., Lobres, Adelfa., Cueto, Arcangel., Dillon, Natalie., Vawdrey, Lynton., Hucks, Louise., Chambers, Donna., Sun, Grace., Cheesman, Jodi., & Australian Centre for International Agricultural Research. (n.d.). *Integrated disease management strategies for the productive, profitable and sustainable production of high quality papaya fruit in the southern Philippines and Australia : final report*.

Paul, M., Rivarez, S., Parac, E. P., Fatima, S., Dimasingkil, M., & Magdalita, P. M. (2021). *Inuence of native endophytic bacteria on the growth and bacterial crown rot tolerance of papaya (Carica papaya)*. https://doi.org/10.21203/rs.3.rs-559032/v1

Pecherina, A., Grinberg, M., Ageyeva, M., Zdobnova, T., Ladeynova, M., Yudintsev, A., Vodeneev, V., & Brilkina, A. (2021). Whole-plant measure of temperature-induced changes in the cytosolic ph of potato plants using genetically encoded fluorescent sensor pt-gfp. *Agriculture (Switzerland)*, *11*(11). https://doi.org/10.3390/agriculture11111131

Pellis, A., Guebitz, G. M., & Nyanhongo, G. S. (2022). Chitosan: Sources, Processing and Modification Techniques. In *Gels* (Vol. 8, Issue 7). MDPI. https://doi.org/10.3390/gels8070393

Pereira, A. do E. S., Oliveira, H. C., & Fraceto, L. F. (2019). Polymeric nanoparticles as an alternative for application of gibberellic acid in sustainable agriculture: a field study. *Scientific Reports*, *9*(1). https://doi.org/10.1038/s41598-019-43494-y

Pham, T. T., Nguyen, T. H., Thi, T. V., Nguyen, T. T., Le, T. D., Vo, D. M. H., Nguyen, D. H., Nguyen, C. K., Nguyen, D. C., Nguyen, T. T., & Bach, L. G. (2019). Investigation of chitosan nanoparticles loaded with Protocatechuic acid (PCA) for the resistance of Pyricularia oryzae Fungus against rice blast. *Polymers*, *11*(1). https://doi.org/10.3390/POLYM11010177

Picchi, V., Gobbi, S., Fattizzo, M., Zefelippo, M., & Faoro, F. (2021). Chitosan nanoparticles loaded with n-acetyl cysteine to mitigate ozone and other possible oxidative stresses in durum wheat. *Plants*, *10*(4). https://doi.org/10.3390/plants10040691

Pirozzi, D., Latte, A., & Sannino, F. (2023). Immobilization of Lipases on Chitosan Hydrogels Improves Their Stability in the Presence of the Products of Triglyceride Oxidation. *Gels*, *9*(10). https://doi.org/10.3390/gels9100776

Rajan, R. K., Hussein, M. Z., Fakurazi, S., Yusoff, K., & Masarudin, M. J. (2019). Increased ROS scavenging and antioxidant efficiency of chlorogenic acid compound delivered via a chitosan nanoparticulate system for efficient in vitro visualization and accumulation in human renal adenocarcinoma cells. *International Journal of Molecular Sciences*, *20*(19). https://doi.org/10.3390/ijms20194667

Rizeq, B. R., Younes, N. N., Rasool, K., & Nasrallah, G. K. (2019). Synthesis, bioapplications, and toxicity evaluation of chitosan-based nanoparticles. In *International Journal of Molecular Sciences* (Vol. 20, Issue 22). MDPI AG. https://doi.org/10.3390/ijms20225776

Roff, M., Noor, M., & Abu Bakar, N. (2019). *TROPICAL FRUIT PESTS AND ITS MANAGEMENT OPTIONS IN MALAYSIA*. https://www.researchgate.net/publication/333419053

Rozana, N. (2017a). Competitiveness of Malaysia's Fruits in the Global Market: Revealed Comparative Advantage Analysis. In *Malaysian Journal of Mathematical Sciences* (Vol. 11).

Rozana, N. (2017b). Competitiveness of Malaysia's Fruits in the Global Market: Revealed Comparative Advantage Analysis. In *Malaysian Journal of Mathematical Sciences* (Vol. 11).

Sabrina Wahid, N., Abu Bakar, N., Azlina Masdor, N., Azhar Hassan, M., Balqis Zamri, N., Suzaida Mohd Nor, N., Zulfadli Sohaime, M., Ainul Bashirah, R., & Jaffri Masaruddin, M. (2021). Encapsulation and characterisation of SAR-inducing recombinant proteins in chitosan nanoparticles for papaya dieback disease management. In *Proceedings of MARDI Science and Technology Exhibition*.

Sampathkumar, K., Tan, K. X., Chye, S., & Loo, J. (2020). Developing Nano-Delivery Systems for Agriculture and Food Applications with Nature-Derived Polymers. *ISCIENCE*, *23*, 101055. https://doi.org/10.1016/j.isci

Santana, I., Wu, H., Hu, P., & Giraldo, J. P. (2020). Targeted delivery of nanomaterials with chemical cargoes in plants enabled by a biorecognition motif. *Nature Communications*, *11*(1). https://doi.org/10.1038/s41467-020-15731-w

Saritha, G. N. G., Anju, T., & Kumar, A. (2022). Nanotechnology - Big impact: How nanotechnology is changing the future of agriculture? *Journal of Agriculture and Food Research*, *10*. https://doi.org/10.1016/j.jafr.2022.100457

Sedyakina, N., Kuskov, A., Velonia, K., Feldman, N., Lutsenko, S., & Avramenko, G. (2020). Modulation of entrapment efficiency and in vitro release properties of BSA-loaded chitosan microparticles cross-linked with citric acid as a potential protein-drug delivery system. *Materials*, *13*(8). https://doi.org/10.3390/MA13081989

Sekeli, R., Hisham Nazaruddin, N., Asyraf Tamizi, A., Mat Amin, N., Wee, C.-Y., Sarip, J., Abdullah, ini, Izzati Saidi, N., Abdul Razak, R., & Zulkifli, Z. (2019). Enhancing Eksotika Papaya Resistance to Dieback Disease through Quorum Quenching. *J. Trop. Plant Physiol*, *11*(1), 1–9.

Sikhondze, S. S., Makoni, P. A., Walker, R. B., & Khamanga, S. M. M. (2023a). Chitosan-Coated SLN: A Potential System for Ocular Delivery of Metronidazole. *Pharmaceutics*, *15*(7). https://doi.org/10.3390/pharmaceutics15071855

Sikhondze, S. S., Makoni, P. A., Walker, R. B., & Khamanga, S. M. M. (2023b). Chitosan-Coated SLN: A Potential System for Ocular Delivery of Metronidazole. *Pharmaceutics*, *15*(7). https://doi.org/10.3390/pharmaceutics15071855

Simpson, E., Sarwar, H., Jack, I., & Lowry, D. (2024). Evaluation of the Potential of Chitosan Nanoparticles as a Delivery Vehicle for Gentamicin for the Treatment of Osteomyelitis. *Antibiotics*, *13*(3). https://doi.org/10.3390/antibiotics13030208

Sirviö, J. A., Kantola, A. M., Komulainen, S., & Filonenko, S. (2021). Aqueous modification of chitosan with itaconic acid to produce strong oxygen barrier film. *Biomacromolecules*, *22*(5), 2119–2128. https://doi.org/10.1021/acs.biomac.1c00216

Sornay, C., Vaur, V., Wagner, A., & Chaubet, G. (2022). An overview of chemo- and site-selectivity aspects in the chemical conjugation of proteins. In *Royal Society Open Science* (Vol. 9, Issue 1). Royal Society Publishing. https://doi.org/10.1098/rsos.211563

Spychalski, M., Kukawka, R., Prasad, R., Borodynko-Filas, N., Stępniewska-Jarosz, S., Turczański, K., & Smiglak, M. (2023). A New Benzothiadiazole Derivative with Systemic Acquired Resistance Activity in the Protection of Zucchini (Cucurbita pepo convar. giromontiina) against Viral and Fungal Pathogens. *Plants*, *12*(1). https://doi.org/10.3390/plants12010043

Suharjo, R., Oktaviana, H. A., Aeny, T. N., Ginting, C., Wardhana, R. A., Nugroho, A., & Ratdiana, R. (2021). Erwinia mallotivora is the causal agent of papaya bacterial crown rot disease in lampung timur, indonesia. *Plant Protection Science*, *57*(2), 122–133. https://doi.org/10.17221/123/2020-PPS

Tamizi, A. A., Abu-Bakar, N., Samsuddin, A. F., Rozano, L., Ahmad-Redzuan, R., & Abdul-Murad, A. M. (2020). Characterisation and mutagenesis study of an alternative sigma factor gene (Hrpl) from erwinia mallotivora reveal its central role in papaya dieback disease. *Biology*, *9*(10), 1–16. https://doi.org/10.3390/biology9100323

Tamizi, A. A., Mat-Amin, N., Weaver, J. A., Olumakaiye, R. T., Akbar, M. A., Jin, S., Bunawan, H., & Alberti, F. (2022). Genome Sequencing

and Analysis of Trichoderma (Hypocreaceae) Isolates Exhibiting Antagonistic Activity against the Papaya Dieback Pathogen, Erwinia mallotivora. *Journal of Fungi*, *8*(3). https://doi.org/10.3390/jof8030246

Tan, G. H., Ali, A., & Siddiqui, Y. (2022). Current strategies, perspectives and challenges in management and control of postharvest diseases of papaya. In *Scientia Horticulturae* (Vol. 301). Elsevier B.V. https://doi.org/10.1016/j.scienta.2022.111139

Tan, G. H., Ali, A., & Siddiqui, Y. (2023). Major fungal postharvest diseases of papaya: Current and prospective diagnosis methods. In *Crop Protection* (Vol. 174). Elsevier Ltd. https://doi.org/10.1016/j.cropro.2023.106399

Tarakanov, R., Shagdarova, B., Lyalina, T., Zhuikova, Y., Il'ina, A., Dzhalilov, F., & Varlamov, V. (2023). Protective Properties of Copper-Loaded Chitosan Nanoparticles against Soybean Pathogens Pseudomonas savastanoi pv. glycinea and Curtobacterium flaccumfaciens pv. flaccumfaciens. *Polymers*, *15*(5). https://doi.org/10.3390/polym15051100

Tokmakov, A. A., Kurotani, A., & Sato, K. I. (2021). Protein pI and Intracellular Localization. In *Frontiers in Molecular Biosciences* (Vol. 8). Frontiers Media S.A. https://doi.org/10.3389/fmolb.2021.775736

Torres-Rodriguez, J. A., Reyes-Pérez, J. J., Castellanos, T., Angulo, C., Quiñones-Aguilar, E. E., & Hernandez-Montiel, L. G. (2021). A biopolymer with antimicrobial properties and plant resistance inducer against phytopathogens: Chitosan. *Notulae Botanicae Horti Agrobotanici Cluj-Napoca*, *49*(1), 1–15. https://doi.org/10.15835/nbha49112231

Valderrama N, A., Jacinto H, C., Lay, J., Flores E, Y., Zavaleta C, D., & Delfín, A. R. (2020). Factorial design for preparing chitosan nanoparticles and its use for loading and controlled release of indole-3-acetic acid with effect on hydroponic lettuce crops. *Biocatalysis and Agricultural Biotechnology*, *26*. https://doi.org/10.1016/j.bcab.2020.101640

Vega-Vásquez, P., Mosier, N. S., & Irudayaraj, J. (2020). Nanoscale Drug Delivery Systems: From Medicine to Agriculture. In *Frontiers in Bioengineering and Biotechnology* (Vol. 8). Frontiers Media S.A. https://doi.org/10.3389/fbioe.2020.00079

Venkateshaiah, A., Padil, V. V. T., Nagalakshmaiah, M., Waclawek, S., Černík, M., & Varma, R. S. (2020). Microscopic techniques for the analysis of micro and nanostructures of biopolymers and their derivatives. In *Polymers* (Vol. 12, Issue 3). MDPI AG. https://doi.org/10.3390/polym12030512

Wang, G., Ren, Y., Bai, X., Su, Y., & Han, J. (2022). Contributions of Beneficial Microorganisms in Soil Remediation and Quality Improvement of Medicinal Plants. In *Plants* (Vol. 11, Issue 23). MDPI. https://doi.org/10.3390/plants11233200

Wang, Y., Yan, Q., Lan, C., Tang, T., Wang, K., Shen, J., & Niu, D. (2023). Nanoparticle carriers enhance RNA stability and uptake efficiency and prolong the protection against Rhizoctonia solani. *Phytopathology Research*, *5*(1). https://doi.org/10.1186/s42483-023-00157-1

Wong, B. X., Chew, C. C., Gaik Tay, K., Al-Qershi, O., Huong, A., & Alzaeemi, S. A. (2023). *Android Based-App Papaya Leaf Disease Identification Using Convolution Neural Network* (Vol. 7). http://arqiipubl.com/ams

Xi, D. K., Yap, S. L., Kumar, N. N., Toh, C. C., Ishikawa, K., & Hori, M. (2023). Plasma-Assisted priming: Improved germination and seedling performance of papaya. *Sains Malaysiana*, *52*(2), 599–611. https://doi.org/10.17576/jsm-2023-5202-21

Xiao, D., Liu, J., Liu, Y., Wang, Y., Zhan, Y., & Liu, Y. (2022). Exogenous Application of a Plant Elicitor Induces Volatile Emission in Wheat and Enhances the Attraction of an Aphid Parasitoid Aphidius gifuensis. *Plants*, *11*(24). https://doi.org/10.3390/plants11243496

Yadav, A., Yadav, K., & Abd-Elsalam, K. A. (2023). Nanofertilizers: Types, Delivery and Advantages in Agricultural Sustainability. *Agrochemicals*, *2*(2), 296–336. https://doi.org/10.3390/agrochemicals2020019

YAVAŞ, İ. (2021). The Effect of Nanoparticle Applications on Plants under Some Stress Conditions. *Turkish Journal of Range and Forage Science*, *2*(2), 52–62. https://doi.org/10.51801/turkjrfs.954843

Zahir, S., Kanti Pal, T., Sengupta, A., Biswas, S., Bar, S., Bose, S., & Nanak, G. (2021). Determination Of Lethal Concentration Fifty (Lc 50) Of Whole Plant Ethanolic Extract Of Amaranthus Viridis, Cynodon Dactylon & Aerva Sanguinolenta On Zebrafish (Danio Rerio) EMBRYOS. *International Journal of Pharmaceutical Sciences and*

Research, *12*(4), 2394–2404. https://doi.org/10.13040/IJPSR.0975-8232.12(4).2394-04

Zaman, M., Butt, M. H., Siddique, W., Iqbal, M. O., Nisar, N., Mumtaz, A., Nazeer, H. Y., Alshammari, A., & Riaz, M. S. (2022). Fabrication of PEGylated Chitosan Nanoparticles Containing Tenofovir Alafenamide: Synthesis and Characterization. *Molecules*, *27*(23). https://doi.org/10.3390/molecules27238401

Zarzar, J., Khan, T., Bhagawati, M., Weiche, B., Sydow-Andersen, J., & Alavattam, S. (2023). High concentration formulation developability approaches and considerations. In *mAbs* (Vol. 15, Issue 1). Taylor and Francis Ltd. https://doi.org/10.1080/19420862.2023.2211185

Zehra, A., Raytekar, N. A., Meena, M., & Swapnil, P. (2021). Efficiency of microbial bio-agents as elicitors in plant defense mechanism under biotic stress: A review. In *Current Research in Microbial Sciences* (Vol. 2). Elsevier Ltd. https://doi.org/10.1016/j.crmicr.2021.100054

Zhang, C., Feng, C., Wang, J., Kong, F., Sun, W., & Wang, F. (2016). Cloning, expression analysis and recombinant expression of a gene encoding a polygalacturonase-inhibiting protein from tobacco, Nicotiana tabacum. *Heliyon*, *2*(5). https://doi.org/10.1016/j.heliyon.2016.e00110

Zhang, H., Goh, N. S., Wang, J. W., Pinals, R. L., González-Grandío, E., Demirer, G. S., Butrus, S., Fakra, S. C., Del Rio Flores, A., Zhai, R., Zhao, B., Park, S. J., & Landry, M. P. (2022). Nanoparticle cellular internalization is not required for RNA delivery to mature plant leaves. *Nature Nanotechnology*, *17*(2), 197–205. https://doi.org/10.1038/s41565-021-01018-8

Zheng, K., Lu, J., Li, J., Yu, Y., Zhang, J., He, Z., Ismail, O. M., Wu, J., Xie, X., Li, X., Xu, G., Dou, D., & Wang, X. (2021). Efficiency of chitosan application against Phytophthora infestans and the activation of defence mechanisms in potato. *International Journal of Biological Macromolecules*, *182*, 1670–1680. https://doi.org/10.1016/j.ijbiomac.2021.05.097

Zhou, X., Chen, Y., Zhao, Y., Gao, F., & Liu, H. (2020). The application of exogenous PopW increases the tolerance of Solanum lycopersicum L. to drought stress through multiple mechanisms. *Physiology and Molecular Biology of Plants*, *26*(12), 2521–2535. https://doi.org/10.1007/s12298-020-00918-8

Zungu, B., Kamdem Paumo, H., Gaorongwe, J. L., Tsuene, G. N., Ruzvidzo, O., & Katata-Seru, L. (2023). Zn nutrients-loaded chitosan nanocomposites and their efficacy as nanopriming agents for maize (Zea mays) seeds. *Frontiers in Chemistry*, *11*. https://doi.org/10.3389/fchem.2023.1243884

APPENDICES

Appendix I: Synthesis of CNP using different CS and TPP volumes

Volume (mL)		Particle size (nm)				
TPP	**CS**	1	2	3	Mean	SD
2.5	0.0	2360.317	2080.230	2276.880	2239.14	143.81
	1.5	672.443	678.947	606.723	652.70	39.95
	3.0	199.733	194.283	206.043	200.02	5.89
	4.5	130.513	130.743	127.500	129.69	1.81
	6.0	64.817	67.500	70.637	67.65	2.91
	7.5	70.220	71.750	71.743	71.24	0.88
CS	**TPP**	1	2	3	Mean	SD
6	0.0	635.663	637.577	605.387	626.21	18.06
	0.5	165.757	164.370	158.533	162.89	3.83
	1.0	80.513	80.027	81.490	80.68	0.75
	1.5	76.093	76.893	77.663	76.88	0.79
	2.0	72.790	73.353	74.620	73.59	0.94
	2.5	64.277	66.853	67.673	66.27	1.77
	3.0	114.280	114.347	113.243	113.96	0.62
	3.5	116.167	116.680	118.053	117.03	0.95
	4.0	124.880	130.500	133.380	129.59	4.32

Volume (mL)		Polydispersity index				
TPP	**CS**	1	2	3	Mean	SD
2.5	0.0	0.360	0.378	0.289	0.342	0.047
	1.5	0.406	0.339	0.391	0.379	0.035
	3.0	0.222	0.218	0.224	0.221	0.003
	4.5	0.239	0.210	0.219	0.223	0.015
	6.0	0.223	0.235	0.188	0.215	0.024
	7.5	0.192	0.176	0.166	0.178	0.013
CS	**TPP**	1	2	3	Mean	SD
6	0.0	0.248	0.339	0.261	0.301	0.039
	0.5	0.233	0.208	0.226	0.223	0.013
	1.0	0.181	0.167	0.197	0.182	0.015
	1.5	0.200	0.205	0.182	0.196	0.012
	2.0	0.212	0.238	0.178	0.209	0.030
	2.5	0.220	0.175	0.171	0.189	0.027
	3.0	0.205	0.217	0.232	0.218	0.013
	3.5	0.186	0.186	0.183	0.185	0.002
	4.0	0.219	0.240	0.248	0.236	0.015

Appendix II: Synthesis of CNP-HrpN using different HrpN concentration

Concentration of HrpN in CNP (mg/mL)	Particle Size (nm)				
	1	2	3	Mean	SD
0	78.24	78.34	78.18	78.25	0.08
0.02	100.76	101.85	103.03	101.80	1.14
0.04	104.73	105.64	108.65	106.34	2.05
0.06	108.55	108.62	109.12	108.76	0.31
0.08	109.02	109.35	111.16	109.84	1.15
1.0	111.67	111.70	112.20	111.86	0.30
	Polydispersity index				
	1	2	3	Mean	SD
0	0.207	0.191	0.175	0.191	0.016
0.02	0.257	0.205	0.176	0.213	0.041
0.04	0.195	0.193	0.175	0.188	0.011
0.06	0.204	0.205	0.215	0.208	0.006
0.08	0.180	0.211	0.233	0.208	0.027
1.0	0.194	0.205	0.188	0.195	0.009

Volume (mL)	Encapsulation Efficiency				
Concentration of HrpN in CNP (mg/mL)	1	2	3	Mean	SD
0.02	84.58	83.33	89.58	85.83	3.30
0.04	80.00	79.71	85.79	81.84	3.43
0.06	71.01	54.55	60.784	62.11	8.31
0.08	50.00	54.55	59.09	54.55	4.55
1.0	59.80	51.96	49.02	53.59	5.57

Appendix III: Release Percentage of HrpN from CNP

CNP-HrpN: 0.02 mg/ml

Time (hour)	Reading 1 (%)	Reading 2 (%)	Reading 3 (%)	Mean (%)	Standard Deviation
1	11.45	12.00	13.45	12.30	1.03
3	33.09	34.76	35.77	34.54	0.57
6	46.21	45.76	47.01	46.33	1.16
24	81.78	81.45	82.01	81.75	0.37
48	89.97	90.21	90.88	90.36	0.36
72	99.32	99.02	98.02	98.79	1.15

CNP-HrpN: 0.04 mg/ml

Time (hour)	Reading 1 (%)	Reading 2 (%)	Reading 3 (%)	Mean (%)	Standard Deviation
1	15.99	16.01	16.23	16.08	0.13
3	41.02	40.45	39.01	40.16	1.17
6	56.87	58.23	51.95	55.68	2.44
24	85.77	83.48	86.11	85.12	4.48
48	98.21	98.79	92.22	96.41	4.71
72	98.80	99.95	99.94	99.56	3.96

CNP-HrpN: 0.06 mg/ml

Time (hour)	Reading 1 (%)	Reading 2 (%)	No.3 (%)	Mean (%)	Standard Deviation
1	18.54	17.95	18.84	18.44	0.45
3	47.77	44.28	42.13	44.73	2.97
6	63.42	61.14	60.11	61.55	1.16
24	88.55	87.45	86.12	87.37	0.61
48	96.67	97.63	94.02	96.10	1.26
72	99.03	99.07	99.02	99.04	1.85

CNP-HrpN: 0.08 mg/ml

Time (hour)	Reading 1 (%)	Reading 2 (%)	Reading 3 (%)	Mean (%)	Standard Deviation
1	18.94	19.95	19.99	19.63	0.59
3	46.59	48.86	44.97	46.81	2.01
6	62.05	63.55	62	62.54	1.19
24	85.55	87.33	88.13	87.01	1.44
48	96.66	94.09	95.12	95.30	2.45
72	99.12	99.34	99.07	99.18	1.40

CNP-HrpN: 1.0 mg/ml

Time (hour)	Reading 1 (%)	Reading 2 (%)	Reading 3 (%)	Mean (%)	Standard Deviation
1	22.03	21.57	20.01	21.20	1.06
3	48.17	49.02	48.02	48.40	0.96
6	64.12	66.67	65.73	65.50	1.00
24	89.12	90.03	88.78	89.31	1.05
48	98.12	97.23	96.14	97.16	1.00
72	99.77	99.12	99.88	99.58	1.14

BIODATA OF STUDENT

Nur Balqis Zamri is currently working on her Master of Science in Nanobiotechnology at Universiti Putra Malaysia. She previously completed her Foundation of Agricultural Sciences and Bachelor of Science in Cell and Molecular Biology at the same university, where she developed skills in molecular biology and nanotechnology. During her studies, Nur Balqis became deeply interested in how molecular biology, nanotechnology and agriculture intersect. Her research has earned her recognition, including the Best Research Paper Award at the 2023 Postgraduate Students Research Paper Competition at Universiti Malaya. Nur Balqis also worked as a Research Officer at Malaysian Agricultural Research and Development Institute (MARDI), where she planned and conducted experiments related to nanobiotechnology in agriculture. She has developed strong interest in scientific writing, nanoparticle formulation, and molecular biology, and she actively participates in international workshops and conferences to further her knowledge. Driven by a passion for combining science with creativity, Nur Balqis aims to develop innovative solutions in nanobiotechnology to support sustainable practices.

LIST OF PUBLICATIONS

Balqis Zamri, N., Wahid, S., Abu Bakar, N., Sohaime, Z., Azlina Masdor, N., Suzaida, N., & Nor, M. (2024). Unlocking the potential of chitosan nanoparticle as a carrier for systemic acquired resistance (SAR)-inducing recombinant protein: A preliminary study. In AsPac J. Mol. Biol. Biotechnol (Vol. 32, Issue 1).

Balqis, Z. N., Sabrina, W. N., Suzaida, M. N., Norliza, A. B., Zulfadli, S. M., Azlina, M. N., ... & Jaffri, M. M. (2022). Toxicology evaluation through zebrafish embryo acute toxicity test on chitosan nanoparticles (CNP) and chitosan nanoparticles loaded with bacterial effector protein, HrpN (CNP-HrpN). Transaction of the Malaysian Society of Plant Physiology.

Zamri, N. B. (2023). Nanotechnology in agriculture: A review of innovative utilization. Malaysian NANO-An International Journal, 3(2), 50-64.

Sabrina Wahid, N., Abu Bakar, N., Azlina Masdor, N., Azhar Hassan, M., Balqis Zamri, N., Suzaida Mohd Nor, N., Zulfadli Sohaime, M., Ainul Bashirah, R., & Jaffri Masaruddin, M. (2021). Encapsulation and characterisation of SAR-inducing recombinant proteins in chitosan nanoparticles for papaya dieback disease management. In Proceedings of MARDI Science and Technology Exhibition.